Uncommon K-foiditic magmas: the case study of Tufo del Palatino (Colli Albani Volcanic District, Italy)

M. Gaeta[1*], B. Bonechi[1], F. Marra[2], C. Perinelli[1]

1: Dipartimento di Scienze della Terra, Sapienza Università di Roma, P.le Aldo Moro 5, 00185, Rome, Italy

2: Istituto Nazionale di Geofisica e Vulcanologia, Via di Vigna Murata 605, 00143 Rome, Italy

*Corresponding author. Telephone: 0039 06 49914916; E-mail: mario.gaeta@uniroma1.it

Abstract

Leucititic rocks, K-foiditic in composition are volumetrically important in the Colli Albani (also known as Alban Hills) volcanic district (Central Italy) especially during the most explosive phases of activity (>200 km^3). The Colli Albani tephra in distal (>500 km) deposits indicates that K-foiditic magma chambers fed large explosive eruptions (i.e., tens of km^3 of pyroclastic rocks). Major oxides, trace elements and Raman spectra were measured on the glasses and minerals occurring in the K-foiditic scoria clasts of the ~530 kyr-old Tufo del Palatino, erupted in the Colli Albani volcanic district. The Colli Albani pre-eruptive magmatic system is characterized by the a_{H2O} <1 and high CO_2 activity in the melt, as testified by the CO_3 in the clinopyroxene melt inclusions, by the early crystallization of CO_3-bearing apatite and by the high CO_2 activity in the free volatile phase that led to crystallization of calcium carbonate in the scoria clast vesicles. The K-foiditic magmas plot on the Cpx+Lc+melt divariant surface of the Ol-Cpx-Lc-Mel-H_2O-CO_2, P ≥0.2 GPa and T ≤1100 °C. The assimilation of cold carbonate by hot magmas is an important open-system process allowing the establishment of a_{H20} <1 condition in the volatile-rich, Colli Albani magma chambers where the stability fields of the olivine and phlogopite are reduced in favour of clinopyroxene and leucite. Trace element modelling indicates large amount of

carbonate assimilation (~12.4 wt%) involved in the differentiation process that origins the K-foiditic magmas starting from a K-rich, phonotephritic parental magma. The large amount of assimilate carbonate is consistent with the peculiar distribution of the latent heat across the crystallization interval of the phonotephritic parental magma. The isenthalpic assimilation process is very efficient in the phonotephritic magma because the crystallization of clinopyroxene and leucite in equilibrium with a K-foiditic melt proceeds over a relatively large temperature interval (>200 °C) and the K-foiditic melt shows low viscosity (10^4Pa·s at 1000 °C). Actually, the low melt viscosity, that increases the growth rate, and the large temperature interval of crystallization are intrinsic factors that increase the release of the latent heat of crystallization from the phonotephritic parental magma. Extrinsic factors enhancing the assimilation process efficiency are the thickness (>4 km) and the depth (down to 5-7 km) of the carbonate substrate in the Colli Albani volcanic district.

Key words: foidite, glass, leucite, ultrapotassic, Colli Albani.

1. Introduction

Leucititic rocks with K-foiditic composition (i.e., $K_2O>Na_2O$) are rare and occur almost exclusively in the Quaternary volcanic districts of Italy (Lustrino et al., 2019). K-foiditic scoria, lava flows and granular hypabyssal rocks are present in the Vulsini Volcanic District (Di Battistini et al., 1998), at Colli Albani Volcanic District (Gaeta, 1998), at Volsci Volcanic Field (e.g., Marra et al., 2021) and at Vesuvius (e.g., Rolandi et al., 2004). Notably, K-foidites are volumetrically important in the Colli Albani volcanic district (hereafter Colli Albani), where most of the explosive products (>200 km^3) show such peculiar compositions (e.g., Marra et al., 2009). Colli Albani glasses have been recognized in the 1.2 Myr of continuous tephrostratigraphic record of Lake Ohrid (Macedonia and Albania) on the basis

of their unique K-foiditic composition (Leicher et al., 2013). The occurrence of Colli Albani tephra in distal archives indicates that K-foiditic magma chambers fed large explosive eruptions that have emplaced several tens of km^3 of pyroclastic rocks (e.g., Freda et al., 2011). Researchers have been attracted by these rare rocks of the Colli Albani since the early 20^{th} century (Washington, 1906). K-foiditic lava flows of Colli Albani were initially considered as primary magmas, and consequentially they were the subject of geochemical and experimental research aimed to ascertain the conditions of their formation in the mantle (e.g., Thompson, 1977). Nevertheless, later volcanological, geochemical and experimental studies ruled out the existence of K-foiditic primary magmas (Freda et al., 1997). The delay in understanding that the K-foidites of Colli Albani are differentiated magmas is due to the difficulty of finding residual glasses in primitive lava flows and glassy scoria clasts with K-foiditic composition. Actually, the lava flows and the scoria clasts are commonly characterized by holocrystalline groundmass in which the high growth rate of leucite is highlighted by the star-like habit (e.g., Palladino et al., 2001; Freda et al., 2011). At low pressure, Colli Albani magmas are characterized by high liquidus temperature (>1200°C; Freda et al., 2008) and low viscosity (10^4Pa·s at 1000 °C; Giordano et al., 2008). The combination of a large undercooling (i.e., $\Delta T = T_{system}-T_{mineral\ liquidus}$) and low viscosity is generally the main factor capable of producing high growth rates (e.g., Bonechi et al., 2020a). The Colli Albani scoria clasts are glassy mainly in the hydromagmatic deposits (e.g., Freda et al., 2006; Gaeta et al., 2011) because the high cooling rate, due to the eruptive dynamic, contrasts the high growth rate of leucite.

In this paper we present new data on the hydromagmatic scoria clasts of the Tufo del Palatino eruptive unit (Colli Albani, Central Italy). This eruptive unit is richest in glasses which allow a privileged geochemical and spectroscopic characterization of the K-foiditic melts from which the leucititic rocks crystalize. We use this case study to discuss the

processes at the origin of the K-foiditic magmas with the aim to answer at the main query emerging from the global rarity of these magmas: why K-foidites?

2. Geological contest and field aspect

The Colli Albani, located along the Tyrrhenian Sea margin of Central Italy, are rooted in an overthickened carbonate succession extending from 0.5 to 1 km of depth down to the transition to the crystalline basement, which tomographic studies tentatively place between 5 and 7 km (Bianchi et al. 2008). "Tufo del Palatino" is the formal unit name of the deposit of the second largest explosive eruption of the oldest activity of the Colli Albani (Tuscolano-Artemisio Phase; Freda et al., 1997; Vulcano Laziale lithosome, Giordano et al., 2006). The oldest activity was characterized by five large caldera-forming eruptive units in the time span 561-365 ka, separated by long quiescent periods of 30-50 kyr (Marra et al., 2009). Pyroclastic-flow deposits up to ~300 km^3 in volume, radially stretching as far as 20 km from the vent, were emplaced during this phase. The Tufo del Palatino (530 ± 2 ka) eruptive unit, had hydromagmatic features, witnessed by the frequent occurrence of accretionary lapilli both in the pyroclastic-flow and the ash-cloud deposits. In mid-distal settings, the Tufo del Palatino is characterized by a basal, laminated ash layer, <5 cm thick, followed by a well-sorted, clast supported, dark grey lapilli layer, 1-2 to 15 cm thick, and by a massive, matrix supported, dark grey pyroclastic-flow deposit with variable thickness of 1 to 4 m, as a function of the morphology of the substrate above which it was emplaced. A light grey to yellowish, faintly pedogenized ash with abundant accretionary lapilli (ash-cloud deposit) closes the eruptive unit of Tufo del Palatino. The pyroclastic-flow deposit displays a peperino-like aspect, due to the occurrence of mm-sized dark grey, poorly vesicular scoriae, along with loose, abundant leucite and pyroxene crystals. Sedimentary (i.e., silico-clastic and carbonatic) and igneous (i.e., lava and granular) lithic clasts are also present.

Macroscopic lamination, due to change of grain size, confers a characteristic planar fracturing of this soft volcanic rock which, for these favourable physical properties, was extensively exploited as building stone ("cappellaccio") in the archaic Roman period (Diffendale et al., 2019 and references therein). Lithified facies of Tufo del Palatino, due to the intense zeolitization and calcite crystallization, occurs in the Tiber Valley north of Rome, which was previously identified with the name of "Peperino della Via Flaminia" (Diffendale et al., 2019). Samples analyzed in the present study were collected at several outcrops located along the Tiber Valley where fluvial incision provides good exposition of the pyroclastic-flow deposits, which elsewhere are buried under a thick, younger volcanic succession (Fig. 1). Moreover, the analyzed samples includes three archaeological samples collected from ancient Roman buildings: the Servian Walls at Stazione Termini (sample TP-ST), the archaic temple of Sant'Omobono (sample TP-SO1; Brocato et al., 2019), and the foundation of Tabularium (sample TP-TAB; Marra et al., 2015).

3. Analytical methods

3.1. Major element and volatiles determinations

Major oxides of glasses and minerals were analyzed at the CNR-Istituto di Geologia Ambientale e Geoingegneria di Roma, with a Cameca SX50 electron microprobe equipped with five wavelength dispersive spectrometers (WDS). Quantitative analyses were performed using 15 kV accelerating voltage and 15 nA beam current. As standards we employed metals for Mn and Cr, jadeite for Na, wollastonite for Si and Ca, orthoclase for K, corundum for Al, magnetite for Fe, rutile for Ti, periclase for Mg, F-apatite for P, phlogopite for F, potassium chloride for Cl, barite for Ba and S, celestine for Sr. Counting times for all elements were 20 s on peak and half time on both backgrounds. Light elements (Na, K) were counted first to prevent loss by volatilization. The PAP correction method was used.

126 Minerals were analyzed using a beam diameter of 1-5 μm whereas to minimize alkali loss
127 during glass analysis, the beam was defocused to 15 μm. In order to evaluate the accuracy
128 of the analyses, repeated analyses of three international secondary standard (Kakanui augite,
129 Iceladic Bir-1 and rhyolite RLS132 glasses from USGS) were made prior to any series of
130 measurements. The mean accuracy from the standard value was about 1% for SiO_2, 2% for
131 Al_2O_3, 5% for K_2O, CaO and FeO, and 8-10% for other elements. Moreover, the analytical
132 precision (2 sigma error) is ≤1% for elements in the concentration range >10 wt % oxide,
133 5% for elements in the range 2-10 wt % oxide and better than 10% for elements in the range
134 0.5-2 wt % oxide. From chemical analyses, the H_2O±CO_2 contents of glasses were estimated
135 according to the by-difference method (Devine et al., 1995; Humphreys et al., 2006). We are
136 aware that this method is not fully reliable given the estimation is affected by element
137 concentrations not measured by EMPA and surface charge effects (Hughes et al., 2019)
138 leading to an overestimation of H_2O concentration. However, the obtained H_2O values are
139 close to those determined by micro-Raman spectroscopy measurements (Le Losq et al.,
140 2012; Di Genova et al., 2017) on the same glasses. Raman spectra were acquired with a
141 Horiba Lab Ram HR 800 spectrometer at the Department of Science, Roma Tre University.
142 Data were collected using a 600 grooves/mm spectrometer grating and CCD detector.
143 According to the internal calibration method of Di Genova et al. (2017) it is possible to
144 estimate the water content as a function of the HW/LW area ratio [HW (High Wavenumbers)
145 is the water region (2700-4000 cm^{-1}) while LW (Low Wavenumbers) is the silicate region
146 (100-1500 cm^{-1}) of the Raman spectra], using the following equation: H_2O (wt%) =
147 (HW/LW)·m, where HW/LW is the water to silicate band ratio and m is the linear fit
148 coefficient. Since Di Genova et al. (2017) provide a list of m coefficients for a range of
149 chemical composition that does not include the foiditic one, we estimated a m coefficient for
150 this latter by processing Raman spectra, acquired on synthetic foiditic glasses (Freda et al.

2008), through a specific Matlab© code (Di Genova et al., 2017). The obtained HW/LW were plotted against the water content of the synthetic samples previously measured in order to obtain a linear fit representative of the calibration curve for the foiditic composition and consequently the *m* coefficient (*m* = 1.9608, R^2 = 0.98). This coefficient has been used to assess the water content in the glasses of Tufo del Palatino. Error in water determination is estimated ± 0.15 wt %.

3.2. Trace elements determination

LA-ICP-MS analyses of glasses and clinopyroxenes were performed on a quadrupole–based ICP-MS iCAP-Q instrument (Thermo Fisher Scientific, Bremen) coupled to a modified NewWave UP 213 laser microprobe (NewWave, USA) installed at Charles University, Prague. Analyses of clinopyroxene crystals were performed using a circular laser beam of 100 μm diameter, a puls frequency of 10 Hz and a laser flux on the sample surface of 3.5 J/cm^2. External calibration of the laser ablation analyses was done using Standard Reference Materials NIST (National Institute of Standards and Technology, USA) 612 with internal standardization using Si, based on electron microprobe measurements. The concentration values for NIST of all measured elements were taken from Pearce et al. (1997). The external reproducibility of this method was checked on repeated analyses of USGS BCR-2G glass as reference material (e.g., Strnad et al., 2005 and reference therein). The isotopes used were selected with respect to their most abundant species, free from isobaric overlap and minimum interferences. Formation of oxides (MO^+/M^+) was monitored using U in NIST 612 directly from ablation and the measured ratios ($^{254}UO^+/^{238}U^+$) was below 10^{-2}. Further details about the analytical protocol and correction strategy have been described by Strnad et al. (2005) and Skála et al. (2009). Detection limits for all elements were calculated as 3σ level of the gas blank.

176

177 **4. Results**

178 **4.1. Texture**

179 Submillimetre, euhedral to subeuhedral crystals of leucite and clinopyroxene impart sparsely
180 porphyritic textures (1-5% by volume of crystals ≥0.5 mm) to juvenile scoria lapilli in Tufo
181 del Palatino. The colour and shape of clinopyroxene crystals are variable from green to light
182 green and equidimensional to elongated respectively (Fig. 2a and 2b). Glass, oxide and
183 apatite inclusions can be present in the larger clinopyroxenes (Fig. 2a). The scoria lapilli
184 contain also rare phlogopite (Fig. 2c) and brown to deep green amphibole. The groundmass
185 ranges from glassy to cryptocrystalline with rounded to polygonal vesicles (Fig. 3a, 3b and
186 3c). Frequently, vesicles show a layer made up of zeolites and, sometimes, are filled with
187 calcium carbonate (Fig. 3d). Typically, leucite in glassy scoria clasts shows star-like shape
188 (Fig. 3b and 3c), due to diffusion-controlled crystal growth, as a clear indication of large
189 undercooling (i.e., T_{System}-$T_{Lct\text{-}liquidus}$) at high cooling rate conditions (Hammer, 2008). In the
190 ash matrix of the Tufo del Palatino millimetric to submillimetre, euhedral to anhedral,
191 colourless clinopyroxene and submillimetre, subhedral to anhedral brown garnet are also
192 present (Fig. 2d).

193 .

194

195 **4.2. Mineral chemistry**

196 *4.2.1. Clinopyroxene*

197 The clinopyroxene is classified as diopside following the scheme of Morimoto (1988) and
198 the variation of the diopside content ($Di_{83\text{-}40}$) is negatively correlated with that of the
199 Tschermak-components (i.e., $CaAl_2SiO_6$, + $CaFeSiAlO_6$, + $CaTiAl_2O_6$ + $CaCrAlSiO_6$ =
200 $\Sigma Ts_{6\text{-}37}$; Fig.4). On the basis of the diopside content and Tschermak-components ($\Sigma Ts_{6\text{-}37}$)

three populations of clinopyroxene can be distinguished (Fig. 4, Table 1). The first population (Group I) has the highest content of diopside (Di_{83-73}), the lowest in Tschermak-components (ΣTs_{6-17}) and it is the most primitive population with Mg/(Mg+Fetot)>0.78 (Table S1). The second population (Group II) has intermediate contents of diopside and ΣTs and contains homogeneous crystals and clinopyroxenes with a rim enriched in diopside (Di_{69}) respect to the core (Di_{56}; Table 2 and Table S1). The third population (Group III) has the lowest values of diopside (Di_{40-49}) and the highest Tschermak-components (ΣTs_{34-37}). These emerald green clinopyroxenes (Fig. 2b) are the most differentiated (Mg/(Mg+Fetot) $\leq$ 0.50) and are, probably, those more similar to the kushiroite among the magmatic, terrestrial clinopyoxenes (Kimura et al., 2009). Moreover, as suggested also by the trace element abundances (see below) the Group III represents clinopyroxenes in equilibrium with differentiated interstitial melt close to the solidus temperature.

4.2.2. Other phases

In addition to the clinopyroxene, numerous mineral phases (Table S1) occur in the Tufo Palatino scoria clasts.

Leucite is often replaced by analcime. Their K_2O content falls within the range of 21.01-20.70 wt %. The Na/K ratio varies from 0.012 to 0.038 wt % while the iron content, reported as FeO, varies from 0.31 to 0.60 wt %.

Mica is phlogopitic (Mg/Fe cation ratio >2) in composition (Fig. 5 and Table S1) with a narrow range of Mg/(Mg + Fe) ratio and TiO_2 content (0.74-0.78 and 2.44-3.29 wt %, respectively). The F content (0.66-1.31 wt %) is lower than that of the lava flow micas (up to 7.3 wt %, Gaeta *et al.*, 2000; Gozzi *et al.*, 2014) but indicates a_{H2O} <1 in the magma that have fed the explosive eruption of the Tufo del Palatino.

225 Amphibole, for the first time identified in the Colli Albani scoria clasts, belongs to the calcic
226 group and has magnesiohastingsite composition (Hawthorne et al., 2012). Similarly to what
227 has been observed in the mica, the F content of amphiboles (0.46-0.49 wt %) is lower than
228 that measured in the lava flow crystals (up to 3.2 wt %, Gaeta and Freda, 2001). However,
229 also the amphibole indicates the a_{H2O} <1 in the Tufo del Palatino magmatic system.
230 Apatite is characterized by significant amount of SiO_2 (1.15-2.47 wt %), SO_3 (1.17-1.98 wt
231 %) and fluorine (3.65-3.85 wt %) and by low amount of P_2O_5 (32.05-36.65 wt %; Table S1).
232 The high SO_3 and SiO_2 contents of apatite could indicate the presence of the substitution
233 mechanism $S^{6+} + Si^{4+} = 2P^{5+}$. However, the absence of a correlation between $SO_3 + SiO_2$
234 and $2P_2O_5$ abundances indicates that others substitution mechanisms should have played an
235 important role. The high and constant content of CaO (52.87-54.04 wt%, Table S1) excludes
236 substitution mechanisms involving Th, LREE and Sr as those discussed by Fabrizio et al.,
237 (2018) for apatites in the hypoabissal granular rocks of Colli Albani. The Raman spectrum
238 of the Palatino apatite shows pattern peaks (500-630 and 1000-1100 cm^{-1} regions; Fig. 6)
239 occurring in the presence of CO_3 (Awonusi et al., 2007), that in the microprobe analyses
240 could be represented by the 100-$EMPA_{total}$ amount. Plots of the analytical data in a (100-
241 $EMPA_{total}$) + SiO_2 versus ($2P_2O_5$) or (100-$EMPA_{total}$) + SO_3 versus ($2P_2O_5$) diagrams (Fig.
242 6) show a very good correlations (R^2 = 0.993 and 0.999, respectively). These correlations
243 suggest the occurrence of the $CO_3 + SO_3=2P_2O_5$ and $CO_3 + SiO_2=2P_2O_5$ substitutions in the
244 apatite of the Tufo del Palatino.
245 Spinel is Ti-bearing magnetite (ulvöspinel mol. = 14 wt %), moderately enriched in MgO
246 and Al_2O_3 (noble spinel mol. = 10 wt %; Table S1).
247 Garnet is a Ti-bearing andradite, it does not show intra-mineral zoning and it is similar in
248 composition to the garnets occurring in the Villa Senni scoria clasts (Freda et al., 1997).
249

4.2.3. Subsolidus phases

Analcime shows Na_2O content (7.25-9.10 wt %; Table S1) that is lower than that observed in various ultrapotassic volcanic complexes (9.17-14.18 wt %; Gupta, 2015). The inner border of vesicles is filled by chabasite (Fig. 3d) characterized by high contents of SrO and BaO (up to 1.12 wt %) while the core of the vesicles is formed by calcium carbonate (Table S1).

4.3. Glass compositions

Tufo del Palatino glasses are foiditic (Fig. 7) and potassic ($K_2O>Na_2O$) in composition (Table 2). These chemical features are in accordance with the leucite-bearing texture that, however, depends by the crystallization conditions (i.e., T, P and a_{vol}). Consequently, the term K-foidite used hereafter can be considered equivalent but more general respect to leucitite. The MgO content (3.55 wt % in average on volatile-free basis), the Mg# = 0.36 (assuming FeO_{tot}=FeO; Table 2) and the comparison with previously analyzed olivine-bearing phonotephrites of Colli Albani, characterized by Mg# = 0.68-0.59 (Gozzi et al., 2014), indicate that Tufo del Palatino glasses represent differentiated melts. Noteworthy, the CIPW normative olivine content ranging from 7.6 to 13.4 wt% leads to a misleading primitive classification (i.e. basanitic leucitites to tephritic leucitites) of the Tufo del Palatino glasses. The lower SiO_2 content is probably the most significant chemical difference with the primitive compositions found, so far, in the Colli Albani (Fig. 7). However, in spite of their evolved chemical composition, the Tufo del Palatino glasses show high CaO contents (12.23 wt % in average of 41 glass analyses, Table S1) as highlighted by the comparison with parental composition of Colli Albani (Fig. 8), as well as with the leucite-bearing rocks of the Mediterranean area with similar MgO contents (Lustrino et al., 2019). In particular, in the CaO vs. MgO diagram a relatively large range of CaO (11.40-13.95 wt % on dry basis;

Fig. 8 and Table S1) clearly emerges. This oxide is present at higher and lower values compared to those of the phonotephritic composition (Fig. 8). Moreover, the comparison with the phonotephritic composition indicates that in the Tufo del Palatino glasses the content of Al_2O_3, FeO, TiO_2 and Na_2O increases and that of P_2O_5 decreases (Fig. 8 and Table 2). Otherwise, the K_2O content (6.01 to 8.83 wt %, Table S1) is not correlated with MgO but is broadly correlated (R^2=0.6) with SiO_2 (43.18-45.47 wt %).

The SO_3 content (2643 ppm = 0.65 wt % in average; Table S1) is higher than that of primitive magmas in the orogenic contest (S = 900-2500 ppm; De Hoog et al., 2001; Wallace, 2005), as well as that of parental magma (Fig. 8). On the basis of the sulfur content two groups of glasses with an average amount of ~3200 ppm and ~2400 ppm can be recognized. The sulfur variation is not correlated with F (Fig. 8) and Cl, suggesting a different behavior of these volatiles during magma differentiation and degassing. Raman spectra show CO_2 content below the instrumental sensibility and water contents of 1.15-1.12 wt % (Table 2 and Fig. 9). These water contents are close to 100-$EMPA_{total}$ value found in the Tufo del Palatino glasses (2.29-3.06 wt %, Table S1) corrected for Fe^{3+} and Fe^{2+} partition [$(FeO+Fe_2O_3)$-$FeOt_{ot}$~0.4 wt %, with the iron partition calculated at the fO_2 of QFM+2; Table 2)] and the trace element contents (~0.9 wt %). Noteworthy, a K-foiditic melt inclusion in the clinopyroxene (Table S1) of the TP-Fall shows higher H_2O respect to the Tufo del Palatino glasses and the presence of CO_3 (Fig. 9).

4.4. Trace elements

In spite of their differentiated chemical composition (i.e., MgO<4 wt%), the K-foiditic glasses of the Tufo del Palatino eruptive unit preserve trace element concentrations distinctive of orogenic, subduction-related magmas. In particular, the primitive mantle-normalized diagrams patterns of the Palatino glasses show very high abundances (>1000

300 times primitive mantle abundances) of Th, U, Pb, very high LILE/HFSE ratios, as shown by
301 marked Nb-Ta and Ti troughs, and slightly decreasing at the heavy rare earth elements-
302 HREE region (Fig. 8). The Cs-Rb trough is clearly ascribable to leucite fractionation (e.g.,
303 Foley and Jenner, 2004; Fabbrizio et al., 2008) and is the only remarkable deviation respect
304 to the pattern of the phonotephritic magmas (Fig. 10).

305 Trace element abundances in clinopyroxenes (Table 3, Table S1 and Fig. 11) are
306 quite variable showing also in some crystals compositional intra-mineral zoning (e.g., cpx-
307 4 in the TP-TAB1 sample). Primitive mantle normalized patterns of clinopyroxenes show an
308 overall similarity with differences in the degree of enrichments of the incompatible elements
309 (Fig 11). This is clearly evidenced, for instance, by the variation in the depth of the Nb, Pb,
310 Zr and Ti negative anomalies with respect to the adjacent elements (Fig. 11). With the
311 exception of the cpx-4 rim in the TP-TAB1 sample that displays a distinctive pattern,
312 variations in incompatible element abundances of Tufo del Palatino clinopyroxenes reflect
313 those observed for major element compositions that, on the basis of diopside (Di) and
314 Tschermak (ΣTs) components, suggested the presence of three clinopyroxene populations
315 (Fig. 4). Crystals having low ΣTs (<0.20) and high Di and Mg# values (Di >0.73 and Mg#
316 >0.67) are characterized by relatively low trace element contents (e.g., Nb =0.07-0.29 ppm,
317 Zr = 100-409 ppm, La = 13-28 ppm) whereas in clinopyroxenes whose Mg# is <0.62 with
318 relatively low Di and high ΣTs (i.e., Group II and III), the concentration of Nb, Zr and La
319 are significant higher (Nb = 0.38-8.37 ppm; Zr=317-939 ppm; La=23-68 ppm). In particular,
320 in Group III clinopyroxene have the highest Nb, Zr and La contents (Fig. 11, Table 3, Table
321 S1). As mentioned above, the incompatible element composition of cpx-4 rim in the TP-
322 TAB1 sample differs from the others because it is characterized by lower contents in Y,
323 LREE/MREE (La_N/Sm_N >3 compared to La_N/Sm_N <2) and LREE/HREE and (La_N/Yb_N =
324 51-65 compared to La_N/Yb_N = 11-36) possibly as a result of the crystallization in equilibrium

with HREE-rich phase. Actually, the distinctive pattern of cpx-4 rim is similar to that of clinopyroxenes crystallized in equilibrium with garnet in the leucite -bearing, granular rocks of Colli Albani (i.e., italites and/or fergusites, Freda et al., 1997; Fabbrizio et al., 2018; Dallai et al., 2004; Shaw, 2018).

5. Discussion

5.1. K-foiditic parental magma

Effusive eruptions in the Colli Albani were fed by phonotephritic to K-foiditic magmas (e.g., Gozzi et al., 2014) while the large explosive eruptions almost exclusively by K-foiditic magmas (e.g., Gaeta, 1998; Palladino et al., 2001; Marra et al., 2009; Freda et al., 2011; Biagio et al., 2013; Leicher et al., 2016). Nevertheless, evidences of the parental phonotephritic magma are common in the products of the large explosive eruptions. A large-scale example is the phonotephritic Vallerano lava flow that predates, without temporal gap, the K-foiditic Pozzolane Rosse eruption (Freda et al., 2011). At smaller scale, clinopyroxene antecrysts in equilibrium with primitive melts are relatively common in the Colli Albani pyroclastites (e.g., Dallai et al., 2004).

The Di-rich population of clinopyroxenes (Group I, Fig. 4) indicates that the Tufo del Palatino scoria clasts are no exception to the rule because these clinopyroxenes are in equilibrium with the Mg#>0.6 typical of the Coli Albani primitive magmas (Table 2). Actually, on the basis of the Fe-Mg distribution coefficient between clinopyroxene and melt ($K_D(\text{Fe-Mg})^{Cpx\text{-}melt} = \text{Fe}_{Cpx} \times \text{Mg}_{melt}/\text{Mg}_{Cpx} \times \text{Fe}_{melt}$, calculated assuming all Fe as Fe^{2+} in both phases) the Group I clinopyroxenes (Fig. 4) are not in equilibrium with the K-foiditic melts, but in equilibrium with the phonotephritic compositions of the primitive Colli Albani lava flows (Table 1).

The latter, as well as the primitive magmas of the Roman Province show peculiar, if not unique, geochemical features (e.g., $K_2O/Na_2O \geq 2$; high LILE/HREE ratio; $^{87}Sr/^{86}Sr \geq 0.709$) and this singularity is due to the composition of the metasomatizing agents that modified the pristine peridotite mantle (e.g., Ammannati et al., 2016; Avanzinelli et al., 2018). Moreover, to better constrain the composition of possible parental magma Tufo del Palatino products, it should be noted that the temporal geochemical variations observed in the Colli Albani magmas indicate that the ultrapotassic magmas originated from a metasomatized mantle source in which phlogopite is the potassium-bearing phase. This is consistent with the $^{87}Sr/^{86}Sr$ and the incompatible trace element decrease of primitive magmas during the eruptive history of the volcanic district (e.g., Gaeta et al., 2006; Boari et al., 2009; Gaeta et al., 2016). Indeed, primitive mantle normalized patterns of the younger primitive compositions (40-308 ka; MgO >5 wt %) of Colli Albani show trace element abundances that are similar or lower than in the oldest AH38f lava flow (474 ka; Fig. 10). Noteworthy, the decrease of incompatible trace element abundances by means of a fractional crystallization process is unrealistic because the younger primitive compositions have lower content of MgO respect to AH38f lava flow (i.e., 4.14-6.43 wt% and 7.07 wt % respectively). Moreover, the younger primitive compositions have lower $^{87}Sr/^{86}Sr$ ratio respect those measured in the Tufo del Palatino clinopyroxene (Table 3) which, instead, is similar those of the AH38f lava flow.

5.2. T, P, volatiles concentration in the pre-eruptive magmatic system

In addition to the clinopyroxene antecrysts (Group I, Fig. 4) in equilibrium with the phonotephritic melt other two group of clinopyroxenes occurs in the scoria clasts of the Tufo del Palatino (Table 1). The largest population (Group II , Fig. 3) has the $K_D(Fe\text{-}Mg)^{Cpx\text{-}melt}$ = 0.20-0.35 that indicate equilibrium conditions ($K_D(Fe\text{-}Mg)^{Cpx\text{-}melt} = 0.28 \pm 0.08$ according to

374 Putirka, 2008)) with the K-foiditic composition of the Tufo del Palatino glasses (Table 2).
375 The third population formed by few crystals (Group III), according to the $K_D(Fe\text{-}Mg)^{Cpx\text{-}glass}$,
376 appear in equilibrium with the K- foiditic compositions characterized by low MgO contents
377 (i.e., <2 wt%, similar to Lionato glasses, Table S1). The equation 33 of the thermometer of
378 Putirka (2008), with a standard error of 87 °C) indicates that clinopyroxene antecrysts and
379 AH38f phonotephrite equilibrate in the range of 1083-1144 °C and the Group II
380 clinopyroxenes and the K-foiditic melt (i.e., Tufo del Palatino glass) between 1048-1098 °C
381 (Table 1 and S1). Lower temperatures in the Palatino pre-eruptive system are suggested by
382 MgO-poor, Group III clinopyroxene, as well as, by the amphibole occurrence that in the
383 alkaline magmas is stable at T<1050°C (e.g., Charles, 1977; Singh et al., 2000; Bonechi et
384 al., 2017, 2020b). The HREE depletion measured in the rims of Group III clinopyroxenes
385 (Fig. 11) suggests local conditions (e.g., the peripheral portion of the magma chamber;
386 Masotta et al., 2010) of even lower temperature compatible with the garnet crystallization
387 (830-920 °C; Scaillet et al., 2008). Anyway, the garnet occurrence, as well as that of
388 amphibole, indicates relatively high pressure condition for the Tufo del Palatino pre-eruptive
389 magmatic system. Pressures of 0.32-0.36 GPa estimated from the Group I clinopyroxene
390 compositions (Table 1 and S1) using the Palk algorithm (Masotta et al., 2013; with a standard
391 error of estimate of 0.12 GPa) are similar to those obtained from the volatile contents in the
392 melt inclusions of Colli Albani mafic cumulate (Gaeta et al., 2009). Using the H_2O + CO_2
393 saturation values measured in the K-melts of Colli Albani at 0.20-0.50 GPa (Behrens et al.,
394 2009), the volatile content in the melt inclusion of the TP-Fall sample (Fig. 9) indicates a
395 pressure of about 0.2 GPa that is in agreement with the barometric estimation obtained from
396 the Group II clinopyroxene compositions (Table 1 and S1). The latter, as well as the
397 amphibole, show high Fe^{3+}/Fe^{2+} ratio due to redox conditions characterized by high values
398 of f_{O2} (i.e., from QFM +1 to QFM +4; Gaeta et al., 2000) but at a_{H2O} <1 as suggested by the

399 F, SO_3, Cl abundances in the K-foiditic glasses (Table 2). The Tufo del Palatino pre-eruptive
400 magmatic system is definitely characterized by the a_{H2O} <1 and high CO_2 activity in the melt,
401 as testified by the early crystallization of CO_3-bearing apatite (Fig. 6), and by the high CO_2
402 activity in the volatile phase which led to the calcium carbonate crystallization in the vesicles
403 of the scoria clasts (Fig. 3d, Table S1). Noteworthy, the volatile contents in the Tufo del
404 Palatino glasses (Table 2 and Table S1) are lower respect those estimate for the pre-eruptive
405 system because the syn-eruptive, glass transition of the Tufo del Palatino magma occurred
406 at low pressure (<0.1 GPa) in agreement with the hydromagmatic style of the eruption.
407
408 **5.3. Phase relationships in the K-foiditic melts**
409 Phase relationships of peculiar silicate melts like the K-foidites still remain enigmatic in
410 spite of the availability of powerful thermodynamic software (e.g., MELTS; Ghiorso and
411 Sack, 1995) and experimental studies of crystallization at controlled conditions (e.g., Gupta,
412 1972; Yoder, 1986; Melzer and Foley, 2000). Actually, in the pseudo-ternary forsterite-
413 leucite-diopside (hereafter Ol-Cpx-Lc) system at atmospheric pressure (Gupta, 1972), the
414 compositions of central Italy leucitites (e.g., Lustrino et al., 2019), as well as the Colli Albani
415 K-foiditic glasses, fall around the olivine-leucite cotectic (Fig. 12), despite the petrographic
416 characteristics of these rocks does not show evidence of olivine+leucite equilibrium in the
417 absence of clinopyroxene. Tufo del Palatino scoria clasts show Group II clinopyroxenes in
418 equilibrium with the K-foiditic melt but also Group I clinopyroxene, crystallized early (i.e.,
419 antecrysts), in a more primitive magma (e.g., AH38f) in equilibrium with the olivine.
420 Moreover, in the groundmass of the K-foiditic lava flows of the Colli Albani the association
421 clinopyroxene+leucite+olivine is also present (Gozzi et al., 2014). The petrographic features
422 of the leucite-bearing rocks of the Colli Albani indicate that the Ol-Cpx-Lc diagram is
423 suitable for representing the crystallization of these rocks but with a different topology from

424 that at atmospheric pressure. On the one hand, the presence of H_2O in the K-foiditic glasses
425 (Table 2 and Fig. 9) and the clinopyroxene-based barometric estimations indicate
426 crystallization conditions at P >1 atm of the phonotephritic parental magmas. On the other
427 hand, the P_{H2O}>1-2 kbar or the high F activity in the system allow the early
428 clinopyroxene+phlogopite crystallization in the phonotephritic magmas. The early
429 crystallization of phlogopite, in turn, causes the departure from the Ol-Cpx-Lc compositional
430 plane with the formation of melts characterized by high silica contents and in equilibrium
431 with K-feldspar ± leucite. Actually, the experiments on F- and H_2O-bearing Cpx-Ks-Ol-Qz
432 system indicate that crystallization, at pressure up to 1.8 GPa, in which phlogopite is present
433 on the liquidus, leads to the formation of phonolites and trachytes but not to K-foidites
434 (Melzer and Foley, 2000). Silica undersaturated melts in equilibrium with phlogopite and
435 leucite ± kalsilite are probably restricted to extremely Ca-poor magmatic system and are not
436 comparable to the composition of the K-foiditic melts of Colli Albani. The crystallization of
437 primitive K-melts at P >1 atm in dry conditions (and/or that does not allow the phlogopite
438 crystallization) it is also unlikely because it occurs at very high temperatures (>1350°C)
439 above that of geothermometric estimation obtained from Group I clinopyroxene (Table 1
440 and S1). Noteworthy, the clustering of the Colli Albani K-foidites in a relatively narrow zone
441 of the Ol-Cpx-Lc diagram suggest the occurrence of a thermal minimum towards which final
442 products of a fractional crystallization converge (Fig. 13). This zone could be represented
443 by melt compositions in equilibrium with Cpx + Lc ± Ol + vapor obtained at 0.2 GPa and
444 a_{H2O} <1 (Fig. 13), starting from a potassic phonotephrite doped with carbonate (Iacono-
445 Marziano et al., 2007; Freda et al., 2008). In particular, the Ol-Cpx-Lc multiple saturation,
446 the abruptly decreases of residual melt (i.e., 57 wt % of crystallization) and the low amount
447 of normative larnite (i.e., 3 wt %) indicate that the composition of the experimental glass
448 obtained by Iacono-Marziano et al., (2007) at 1100 °C and 0.2 GPa is almost representative

449 of a thermal minimum in the Ol-Cpx-Lc system. As the experimental clinopyroxenes are
450 solid solutions with large chemical variations it is not an invariant point. The Ol-Cpx-
451 Lc+melt+vapor equilibrium replaces at 1 atm <P <0.5 GPa (i.e. the experimental condition
452 of Freda et al., 2008) the reaction point Ol + Cpx + Melt = Cpx + Phl + Melt in the system
453 Cpx-Ks-Ol-Qz. Noteworthy, from the point of phlogopite crystallization starts the
454 univariant boundary line Cpx + Phl + Melt that is a piercing point in the Ol-Cpx-Lc plan
455 leading to differentiated compositions of the system Cpx-Ks-Ol-Qz. These compositions are
456 impoverished in magnesium and calcium, and they are in equilibrium with K-
457 feldspar±leucite (i.e., phonolitic compositions; Melzer and Foley, 2000). Otherwise, in
458 absence of phlogopite crystallization, the plane Ol-Cpx-Lc it is considered a thermal barrier
459 in the system Cpx-Ks-Ol-Qz (Yoder, 1986) that divided the crystallization paths toward K-
460 foidites (i.e., in the Ol-Cpx-Lc-Ks volume) from those towards silica oversaturated melts
461 (i.e., in the Ol-Cpx-Lc-Qz volume). It is worth stressing that in the system Cpx-Ks-Ol-Qz at
462 P >1 atm the change from reaction point involving the phlogopite to a point in which Ol +
463 Cpx-Lc + melt is in equilibrium seems to be obtainable only through the addition of calcite
464 or dolomite that through the release of CO_2 brings the system at the volatiles saturation
465 conditions but with a_{H2O} <1 (Freda et al., 2008). These peculiar conditions allow the
466 expansion of the leucite and clinopyroxene stability field at the expense of phlogopite (i.e.,
467 the a_{H2O} <1 effect) and olivine (i.e., the P >1 atm effect) and the appearance of the Ol-Cpx-
468 Lc-melt equilibrium at temperatures compatible with those here obtained from the
469 geothermometers (Table 1 and S1). The phase relationships reported in Figure 12 are valid
470 for potassic melts with a normative larnite content <10 wt %. In the Ol-Cpx-Lc-Mel
471 (melilite) volume, at 0.2 GPa and a_{H2O} <1, the equilibrium Ol-Cpx-Lc-melt disappears at Fo
472 <10 wt % and T <1100 °C and below this temperature the melt composition is in equilibrium
473 with clinopyroxene and leucite. The disappearance of olivine is due to the increase of

474 calcium activity that drives the reaction $Mg_2SiO_4 + 2CaO + 3SiO_2^{melt} = 2CaMgSi_2O_6$ to the
475 right and, in turn, changes the Ol-Cpx-Lc-melt piercing point into a reaction point. In the Ol-
476 Cpx-Lc-Mel system from the reaction point starts a divergent surface containing the Cpx-
477 Lc-melt phases. This divariant surface converges toward the thermal minimum of the Ol-
478 Cpx-Lc-Mel system where Cpx + Lc + Mel + melt coexist. The K-foiditic melts of Colli
479 Albani are contained on this surface and plot close to the Cpx + Lc cotectic line when the
480 glass composition is projected from the melilite corner on the Ol-Cpx-Lc system at $P \geq 0.2$
481 GPa and $a_{H2O} < 1$ (Fig. 12).
482
483 **5.4. Role of the carbonate assimilation**
484 The thermal barrier represented by the Ol-Cpx-Lc surface in the Cpx-Ks-Ol-Qz system does
485 not act in the first steps of the primitive potassic magmas differentiation. Actually, in the
486 Cpx-Ks-Ol-Qz system, the crystallization path starts within the olivine + melt phase volume
487 and/or on the Ol + Cpx + melt surface where the degrees of freedom of are high. In this step
488 of the magmatic differentiation, unless the magmas were not already strongly undersaturated
489 in silica, it is relatively easy that changes in pressure, volatile activities and oxygen fugacity
490 bring the primitive potassic melts towards phonolitic and/or silica oversaturated
491 compositions. The key effect of early phlogopite crystallization on the differentiation of
492 primitive potassic magmas (Melzer and Foley, 2000) has been previously discussed. The
493 lower values and narrow range of Mg# of the Tufo del Palatino phlogopite with respect to
494 Volsci Volcanic Field (VVF; Marra et al. 2021) consistently indicates a narrow phlogopite
495 stability field in the Colli Albani magmas (Fig 5). The VVF Lct-bearing scoria clasts are
496 characterized by the association of Phl with Ol in the phenocryst assemblage, which instead
497 is lacking in the Colli Albani scoria clasts (e.g., Freda et al., 1997, 2006, 2011; Palladino et
498 al., 2001; Marra et al., 2009; Gozzi et al., 2014; Gaeta et al., 2016). Other important effects

499 that increase the silica activity in the melt, during the differentiation of primitive potassic
500 magmas, are: 1) increase of the olivine stability field, caused by low oxygen fugacity and/or
501 low pressure conditions (e.g., Conte et al., 2009); 2) early crystallization of clinopyroxene
502 at high oxygen fugacity that shows a relatively low silica content due to increase of the
503 $CaFeSiAlO_6$ component in solid solution (e.g., Dolfi, 1996), and obviously 3) fractional
504 crystallization coupled with the assimilation of sialic crustal rocks (e.g., Sabatini Volcanic
505 District; Sottili et al., 2019). The assimilation of carbonate by magmas is an important open-
506 system process preventing primitive melts move away from the plane Ol-Cpx-Lc towards
507 phonolitic and/or silica oversaturated compositions. This process has been extensively
508 documented at the Colli Albani (e.g., Freda et al., 1997, 2008, 2011; Dallai et al., 2004;
509 Gaeta et al., 2006, 2009; Iacono Marziano et al., 2007; Mollo et al., 2010; Di Rocco et al.,
510 2012; Gozzi et al., 2014) and it is no coincidence that most of the known K-foidites come
511 from this district. The pristine composition of the Tufo del Palatino glasses allows to obtain
512 further information on the mass of carbonate involved in the assimilation process at the
513 origin of the K-foiditic melts. Major element mass balance calculations indicate that it is
514 possible to obtain the K-foiditic compositions of the Tufo del Palatino glasses starting from
515 the parental magma (i.e., the phonotephrite AH38f, Table 2) by subtracting a solid
516 assemblage made of Cpx (37.0 wt %) + Lc (24.9 wt %) + Mgt (3.8 wt %) + Ap (1.6 wt %;
517 mineral composition are indicated in Table S1). In order to obtain low square residuals (i.e.,
518 $\Sigma r^2 = 0.4$) in the mass balance calculations, we must also consider the assimilation of ~4 wt
519 % of calcite corresponding to a low (<0.1) M^o_a/M^o_m ratio, where M^o_m is the mass of pristine
520 melt to which assimilant mass M^o_a is added. Results of mass balance calculations are in
521 agreement with the mineralogical composition and the texture (e.g., Ti-mgt and apatite
522 inclusions in clinopyroxenes; Fig. 2a) observed in the Tufo del Palatino scoria clasts and
523 with the phase relationships observed in the assimilation experiments (Iacono Marziano et

524 al., 2007; Freda et al., 2008). Trace elements are much more sensible tracers, being able to
525 distinguish between closed-system (i.e., fractional crystallization) and open-system (i.e.,
526 magma mixing and assimilation fractional crystallization) processes, since their low
527 concentrations in crystals and melts vary significantly. Starting from the trace element
528 abundances in the AH38f phonotephrite (i.e., the parental magma) the FC model reproduces
529 well the leucite compatible elements (i.e., Rb, Cs) but increases the incompatible trace
530 elements with respect to what measured in the Tufo del Palatino glasses (Fig. 13a). A similar
531 result is obtained in the fractional crystallization of the AH38f phonotephritic magma open
532 to carbonate assimilation using the AFC algorithm proposed by DePaolo (1981). Otherwise,
533 the trace abundance in the Tufo del Palatino glasses is well reproduced (Fig. 13b) with a
534 calcite-assimilation fractional crystallization model using the FCA algorithm (Cribb and
535 Barton, 1996). The FCA model more faithfully reproduces the nature of the carbonate
536 assimilation process because implicitly considers CO_2 degassing that makes the mass
537 assimilated and the mass crystallized independent. Interesting, the FCA model based on the
538 trace elements (Fig. 13b) indicates a large amount of carbonate (~12.4 wt %) involved in the
539 assimilation process. The ability of magmatic systems to the continuous CO_2-degassing is a
540 limiting factor for the assimilation of so large amount of carbonate at low pressure (<300
541 MPa). Moreover, in case of high ratio M^o_a/M^o_m, the assimilation of cold (~350 °C) wall rock
542 induces considerable cooling of the magma. Nevertheless, magma cooling is compensated
543 by the latent heat of crystallization that, in turn, is function of two parameters: the
544 temperature interval of crystallization and the viscosity of the melt. These two parameters
545 are not independent each other. On one hand, the enlargement of the temperature interval of
546 crystallization depends by the decrease of the glass transition and solidus temperatures. On
547 the other hand, the glass transition temperature is related to the melt viscosity that controls
548 also the crystal growth rate. Actually, In isothermal conditions, the crystal growth rate is

549 function of the melt polymerization that enhancing the melt viscosity lowers the diffusivity
550 of elements in the melt (Bonechi et al. 2020a). The peculiar phase relations and the melt
551 rheology of the K-foiditic magmas, largely different from those occurring in other
552 differentiated potassic magmas (i.e., phonolite or trachyte), lead to unique distribution of the
553 latent heat across the crystallization interval of the K-foidites (e.g., Lange et al., 1994). The
554 experiments on the potassic phonotephrite doped with carbonate (Freda et al., 2008) indicate
555 that the crystallization of clinopyroxene and leucite in equilibrium with a K-foiditic melt
556 proceed over a relatively large (>200 °C) temperature interval (Fig. 14a). In the Colli Albani
557 rocks, this large temperature interval is confirmed by the occurrence of garnet in the scoria
558 clasts (Freda et al., 1997; this work), as well as by magmatic calcite ($T_{dissociation}$<900°C) in
559 the groundmass of the lava flows (Gozzi et al., 2014). Moreover, K-foiditic melts are
560 significantly less viscous than the phonolitic and trachytic melts (Fig. 14b), allowing a rapid
561 nucleation and growth of leucite and clinopyroxene (e.g., Bonechi et al., 2020a). The syn-
562 eruptive, high growth rate of leucite is clearly indicated by the star-like habit (Fig. 3b), while
563 the apatite inclusions (Fig. 2a) sustain the high growth rate of clinopyroxene during the
564 differentiation process of the phonotephritic parental magma. The phosphorus saturation in
565 the boundary layer led to apatite precipitation and its entrapment at the clinopyroxene rim.
566 As observed in many experimental studies (e.g., Bonechi et al., 2020a) high growth rates are
567 favoured by large degree of undercooling. Efficiency of the carbonate assimilation process
568 that origin K-foiditic magmas in the Colli Albani magmatic system is due to the combination
569 and/or the feedback of the low melt viscosity, the large temperature interval of crystallization
570 and the undercooling.
571
572 **6. Conclusions**

573 The K-foiditic magmas of the Colli Albani Volcanic District originate from the combination
574 of the mantle metasomatism (not discussed) and the crustal assimilation which cannot be
575 responsible for the rarity of this type of magmatism as they are active petrological processes
576 on a global scale, and they have certainly been in the past too. Nevertheless, these are open
577 system processes with high degrees of freedom that can greatly affect the final results.
578 Closed-system magmatic differentiation of the ultrapotassic primitive magmas is
579 characterized by the fractional crystallization of olivine, olivine + clinopyroxene and by the
580 early crystallization of phlogopite (i.e., together the clinopyroxene) which leads to phonolitic
581 or trachytic melts but not foiditic melts. K-foiditic magmas, similar to those that fed Tufo
582 del Palatino explosive eruption, are the result of the fractional crystallization of
583 clinopyroxene ± olivine and clinopyroxene + leucite from phonotephritic parental magmas.
584 The reduction of the olivine and phlogopite stability fields in favor of those of clinopyroxene
585 and leucite seems to occur only during the fractional crystallization in a system open to the
586 assimilation of carbonate. The efficiency of this process is due to the combination of intrinsic
587 factors of K-foiditic magmas, which can be considered of general value, such as the low
588 viscosity and the cotectic crystallization of clinopyroxene and leucite in an extended
589 temperature range and a local factor linked exclusively to the geological contest of the Colli
590 Albani Volcanic district: the thickness and the depth of the carbonate substrate.
591
592 **Acknowledgment**
593 We are very grateful to the Editor Michael Roden and two anonymous reviewers for their
594 helpful and constructive comments. We thank to C. Romano (Roma Tre University) for the
595 access to the RAMAN facility and M. Serracino (CNR-IGAG) for assistance during EPMA
596 analytical sessions.
597

598 **Funding**

599 This research has been conducted with the financial support of the HP-HT Laboratory at the
600 Department of Earth Sciences of Sapienza - University of Rome

601

602 **References**

603 Ammannati, E., Jacob, D., Avanzinelli, R., Foley, S.F., 2016. Low Ni olivine in silica-
604 undersaturated ultrapotassic igneous rocks as evidence for carbonate metasomatism in the
605 mantle. Earth Planet. Sci. Lett. 444, 64–74.

606 Avanzinelli, R., Casalini, M., Elliott, T., Conticelli, S., 2018. Carbon fluxes from subducted
607 carbonates revealed by uranium excess at Mount Vesuvius, Italy. Geology 46, 259–262.
608 https://doi.org/10.1130/G39766.1

609 Awonusi, A., Morris, M.D., Tecklenburg, M.M.J., 2007. Carbonate assignment and
610 calibration in the Raman spectrum of apatite. Calcif. Tissue Int. 81, 46–52.
611 https://doi.org/10.1007/s00223-007-9034-0

612 Bianchi, I., Piana Agostinetti, N., De Gori, P., Chiarabba, C., 2008. Deep structure of the
613 Colli Albani volcanic district (central Italy) from receiver functions analysis. J Geophys Res
614 113:B09313. https://doi:10.1029/2007JB005548

615 Behrens, H., Misiti, V., Freda, C., Vetere, F., Botcharnikov, R.E., Scarlato, P., 2009.
616 Solubility of H_2O and CO_2 in ultrapotassic melts at 1200 and 1250 °C and pressure from 50
617 to 500 MPa. Am. Mineral. 94, 105–120. https://doi.org/10.2138/am.2009.2796

618 Boari, E., Avanzinelli, R., Melluso, L., Giordano, G., Mattei, M., De Benedetti, A.A., Morra,
619 V., Conticelli, S., 2009. Isotope geochemistry (Sr-Nd-Pb) and petrogenesis of leucite-
620 bearing volcanic rocks from "Colli Albani" volcano, roman magmatic province, central
621 Italy: Inferences on volcano evolution and magma genesis. Bull. Volcanol. 71, 977–1005.
622 https://doi.org/10.1007/s00445-009-0278-6

623 Bonechi, B., Perinelli, C., Gaeta, M., 2020a. Clinopyroxene growth rates at high pressure:
624 constraints on magma recharge of the deep reservoir of the Campi Flegrei Volcanic District
625 (south Italy). Bull. Volcanol. 82, 5. https://doi.org/10.1007/s00445-019-1342-5
626 Bonechi, B., Perinelli, C., Gaeta, M., Tecchiato, V., Fabbrizio, A., 2020b. Amphibole growth
627 from a primitive alkaline basalt at 0.8 GPa: time-dependent compositional evolution, growth
628 rate and competition with clinopyroxene. Lithos 354–355, 105272.
629 Bonechi, B., Perinelli, C., Gaeta, M., Tecchiato, V., Granati, S.F., 2017. Experimental
630 constraints on amphibole stability in primitive alkaline and calc-alkaline magmas. Period.
631 Mineral. 86, 231–245. https://doi.org/10.2451/2017PM735
632 Bonechi, B., Perinelli, C., Gaeta, M., Fabbrizio, A., Petrelli, M. & Strnad L. Trace element
633 partitioning between clinopyroxene and alkali basaltic melts: investigation at high pressure
634 on a primitive composition from the Campi Flegrei Volcanic district (Italy). Geochimica et
635 Cosmochimica Acta, https://doi.org/10.1016/j.gca.2021.04.023.
636 Brocato, P., Diffendale, D.P., Giuliomaria, D.D., Gaeta, M., Marra, F., Terrenato, N., 2019.
637 A previously unidentified tuff in the archaic temple podium at sant'omobono, rome and its
638 broader implications. Journal of Mediterranean Archaeology. 32, 114–136.
639 Charles, R.W., 1977. The phase equilibria of intermediate compositions on the pseudo-
640 binary $Na_2CaMg_5Si_8O_{22}(OH)_2$, $Na_2Ca\ Fe_5Si_8O_{22}(OH)_2$. Am. J. Sci. 277, 594–625.
641 https://doi.org/10.2475/ajs.277.5.594
642 Conte, A.M., Dolfi, D., Gaeta, M., Misiti, V., Mollo, S., Perinelli, C., 2009. Experimental
643 constraints on evolution of leucite-basanite magma at 1 and 10^{-4} GPa : implications for
644 parental compositions of Roman high-potassium magmas. Eur. J. Mineral. 21, 763–782.
645 https://doi.org/10.1127/0935-1221/2009/0021-1934
646 Cribb, J., Barton, M., 1996. Geochemical effects of decoupled fractional crystallization and
647 crustal assimilation. Lithos 37, 293–307.

Dallai, L., Freda, C., Gaeta, M., 2004. Oxygen isotope geochemistry of pyroclastic clinopyroxene monitors carbonate contributions to Roman-type ultrapotassic magmas. Contrib. Mineral. Petrol. 148, 247–263. https://doi.org/10.1007/s00410-004-0602-2

De Hoog, J.C.M., Mason, P.R.D., Van Bergen, M.J., 2001. Sulfur and chalcophile elements in subduction zones: Constraints from a laser ablation ICP-MS study of melt inclusions from Galunggung volcano, Indonesia. Geochim. Cosmochim. Acta 65, 3147–3164. https://doi.org/10.1016/S0016-7037(01)00634-2

Devine, J.D., Gardner, J.E., Brack, H.P., Layne, G.D., Rutherford, M.J., 1995. Comparison of microanalytical methods for estimating H_2O contents of silicic volcanic glasses. Am. Mineral. 80, 319–328. https://doi.org/10.2138/am-1995-3-413

Di Battistini, G., Montanini, A., Vernia, L., Bargossi, G.M., Castorina, F., 1998. Petrology and geochemistry of ultrapotassic rocks from the Montefiascone Volcanic Complex (Central Italy): magmatic evolution and petrogenesis. Lithos 43, 169–195.

Di Genova, D., Sicola, S., Romano, C., Vona, A., Fanara, S., Spina, L., 2017. Effect of iron and nanolites on Raman spectra of volcanic glasses: A reassessment of existing strategies to estimate the water content. Chem. Geol. 475, 76–86. https://doi.org/10.1016/j.chemgeo.2017.10.035

Di Rocco, T., Freda, C., Gaeta, M., Mollo, S., Dallai, L., 2012. Magma chambers emplaced in carbonate substrate: Petrogenesis of skarn and cumulate rocks and implications for CO_2 degassing in volcanic areas. J. Petrol. 53, 2307–2332. https://doi.org/10.1093/petrology/egs051

Diffendale, D.P., Marra, F., Gaeta, M., Terrenato, N., 2019. Combining geochemistry and petrography to provenance Lionato and Lapis Albanus tuffs used in Roman temples at Sant'Omobono, Rome, Italy. Geoarchaeology 34, 187–199. https://doi.org/10.1002/gea.21702

673 Dolfi, D., 1996. Preliminary results on the effect of oxygen fugacity on magmatic
674 clinopyroxene and coexisting liquid compositions. Period. Mineral. 65, 5–14.
675 Ersoy, Y., Helvaci, C., 2010. FC-AFC-FCA and mixing modeler: A Microsoft® Excel©
676 spreadsheet program for modeling geochemical differentiation of magma by crystal
677 fractionation, crustal assimilation and mixing. Comput. Geosci. 36, 383–390.
678 https://doi.org/10.1016/j.cageo.2009.06.007
679 Fabbrizio, A., Gaeta, M., Carroll, M.R., Petrelli, M., 2018. Crystallization induced Sulfur
680 and REE zoning in apatite: The example of the Colli Albani's magmatic system. Eur. J.
681 Mineral. 125–133.
682 Fabbrizio, A., Schmidt, M. W., Günther, D., Eikenberg, J., 2008. Experimental
683 determination of radium partitioning between leucite and phonolite melt and ^{226}Ra-
684 disequilibrium crystallization ages of leucite. Chemical Geology. 255, 377–387.
685 Foley, S.F., Jenner, G.A., 2004. Trace element partitioning in lamproitic magmas-the
686 Gaussberg olivine leucitite. Lithos 75, 19–38. https://doi.org/10.1016/j.lithos.2003.12.020
687 Freda, C., Gaeta, M., Giaccio, B., Marra, F., Palladino, D.M., Scarlato, P., Sottili, G., 2011.
688 CO_2-driven large mafic explosive eruptions: The Pozzolane Rosse case study from the Colli
689 Albani Volcanic District (Italy). Bull. Volcanol. 73, 241–256.
690 https://doi.org/10.1007/s00445-010-0406-3
691 Freda, C., Gaeta, M., Karner, D.B., Marra, F., Renne, P.R., Taddeucci, J., Scarlato, P.,
692 Christensen, J.N., Dallai, L., 2006. Eruptive history and petrologic evolution of the Albano
693 multiple maar (Alban Hills, Central Italy). Bull. Volcanol. 68, 567–591.
694 https://doi.org/10.1007/s00445-005-0033-6
695 Freda, C., Gaeta, M., Misiti, V., Mollo, S., Dolfi, D., Scarlato, P., 2008. Magma-carbonate
696 interaction: An experimental study on ultrapotassic rocks from Alban Hills (Central Italy).
697 Lithos 101, 397–415. https://doi.org/10.6133/apjcn.092017.05

698 Freda, C., Gaeta, M., Palladino, D.M., Trigila, R., 1997. The Villa Senni Eruption (Alban
699 Hills, central Italy): The role of H_2O and CO_2 on the magma chamber evolution and on the
700 eruptive scenario. J. Volcanol. Geotherm. Res. 78, 103–120. https://doi.org/10.1016/S0377-
701 0273(97)00007-3
702 Gaeta, M., 1998. Petrogenetic implications of Ba-sanidine in the Lionato Tuff (Colli Albani
703 Volcanic District, Central Italy). Mineral. Mag. 62, 697–701.
704 https://doi.org/10.1180/002646198547927
705 Gaeta, M., Di Rocco, T., Freda, C., 2009. Carbonate assimilation in open magmatic systems:
706 The role of melt-bearing skarns and cumulate-forming processes. J. Petrol. 50, 361–385.
707 https://doi.org/10.1093/petrology/egp002
708 Gaeta, M., Fabrizio, G., Cavarretta, G., 2000. F-phlogopites in the Alban Hills Volcanic
709 District (Central Italy): Indications regarding the role of volatiles in magmatic
710 crystallisation. J. Volcanol. Geotherm. Res. 99, 179–193. https://doi.org/10.1016/S0377-
711 0273(00)00172-4
712 Gaeta, M., Freda, C., 2001. Strontian fluoro-magnesiohastingsite in Alban Hills lavas
713 (Central Italy): constraints on crystallization conditions. Mineral. Mag. 65, 787–795.
714 https://doi.org/10.1180/0026461016560009
715 Gaeta, M., Freda, C., Christensen, J.N., Dallai, L., Marra, F., Karner, D.B., Scarlato, P.,
716 2006. Time-dependent geochemistry of clinopyroxene from the Alban Hills (Central Italy):
717 Clues to the source and evolution of ultrapotassic magmas. Lithos 86, 330–346.
718 https://doi.org/10.1016/j.lithos.2005.05.010
719 Gaeta, M., Freda, C., Marra, F., Di Rocco, T., Gozzi, F., Arienzo, I., Giaccio, B., Scarlato,
720 P., 2011. Petrology of the most recent ultrapotassic magmas from the Roman Province
721 (Central Italy). Lithos 127, 298–308.

722 Gaeta, M., Freda, C., Marra, F., Arienzo, I., Gozzi, F., Jicha, B., Di Rocco, T., 2016.
723 Paleozoic metasomatism at the origin of Mediterranean ultrapotassic magmas: Constraints
724 from time-dependent geochemistry of Colli Albani volcanic products (Central Italy). Lithos
725 244, 151–164. https://doi.org/10.1016/j.lithos.2015.11.034
726 Ghiorso, M.S., Sack, R.O., 1995. Chemical mass transfer in magmatic processes IV. A
727 revised and internally consistent thermodynamic model for the interpolation and
728 extrapolation of liquid-solid equilibria in magmatic systems at elevated temperatures and
729 pressures. Contrib. Mineral. Petrol. 119, 197–212. https://doi.org/10.1007/BF00307281
730 Giaccio, B., Arienzo, I., Sottili, G., Castorina, F., Gaeta, M., Nomade, S., Galli, P., Messina,
731 P., 2013. Isotopic (Sr–Nd) and major element fingerprinting of distal tephras: an appli-
732 cation to the Middle–Late Pleistocene markers from the Colli Albani volcano, central Italy.
733 Quaternary Science Reviews 67, 190–206.
734 Giordano, G., De Benedetti, A.A., Diana, A., Diano, G., Gaudioso, F., Marasco, F., Miceli,
735 M., Mollo, S., Cas, R.A.F., Funiciello, R., 2006. The Colli Albani mafic caldera (Roma,
736 Italy): Stratigraphy, structure and petrology. J. Volcanol. Geotherm. Res. 155, 49–80.
737 https://doi.org/10.1016/j.jvolgeores.2006.02.009
738 Giordano, D., Russell, J. K. & Dingwell, D. B. (2008). Viscosity of magmatic liquids: a
739 model. Earth and Planetary Science Letters 271, 123-134.
740 Giordano, D., González-García, D., Russell, J.K., Raneri, S., Bersani, D., Fornasini, L., Di
741 Genova, D., Ferrando, S., Kaliwoda, M., Lottici, P.P., Smit, M., Dingwell, D.B., 2020. A
742 calibrated database of Raman spectra for natural silicate glasses: implications for modelling
743 melt physical properties. J. Raman Spectrosc. 51, 1822–1838.
744 https://doi.org/10.1002/jrs.5675

745 Gozzi, F., Gaeta, M., Freda, C., Mollo, S., Di Rocco, T., Marra, F., Dallai, L., Pack, A.,
746 2014. Primary magmatic calcite reveals origin from crustal carbonate. Lithos 190–191, 191–
747 203. https://doi.org/10.1016/j.lithos.2013.12.008
748 Gupta, A., 2015. Origin of potassium-rich silica-deficient igneous rocks. Springer, New
749 Delhi, India.
750 Gupta, A., 1972. The system Forsterite-Diopside-Akermanite-Leucite and its significance in
751 the origin of potassium-rich mafic and ultramafic volcanic rocks.. Am. Mineral. 57, 1242–
752 1259.
753 Hammer, J.E., 2008. Experimental studies of the kinetics and energetics of magma
754 crystallization. In: Putirka KD, Tepley III FJ (eds) Minerals, inclusions and volcanic
755 processes. Rev Mineral Geochemistry, 9–59.
756 Hawthorne, F.C., Oberti, R., Harlow, G.E., Maresch, W. V, Martin, R.F., Schumacher, J.C.,
757 Welch, M.D., 2012. Nomenclature of the amphibole supergroup. Am. Mineral. 97, 2031–
758 2048.
759 Hughes, E.C., Buse, B., Kearns, S.L., Blundy, J.D., Kilgour, G.N., Mader, H.M., 2019. Low
760 analytical totals in EPMA of hydrous silicate glass due t sub-surface charging: Obtaining
761 accurate volatiles by difference. Chem. Geol. 505, 48–56.
762 Humphreys, M.C.S., Kearns, S.L., Blundy, J.D., 2006. SIMS investigation of electron-beam
763 damage to hydrous, rhyolitic glasses: implications for melt inclusion analysis. Am. Mineral.
764 91, 667–679.
765 Iacono Marziano, G., Gaillard, F., Pichavant, M., 2007. Limestone assimilation and the
766 origin of CO_2 emissions at the Alban Hills (Central Italy): Constraints from experimental
767 petrology. J. Volcanol. Geotherm. Res. 166, 91–105.
768 https://doi.org/10.1016/j.jvolgeores.2007.07.001

769 Kimura, M., Mikouchi, T., Suzuki, A., Miyahara, M., Ohtani, E., El Goresy, A., 2009.
770 Kushiroite, $CaAlAlSiO_6$: A new mineral of the pyroxene group from the ALH 85085 CH
771 chondrite, and its genetic significance in refractory inclusions. Am. Mineral. . 94, 1479–
772 1482.
773 Lange, R.A., Cashman, K. V., Navrotsky, A., 1994. Direct measurements of latent heat
774 during crystallization and melting of a ugandite and an olivine basalt. Contrib. Mineral.
775 Petrol. 118, 169–181. https://doi.org/10.1007/BF01052867
776 Le Bas, M.J., W, L.M.R., Streckeisen, A., Zanettin, B., 1986. A chemical classification of
777 volcanic rocks based on the total alkali-silica diagram. J. Petrol.
778 https://doi.org/10.1093/petrology/27.3.745
779 Le Losq, C., Neuville, D.R., Moretti, R., Roux, J., 2012. Determination of water content in
780 silicate glasses using Raman spectrometry: Implications for the study of explosive
781 volcanism. Am. Mineral. 97, 779–790. https://doi.org/10.2138/am.2012.3831
782 Leake, B.E., Woolley, A.R., S, C.E., A, M.C.G.U.S., Canada, J.D.G., Hawthorne, F.C.,
783 Kisch, H.J., Krivovichev, V.G., Canada, J.A.M., Maresch, W. V, Schumacher, J.C., France,
784 D.C.S., Stephenson, N.C.N., Whittaker, E.J.W., 1997. Nomenclature of Amphiboles: report
785 of the subcommittee on amphiboles of the international mineralogical association,
786 commission on new minerals and mineral names. Can. Mineral. 35, 219–246.
787 Leicher, N., Zanchetta, G., Sulpizio, R., Giaccio, B., Wagner, B., Nomade, S., Francke, A.,
788 Del Carlo, P., 2016. First tephrostratigraphic results of the DEEP site record from Lake
789 Ohrid (Macedonia and Albania). Biogeosciences, 13, 2151–2178.
790 Lustrino, M., Fedele, L., Agostini, S., Prelević, D., Salari, G., 2019. Leucitites within and
791 around the Mediterranean area. Lithos 324–325, 216–233.
792 https://doi.org/10.1016/j.lithos.2018.11.007

793 Masotta, M., Gaeta, M., Gozzi, F., Marra, F., Palladino, D.M., Sottili, G., 2010. H2O- and
794 temperature-zoning in magma chambers: The example of the Tufo Giallo della Via Tiberina
795 eruptions (Sabatini Volcanic District, central Italy). Lithos, 118, 119–130.
796 Marra, F., Danti, A., Gaeta, M., 2015. The volcanic aggregate of ancient Roman mortars
797 from the Capitoline Hill: Petrographic criteria for identification of Rome's pozzolans and
798 historical implications. J. Volcanol. Geotherm. Res., 308, 113–126.
799 Marra, F., Cardello, L., Gaeta, M., Jicha, B., Montone, P., Niespolo, E., Nomade, S.,
800 Palladino, D.M., Pereira, A., De Luca, G., Florindo, F., Frepoli, A., Renne, P., Sottili, G.,
801 2021. The Volsci Volcanic Field (central Italy): an open window on continental subduction
802 processes. Int. J. Earth Sci. in press.
803 Marra, F., Karner, D.B., Freda, C., Gaeta, M., Renne, P., 2009. Large mafic eruptions at
804 Alban Hills Volcanic District (Central Italy): Chronostratigraphy, petrography and eruptive
805 behavior. J. Volcanol. Geotherm. Res. 179, 217–232.
806 https://doi.org/10.1016/j.jvolgeores.2008.11.009
807 McDonough, W.F., Sun, S. s., 1995. The composition of the Earth. Chem. Geol. 120, 223–
808 253. https://doi.org/10.1016/0009-2541(94)00140-4
809 Melzer, S., Foley, S.F., 2000. Phase relations and fractionation sequences in potassic magma
810 series modelled in the system $CaMgSi_2O_6$-$KAlSiO_4$-Mg_2SiO_4-SiO_2-F_2O_{-1} at 1 bar to 18 kbar.
811 Contrib. Mineral. Petrol. 138, 186–197. https://doi.org/10.1007/s004100050017
812 Mollo, S., Gaeta, M., Freda, C., Di Rocco, T., Misiti, V., Scarlato, P., 2010. Carbonate
813 assimilation in magmas: A reappraisal based on experimental petrology. Lithos 114, 503–
814 514. https://doi.org/10.1016/j.lithos.2009.10.013
815 Morimoto, N., 1988. Nomenclature of Pyroxenes. Mineral. Petrol. 39, 55–76.
816 https://doi.org/10.1007/BF01226262

817 Palladino, D.M., Gaeta, M., Marra, F., 2001. A large K-foiditic hydromagmatic eruption
818 from the early activity of the Alban Hills Volcanic District, Italy. Bull. Volcanol. 63, 345–
819 359. https://doi.org/10.1007/s004450100150
820 Pearce, N.J.G., Perkins, W.T., Westgate, J.A., Gorton, M.P., Jackson, S.E., Neal, C.R.,
821 Chenery, S.P., 1997. A compilation of new and published major and trace element data for
822 NIST SRM 610 and NIST SRM 612 glass reference materials. Geostand. Newsl. 21, 115–
823 144. https://doi.org/10.1111/j.1751-908X.1997.tb00538.x
824 Putirka, K.D., 2008. Thermometers and Barometers for Volcanic Systems, in: Putirka, K.D.,
825 Tepley III, F.J. (Eds.), Minerals, Inclusions And Volcanic Processes. Reviews in Mineralogy
826 and Geochemistry, pp. 61–120. https://doi.org/10.2138/rmg.2008.69.3
827 Rolandi, G., Munno, R. & Postiglione, I. (2004). The A.D. 472 eruption of the Somma
828 volcano. Journal of Volcanology and Geothermal Research 129, 291–319.
829 Scaillet, B., Pichavant, M., Cioni, R., 2008. Upward migration of Vesuvius magma chamber
830 over the past 20,000 years. Nature 455, 216–219. https://doi.org/10.1038/nature07232
831 Singh, P., Arima, M., Gupta, A., 2000. Phase equilibrium constraints on the petrogenesis of
832 nephelinites with reference to the system diopside nepheline under variable P T conditions
833 in the presence or absence of water. J. Mineral. Petrol. Sci. 95, 113–124.
834 Shaw, C.S.J., 2018. Evidence for the presence of carbonate melt during the formation of
835 cumulates in the Colli Albani Volcanic District, Italy. Lithos. 310–311, 105–119.
836 Skála, R., Strnad, L., McCammon, C., Čada, M., 2009. Moldavites from the Cheb Basin,
837 Czech Republic. Geochim. Cosmochim. Acta 73, 1145–1179.
838 https://doi.org/10.1016/j.gca.2008.11.003
839 Sottili, G., Arienzo, I., Castorina, F., Gaeta, M., Giaccio, B., Marra, F., Palladino, D.M.,
840 2019. Time-dependent Sr and Nd isotope variations during the evolution of the ultrapotassic

841 Sabatini Volcanic District (Roman province, Central Italy). Bull. Volcanol. 81.
842 https://doi.org/10.1007/s00445-019-1324-7
843 Strnad, L., Mihaljevic, M., Sebek, O., 2005. Laser Ablation and Solution ICP-MS
844 Determination of Rare Earth Elements in USGS BIR-1G, BHVO-2G and BCR-2G Glass
845 Reference Materials. Geostand. Geoanalytical Res. 29, 303–314.
846 https://doi.org/10.1111/j.1751-908x.2005.tb00902.x
847 Thompson, R. (1977). Primary basalts and magma genesis. III. Alban Hills, Roman
848 Comagmatic Province, Central Italy. Contributions to Mineralogy and Petrology 60, 91–
849 108.
850 Wallace, P.J., 2005. Volatiles in subduction zone magmas: Concentrations and fluxes based
851 on melt inclusion and volcanic gas data. J. Volcanol. Geotherm. Res. 140, 217–240.
852 https://doi.org/10.1016/j.jvolgeores.2004.07.023
853 Washington, H., 1906. The Roman comagmatic region. Carnegie Inst. Washingt. 56, 206–
854 214.
855 Yoder, H.S., 1986. Potassium-rich Rocks: Phase Analysis and Heteromorphic Relations. J.
856 Petrol. 27, 1215–1228. https://doi.org/10.1093/petrology/27.5.1215
857

858 **Figure captions**

859 **Figure 1 -** Stratigraphic successions and chronological constraints available for Colli Albani
860 Volcanic District (a). Simplified geologic map of the Colli Albani Volcanic District with the
861 same colours used in the stratigraphic successions (b). Satellite image showing the outcrop
862 area of the pyroclastic-flow deposits of Tufo del Palatino and the sites (geographic
863 coordinates in Table S1) where the analyzed samples were collected: 1) TP-Fall; 2) TP-ST;
864 3) TP-SO1; 4) TP-CH, 5) TP-RT; 6) TP-TAB; 7) TP-VM; 8) TP-VP; 9) TP-VG; 10) TP-
865 EU; 11) TP-PVF (c).

Figure 2 - Photomicrographs of the Tufo del Palatino scoria clasts in plane-polarized light. Group II, pale green, euhedral clinopyroxene with Ti-magnetite, apatite and melt inclusions (a). Group III, deep green clinopyroxene in equilibrium with MgO-poor melt and garnet (b). Microphenocryst of phlogopite in a cryptocrystalline scoria clast with star-like leucites and calcite-bearing vesicles (c). Subhedral, brown garnet (d). Cpx: clinopyroxene; Ti-Mgt: Ti-magnetite; Amph: amphibole; Cc: calcite.

Figure 3 - Photomicrographs of the Tufo del Palatino scoria clasts in plane-polarized light (a, b, c) and crossed polars (d). Aphyric, glassy scoria clast with scarce vesiculation (a). Glassy scoria clast showing scarce leucite microcrysts characterized by star-like habit and calcite-bearing vesicles (b). Glassy scoria clast showing leucite microcrysts ranging from euhedral to star-like (c). Detail of a large vesicle showing the zeolite rim and the calcite core (d). Cpx: clinopyroxene; Ti-Mgt: Ti-magnetite; Amph: amphibole; Cc: calcite.

Figure 4 - Binary covariation plot of diopside (Di) vs Tschermak (Ts) components expressed as the sum of kushiroite ($CaAl_2SiO_6$), essenite ($CaFeSiAlO_6$), CaTi-Tschermak (CaTiTs, $CaTiAl_2O_6$) and CaCr-Tschermak (CaCrTs, $CaCrAlSiO_6$) for clinopyroxenes in the Tufo del Palatino scoria clasts.

Figure 5 - Phlogopite chemical compositions from Tufo del Palatino (this work), Colli Albani (data from Gaeta et al., 2000) and Volsci Volcanic Field (yellow field, data from Marra et al., 2021) scoria clasts, reported in the Ti-Mg/(Mg + Fe^{2+}) (upper) and F-Mg/(Mg + Fe^{2+}) (lower) diagrams.

Figure 6 - Raman spectra of Tufo del Palatino apatite. Insets are Raman spectra portions (Awonusi et al., 2007) of CO_3-bearing apatite from 0.03 wt % in a-spectra to 7.9 wt % in f-spectra. Raman spectra were processed (baseline correction and smoothing) using the Spectragryph© software (F. Menges, "Spectragryph - optical spectroscopy software", Version 1.2.14, 2016-2020, http://www.effemm2.de/spectragryph/) (a). Plots illustrating a

linear relationship between: (100-$EMPA_{tot}$) + SO_3 vs $2P_2O_5$ wt % (b) and (100-$EMPA_{tot}$) + SO_3 vs $2P_2O_5$ wt % (c) in the apatite crystals of the Tufo del Palatino scoria clasts. The (100-$EMPA_{tot}$) wt % content is representative of the CO_3 content in the apatite.

Figure 7 - Total alkali versus silica classification diagram (Le Bas et al., 1986) of the Tufo del Palatino glasses and the parental magma (AH38f).

Figure 8 - Major oxide vs MgO (a,b and c) and S vs F (d) co-variations for the Tufo del Palatino glasses and the parental magma (AH38f). Symbols are as in Fig. 7.

Figure 9 – Raman spectra for the melt inclusion (TP-Fall) and glasses (TP-SO1 and TP-VM). The melt inclusion shows higher H_2O respect to the glasses and the presence of CO_3. Green field indicates the silicates region (200-1400 cm^{-1}) while the light blue field indicates the water region (2700-4000 cm^{-1}). H_2O^{Raman} is the water content estimated following the methods of Di Genova et al. (2017) (see §Analytical Methods for detail). Details of the Raman processing as in Fig. 7.

Figure 10 - Primitive Mantle normalized (McDonough and Sun, 1995) trace element abundances for Tufo del Palatino glasses and primitive lava flows from Colli Albani volcanic district. MdT, AH32, AH7a and AH38f have MgO content (wt %) of 5.15, 4.54, 6.43 and 7.07, respectively.

Figure 11 - Primitive Mantle normalized (McDonough and Sun, 1995) trace element abundances for Tufo del Palatino clinopyroxenes. Clinopyroxenes were arranged in Cpx groupI, Cpx group II and Cpx group III as function of their content in diopside (Di) and Tshermak (STs) components (see the text).

Figure 12 - Olivine (Ol), clinopyroxene (Cpx), leucite (Lc) compositional (wt%) plane showing the phase relations at 0.2 GPa and a_{H2O} <1 and at 0.001 GPa. The Ol, Cpx and Lc normative compositions reported in the diagram are calculated assuming $An_{Normative}$ = $CaAl_2Si_2O_8$ = $CaAl_2SiO_6$ + SiO_2, Cpx = $Di_{Normative}$ + $CaAl_2SiO_6$ and Lc = $Lc_{Normative}$ +

$Ne_{Normative} + SiO_2$, $Ol = Ol_{Normative}$. K-foiditic glasses of Colli Albani after Gaeta (1998) and Marra et al. (2009). Experimental data after Gupta (1972), Iacono Marziano et a*l*. (2007) and Freda et al. (2008).

Figure 13 - Primitive Mantle normalized (McDonough and Sun, 1995) trace elements patterns for phonotephrite (AH38f, Table 3 and S1), the average of the Tufo del Palatino glass compositions, and the predicted composition of differentiated melts obtained after fractional crystallization (FC in a), combined (AFC in b) and decoupled (FCA in c) fractional crystallization and assimilation from the AH38f phonotephrite assumed as primitive parental magma. In the three models the amount of residual melt is 37 wt % and removed solid is formed by clinopyroxene (38.9 wt %), leucite (19.3 wt %), Ti-magnetite (3.6 wt %) and apatite (1.2 wt %). The relative ratio of assimilated material to crystallized material (r) in the AFC and FCA models is r = 0.2 with the assimilated calcite composition after Gozzi *et al.* (2014). The modelled compositions were calculated by using the Excel© spreadsheet program of Ersoy and Helvaci (2010) implemented with the $K_{Dleucite/melt}$ (Foley and Jenner, 2004) and $K_{Dclinopyroxene/melt}$ (Bonechi *et al.*, 2021).

Figure 14 - Phase relationships for the hydrous-carbonated parental phonotephritic composition reported in the pressure vs temperature space (modified from Freda et al., 2011). The diagram illustrates the large temperature range of clinopyroxene and leucite crystallization in equilibrium with K-foiditic melt (a). The diagram shows the variation of the viscosity with the SiO_2 content for K-foiditic glass (in blue; this study) and phonolitic and trachytic glasses (in green; database of Giordano et al., 2019). Viscosity data were calculated using the Excel© spreadsheet of Giordano et al. (2008) at atmospheric pressure and T = 1000°C (b).

Uncommon K-foiditic magmas: the case study of Tufo del Palatino (Colli Albani Volcanic District, Italy)

M. Gaeta[1*], B. Bonechi[1], F. Marra[2], C. Perinelli[1]

1: Dipartimento di Scienze della Terra, Sapienza Università di Roma, P.le Aldo Moro 5, 00185, 7 Rome, Italy

2: Istituto Nazionale di Geofisica e Vulcanologia, Via di Vigna Murata 605, 00143 Rome, Italy

*Corresponding author. Telephone: 0039 06 49914916; E-mail: mario.gaeta@uniroma1.it

Abstract

Leucititic rocks, K-foiditic in composition are volumetrically important in the Colli Albani (also known as Alban Hills) volcanic district (Central Italy) especially during the most explosive phases of activity (>200 km^3). The Colli Albani tephra in distal (>500 km) deposits indicates that K-foiditic magma chambers fed large explosive eruptions (i.e., tens of km^3 of pyroclastic rocks). Major oxides, trace elements and Raman spectra were measured on the glasses and minerals occurring in the K-foiditic scoria clasts of the ~530 kyr-old Tufo del Palatino, erupted in the Colli Albani volcanic district. The Colli Albani pre-eruptive magmatic system is characterized by the a_{H2O} <1 and high CO_2 activity in the melt, as testified by the CO_3 in the clinopyroxene melt inclusions, by the early crystallization of CO_3-bearing apatite and by the high CO_2 activity in the free volatile phase that led to crystallization of calcium carbonate in the scoria clast vesicles. The K-foiditic magmas plot on the Cpx+Lc+melt divariant surface of the Ol-Cpx-Lc-Mel-H_2O-CO_2, P ≥0.2 GPa and T ≤1100 °C. The assimilation of cold carbonate by hot magmas is an important open-system process allowing the establishment of a_{H20} <1 condition in the volatile-rich, Colli Albani magma chambers where the stability fields of the olivine and phlogopite are reduced in favour of clinopyroxene and leucite. Trace element modelling indicates large amount of

carbonate assimilation (~12.4 wt%) involved in the differentiation process that origins the K-foiditic magmas starting from a K-rich, phonotephritic parental magma. The large amount of assimilate carbonate is consistent with the peculiar distribution of the latent heat across the crystallization interval of the phonotephritic parental magma. The isenthalpic assimilation process is very efficient in the phonotephritic magma because the crystallization of clinopyroxene and leucite in equilibrium with a K-foiditic melt proceeds over a relatively large temperature interval (>200 °C) and the K-foiditic melt shows low viscosity (10^4Pa·s at 1000 °C). Actually, the low melt viscosity, that increases the growth rate, and the large temperature interval of crystallization are intrinsic factors that increase the release of the latent heat of crystallization from the phonotephritic parental magma. Extrinsic factors enhancing the assimilation process efficiency are the thickness (>4 km) and the depth (down to 5-7 km) of the carbonate substrate in the Colli Albani volcanic district.

Key words: foidite, glass, leucite, ultrapotassic, Colli Albani.

1. Introduction

Leucititic rocks with K-foiditic composition (i.e., $K_2O>Na_2O$) are rare and occur almost exclusively in the Quaternary volcanic districts of Italy (Lustrino et al., 2019). K-foiditic scoria, lava flows and granular hypabyssal rocks are present in the Vulsini Volcanic District (Di Battistini et al., 1998), at Colli Albani Volcanic District (Gaeta, 1998), at Volsci Volcanic Field (e.g., Marra et al., 2021) and at Vesuvius (e.g., Rolandi et al., 2004). Notably, K-foidites are volumetrically important in the Colli Albani volcanic district (hereafter Colli Albani), where most of the explosive products (>200 km^3) show such peculiar compositions (e.g., Marra et al., 2009). Colli Albani glasses have been recognized in the 1.2 Myr of continuous tephrostratigraphic record of Lake Ohrid (Macedonia and Albania) on the basis

of their unique K-foiditic composition (Leicher et al., 2013). The occurrence of Colli Albani tephra in distal archives indicates that K-foiditic magma chambers fed large explosive eruptions that have emplaced several tens of km^3 of pyroclastic rocks (e.g., Freda et al., 2011). Researchers have been attracted by these rare rocks of the Colli Albani since the early 20^{th} century (Washington, 1906). K-foiditic lava flows of Colli Albani were initially considered as primary magmas, and consequentially they were the subject of geochemical and experimental research aimed to ascertain the conditions of their formation in the mantle (e.g., Thompson, 1977). Nevertheless, later volcanological, geochemical and experimental studies ruled out the existence of K-foiditic primary magmas (Freda et al., 1997). The delay in understanding that the K-foidites of Colli Albani are differentiated magmas is due to the difficulty of finding residual glasses in primitive lava flows and glassy scoria clasts with K-foiditic composition. Actually, the lava flows and the scoria clasts are commonly characterized by holocrystalline groundmass in which the high growth rate of leucite is highlighted by the star-like habit (e.g., Palladino et al., 2001; Freda et al., 2011). At low pressure, Colli Albani magmas are characterized by high liquidus temperature (>1200°C; Freda et al., 2008) and low viscosity (10^4Pa·s at 1000 °C; Giordano et al., 2008). The combination of a large undercooling (i.e., $\Delta T = T_{system}-T_{mineral\ liquidus}$) and low viscosity is generally the main factor capable of producing high growth rates (e.g., Bonechi et al., 2020a). The Colli Albani scoria clasts are glassy mainly in the hydromagmatic deposits (e.g., Freda et al., 2006; Gaeta et al., 2011) because the high cooling rate, due to the eruptive dynamic, contrasts the high growth rate of leucite.

In this paper we present new data on the hydromagmatic scoria clasts of the Tufo del Palatino eruptive unit (Colli Albani, Central Italy). This eruptive unit is richest in glasses which allow a privileged geochemical and spectroscopic characterization of the K-foiditic melts from which the leucititic rocks crystalize. We use this case study to discuss the

processes at the origin of the K-foiditic magmas with the aim to answer at the main query emerging from the global rarity of these magmas: why K-foidites?

2. Geological contest and field aspect

The Colli Albani, located along the Tyrrhenian Sea margin of Central Italy, are rooted in an overthickened carbonate succession extending from 0.5 to 1 km of depth down to the transition to the crystalline basement, which tomographic studies tentatively place between 5 and 7 km (Bianchi et al. 2008). "Tufo del Palatino" is the formal unit name of the deposit of the second largest explosive eruption of the oldest activity of the Colli Albani (Tuscolano-Artemisio Phase; Freda et al., 1997; Vulcano Laziale lithosome, Giordano et al., 2006). The oldest activity was characterized by five large caldera-forming eruptive units in the time span 561-365 ka, separated by long quiescent periods of 30-50 kyr (Marra et al., 2009). Pyroclastic-flow deposits up to ~300 km^3 in volume, radially stretching as far as 20 km from the vent, were emplaced during this phase. The Tufo del Palatino (530 ± 2 ka) eruptive unit, had hydromagmatic features, witnessed by the frequent occurrence of accretionary lapilli both in the pyroclastic-flow and the ash-cloud deposits. In mid-distal settings, the Tufo del Palatino is characterized by a basal, laminated ash layer, <5 cm thick, followed by a well-sorted, clast supported, dark grey lapilli layer, 1-2 to 15 cm thick, and by a massive, matrix supported, dark grey pyroclastic-flow deposit with variable thickness of 1 to 4 m, as a function of the morphology of the substrate above which it was emplaced. A light grey to yellowish, faintly pedogenized ash with abundant accretionary lapilli (ash-cloud deposit) closes the eruptive unit of Tufo del Palatino. The pyroclastic-flow deposit displays a peperino-like aspect, due to the occurrence of mm-sized dark grey, poorly vesicular scoriae, along with loose, abundant leucite and pyroxene crystals. Sedimentary (i.e., silico-clastic and carbonatic) and igneous (i.e., lava and granular) lithic clasts are also present.

Macroscopic lamination, due to change of grain size, confers a characteristic planar fracturing of this soft volcanic rock which, for these favourable physical properties, was extensively exploited as building stone ("cappellaccio") in the archaic Roman period (Diffendale et al., 2019 and references therein). Lithified facies of Tufo del Palatino, due to the intense zeolitization and calcite crystallization, occurs in the Tiber Valley north of Rome, which was previously identified with the name of "Peperino della Via Flaminia" (Diffendale et al., 2019). Samples analyzed in the present study were collected at several outcrops located along the Tiber Valley where fluvial incision provides good exposition of the pyroclastic-flow deposits, which elsewhere are buried under a thick, younger volcanic succession (Fig. 1). Moreover, the analyzed samples includes three archaeological samples collected from ancient Roman buildings: the Servian Walls at Stazione Termini (sample TP-ST), the archaic temple of Sant'Omobono (sample TP-SO1; Brocato et al., 2019), and the foundation of Tabularium (sample TP-TAB; Marra et al., 2015).

3. Analytical methods

3.1. Major element and volatiles determinations

Major oxides of glasses and minerals were analyzed at the CNR-Istituto di Geologia Ambientale e Geoingegneria di Roma, with a Cameca SX50 electron microprobe equipped with five wavelength dispersive spectrometers (WDS). Quantitative analyses were performed using 15 kV accelerating voltage and 15 nA beam current. As standards we employed metals for Mn and Cr, jadeite for Na, wollastonite for Si and Ca, orthoclase for K, corundum for Al, magnetite for Fe, rutile for Ti, periclase for Mg, F-apatite for P, phlogopite for F, potassium chloride for Cl, barite for Ba and S, celestine for Sr. Counting times for all elements were 20 s on peak and half time on both backgrounds. Light elements (Na, K) were counted first to prevent loss by volatilization. The PAP correction method was used.

126 Minerals were analyzed using a beam diameter of 1-5 μm whereas to minimize alkali loss
127 during glass analysis, the beam was defocused to 15 μm. In order to evaluate the accuracy
128 of the analyses, repeated analyses of three international secondary standard (Kakanui augite,
129 Iceladic Bir-1 and rhyolite RLS132 glasses from USGS) were made prior to any series of
130 measurements. The mean accuracy from the standard value was about 1% for SiO_2, 2% for
131 Al_2O_3, 5% for K_2O, CaO and FeO, and 8-10% for other elements. Moreover, the analytical
132 precision (2 sigma error) is ≤1% for elements in the concentration range >10 wt % oxide,
133 5% for elements in the range 2-10 wt % oxide and better than 10% for elements in the range
134 0.5-2 wt % oxide. From chemical analyses, the H_2O±CO_2 contents of glasses were estimated
135 according to the by-difference method (Devine et al., 1995; Humphreys et al., 2006). We are
136 aware that this method is not fully reliable given the estimation is affected by element
137 concentrations not measured by EMPA and surface charge effects (Hughes et al., 2019)
138 leading to an overestimation of H_2O concentration. However, the obtained H_2O values are
139 close to those determined by micro-Raman spectroscopy measurements (Le Losq et al.,
140 2012; Di Genova et al., 2017) on the same glasses. Raman spectra were acquired with a
141 Horiba Lab Ram HR 800 spectrometer at the Department of Science, Roma Tre University.
142 Data were collected using a 600 grooves/mm spectrometer grating and CCD detector.
143 According to the internal calibration method of Di Genova et al. (2017) it is possible to
144 estimate the water content as a function of the HW/LW area ratio [HW (High Wavenumbers)
145 is the water region (2700-4000 cm^{-1}) while LW (Low Wavenumbers) is the silicate region
146 (100-1500 cm^{-1}) of the Raman spectra], using the following equation: H_2O (wt%) =
147 (HW/LW)·m, where HW/LW is the water to silicate band ratio and m is the linear fit
148 coefficient. Since Di Genova et al. (2017) provide a list of m coefficients for a range of
149 chemical composition that does not include the foiditic one, we estimated a m coefficient for
150 this latter by processing Raman spectra, acquired on synthetic foiditic glasses (Freda et al.

151 2008), through a specific Matlab© code (Di Genova et al., 2017). The obtained HW/LW
152 were plotted against the water content of the synthetic samples previously measured in order
153 to obtain a linear fit representative of the calibration curve for the foiditic composition and
154 consequently the *m* coefficient (*m* = 1.9608, R^2 = 0.98). This coefficient has been used to
155 assess the water content in the glasses of Tufo del Palatino. Error in water determination is
156 estimated ± 0.15 wt %.
157
158 **3.2. Trace elements determination**
159 LA-ICP-MS analyses of glasses and clinopyroxenes were performed on a quadrupole–based
160 ICP-MS iCAP-Q instrument (Thermo Fisher Scientific, Bremen) coupled to a modified
161 NewWave UP 213 laser microprobe (NewWave, USA) installed at Charles University,
162 Prague. Analyses of clinopyroxene crystals were performed using a circular laser beam of
163 100 μm diameter, a puls frequency of 10 Hz and a laser flux on the sample surface of 3.5
164 J/cm^2. External calibration of the laser ablation analyses was done using Standard Reference
165 Materials NIST (National Institute of Standards and Technology, USA) 612 with internal
166 standardization using Si, based on electron microprobe measurements. The concentration
167 values for NIST of all measured elements were taken from Pearce et al. (1997). The external
168 reproducibility of this method was checked on repeated analyses of USGS BCR-2G glass as
169 reference material (e.g., Strnad et al., 2005 and reference therein). The isotopes used were
170 selected with respect to their most abundant species, free from isobaric overlap and
171 minimum interferences. Formation of oxides (MO^+/M^+) was monitored using U in NIST 612
172 directly from ablation and the measured ratios ($^{254}UO^+/^{238}U^+$) was below 10^{-2}. Further details
173 about the analytical protocol and correction strategy have been described by Strnad et al.
174 (2005) and Skála et al. (2009). Detection limits for all elements were calculated as 3σ level
175 of the gas blank.

4. Results

4.1. Texture

Submillimetre, euhedral to subeuhedral crystals of leucite and clinopyroxene impart sparsely porphyritic textures (1-5% by volume of crystals ≥0.5 mm) to juvenile scoria lapilli in Tufo del Palatino. The colour and shape of clinopyroxene crystals are variable from green to light green and equidimensional to elongated respectively (Fig. 2a and 2b). Glass, oxide and apatite inclusions can be present in the larger clinopyroxenes (Fig. 2a). The scoria lapilli contain also rare phlogopite (Fig. 2c) and brown to deep green amphibole. The groundmass ranges from glassy to cryptocrystalline with rounded to polygonal vesicles (Fig. 3a, 3b and 3c). Frequently, vesicles show a layer made up of zeolites and, sometimes, are filled with calcium carbonate (Fig. 3d). Typically, leucite in glassy scoria clasts shows star-like shape (Fig. 3b and 3c), due to diffusion-controlled crystal growth, as a clear indication of large undercooling (i.e., T_{System}-$T_{Lct\text{-}liquidus}$) at high cooling rate conditions (Hammer, 2008). In the ash matrix of the Tufo del Palatino millimetric to submillimetre, euhedral to anhedral, colourless clinopyroxene and submillimetre, subhedral to anhedral brown garnet are also present (Fig. 2d).

.

4.2. Mineral chemistry

4.2.1. Clinopyroxene

The clinopyroxene is classified as diopside following the scheme of Morimoto (1988) and the variation of the diopside content ($Di_{83\text{-}40}$) is negatively correlated with that of the Tschermak-components (i.e., $CaAl_2SiO_6$, + $CaFeSiAlO_6$, + $CaTiAl_2O_6$ + $CaCrAlSiO_6$ = $\Sigma Ts_{6\text{-}37}$; Fig.4). On the basis of the diopside content and Tschermak-components ($\Sigma Ts_{6\text{-}37}$)

three populations of clinopyroxene can be distinguished (Fig. 4, Table 1). The first population (Group I) has the highest content of diopside (Di_{83-73}), the lowest in Tschermak-components (ΣTs_{6-17}) and it is the most primitive population with Mg/(Mg+Fetot)>0.78 (Table S1). The second population (Group II) has intermediate contents of diopside and ΣTs and contains homogeneous crystals and clinopyroxenes with a rim enriched in diopside (Di_{69}) respect to the core (Di_{56}; Table 2 and Table S1). The third population (Group III) has the lowest values of diopside (Di_{40-49}) and the highest Tschermak-components (ΣTs_{34-37}). These emerald green clinopyroxenes (Fig. 2b) are the most differentiated (Mg/(Mg+Fetot) $\leq$ 0.50) and are, probably, those more similar to the kushiroite among the magmatic, terrestrial clinopyoxenes (Kimura et al., 2009). Moreover, as suggested also by the trace element abundances (see below) the Group III represents clinopyroxenes in equilibrium with differentiated interstitial melt close to the solidus temperature.

4.2.2. Other phases

In addition to the clinopyroxene, numerous mineral phases (Table S1) occur in the Tufo Palatino scoria clasts.

Leucite is often replaced by analcime. Their K_2O content falls within the range of 21.01-20.70 wt %. The Na/K ratio varies from 0.012 to 0.038 wt % while the iron content, reported as FeO, varies from 0.31 to 0.60 wt %.

Mica is phlogopitic (Mg/Fe cation ratio >2) in composition (Fig. 5 and Table S1) with a narrow range of Mg/(Mg + Fe) ratio and TiO_2 content (0.74-0.78 and 2.44-3.29 wt %, respectively). The F content (0.66-1.31 wt %) is lower than that of the lava flow micas (up to 7.3 wt %, Gaeta *et al.*, 2000; Gozzi *et al.*, 2014) but indicates a_{H2O} <1 in the magma that have fed the explosive eruption of the Tufo del Palatino.

225 Amphibole, for the first time identified in the Colli Albani scoria clasts, belongs to the calcic
226 group and has magnesiohastingsite composition (Hawthorne et al., 2012). Similarly to what
227 has been observed in the mica, the F content of amphiboles (0.46-0.49 wt %) is lower than
228 that measured in the lava flow crystals (up to 3.2 wt %, Gaeta and Freda, 2001). However,
229 also the amphibole indicates the a_{H2O} <1 in the Tufo del Palatino magmatic system.
230 Apatite is characterized by significant amount of SiO_2 (1.15-2.47 wt %), SO_3 (1.17-1.98 wt
231 %) and fluorine (3.65-3.85 wt %) and by low amount of P_2O_5 (32.05-36.65 wt %; Table S1).
232 The high SO_3 and SiO_2 contents of apatite could indicate the presence of the substitution
233 mechanism $S^{6+} + Si^{4+} = 2P^{5+}$. However, the absence of a correlation between $SO_3 + SiO_2$
234 and $2P_2O_5$ abundances indicates that others substitution mechanisms should have played an
235 important role. The high and constant content of CaO (52.87-54.04 wt%, Table S1) excludes
236 substitution mechanisms involving Th, LREE and Sr as those discussed by Fabrizio et al.,
237 (2018) for apatites in the hypoabissal granular rocks of Colli Albani. The Raman spectrum
238 of the Palatino apatite shows pattern peaks (500-630 and 1000-1100 cm^{-1} regions; Fig. 6)
239 occurring in the presence of CO_3 (Awonusi et al., 2007), that in the microprobe analyses
240 could be represented by the 100-$EMPA_{total}$ amount. Plots of the analytical data in a (100-
241 $EMPA_{total}$) + SiO_2 versus ($2P_2O_5$) or (100-$EMPA_{total}$) + SO_3 versus ($2P_2O_5$) diagrams (Fig.
242 6) show a very good correlations (R^2 = 0.993 and 0.999, respectively). These correlations
243 suggest the occurrence of the $CO_3 + SO_3=2P_2O_5$ and $CO_3 + SiO_2=2P_2O_5$ substitutions in the
244 apatite of the Tufo del Palatino.
245 Spinel is Ti-bearing magnetite (ulvöspinel mol. = 14 wt %), moderately enriched in MgO
246 and Al_2O_3 (noble spinel mol. = 10 wt %; Table S1).
247 Garnet is a Ti-bearing andradite, it does not show intra-mineral zoning and it is similar in
248 composition to the garnets occurring in the Villa Senni scoria clasts (Freda et al., 1997).
249

4.2.3. Subsolidus phases

Analcime shows Na_2O content (7.25-9.10 wt %; Table S1) that is lower than that observed in various ultrapotassic volcanic complexes (9.17-14.18 wt %; Gupta, 2015). The inner border of vesicles is filled by chabasite (Fig. 3d) characterized by high contents of SrO and BaO (up to 1.12 wt %) while the core of the vesicles is formed by calcium carbonate (Table S1).

4.3. Glass compositions

Tufo del Palatino glasses are foiditic (Fig. 7) and potassic ($K_2O>Na_2O$) in composition (Table 2). These chemical features are in accordance with the leucite-bearing texture that, however, depends by the crystallization conditions (i.e., T, P and a_{vol}). Consequently, the term K-foidite used hereafter can be considered equivalent but more general respect to leucitite. The MgO content (3.55 wt % in average on volatile-free basis), the Mg# = 0.36 (assuming FeO_{tot}=FeO; Table 2) and the comparison with previously analyzed olivine-bearing phonotephrites of Colli Albani, characterized by Mg# = 0.68-0.59 (Gozzi et al., 2014), indicate that Tufo del Palatino glasses represent differentiated melts. Noteworthy, the CIPW normative olivine content ranging from 7.6 to 13.4 wt% leads to a misleading primitive classification (i.e. basanitic leucitites to tephritic leucitites) of the Tufo del Palatino glasses. The lower SiO_2 content is probably the most significant chemical difference with the primitive compositions found, so far, in the Colli Albani (Fig. 7). However, in spite of their evolved chemical composition, the Tufo del Palatino glasses show high CaO contents (12.23 wt % in average of 41 glass analyses, Table S1) as highlighted by the comparison with parental composition of Colli Albani (Fig. 8), as well as with the leucite-bearing rocks of the Mediterranean area with similar MgO contents (Lustrino et al., 2019). In particular, in the CaO vs. MgO diagram a relatively large range of CaO (11.40-13.95 wt % on dry basis;

Fig. 8 and Table S1) clearly emerges. This oxide is present at higher and lower values compared to those of the phonotephritic composition (Fig. 8). Moreover, the comparison with the phonotephritic composition indicates that in the Tufo del Palatino glasses the content of Al_2O_3, FeO, TiO_2 and Na_2O increases and that of P_2O_5 decreases (Fig. 8 and Table 2). Otherwise, the K_2O content (6.01 to 8.83 wt %, Table S1) is not correlated with MgO but is broadly correlated (R^2=0.6) with SiO_2 (43.18-45.47 wt %).

The SO_3 content (2643 ppm = 0.65 wt % in average; Table S1) is higher than that of primitive magmas in the orogenic contest (S = 900-2500 ppm; De Hoog et al., 2001; Wallace, 2005), as well as that of parental magma (Fig. 8). On the basis of the sulfur content two groups of glasses with an average amount of ~3200 ppm and ~2400 ppm can be recognized. The sulfur variation is not correlated with F (Fig. 8) and Cl, suggesting a different behavior of these volatiles during magma differentiation and degassing. Raman spectra show CO_2 content below the instrumental sensibility and water contents of 1.15-1.12 wt % (Table 2 and Fig. 9). These water contents are close to 100-$EMPA_{total}$ value found in the Tufo del Palatino glasses (2.29-3.06 wt %, Table S1) corrected for Fe^{3+} and Fe^{2+} partition [$(FeO+Fe_2O_3)$-$FeOt_{ot}$~0.4 wt %, with the iron partition calculated at the fO_2 of QFM+2; Table 2)] and the trace element contents (~0.9 wt %). Noteworthy, a K-foiditic melt inclusion in the clinopyroxene (Table S1) of the TP-Fall shows higher H_2O respect to the Tufo del Palatino glasses and the presence of CO_3 (Fig. 9).

4.4. Trace elements

In spite of their differentiated chemical composition (i.e., MgO<4 wt%), the K-foiditic glasses of the Tufo del Palatino eruptive unit preserve trace element concentrations distinctive of orogenic, subduction-related magmas. In particular, the primitive mantle-normalized diagrams patterns of the Palatino glasses show very high abundances (>1000

300 times primitive mantle abundances) of Th, U, Pb, very high LILE/HFSE ratios, as shown by
301 marked Nb-Ta and Ti troughs, and slightly decreasing at the heavy rare earth elements-
302 HREE region (Fig. 8). The Cs-Rb trough is clearly ascribable to leucite fractionation (e.g.,
303 Foley and Jenner, 2004; Fabbrizio et al., 2008) and is the only remarkable deviation respect
304 to the pattern of the phonotephritic magmas (Fig. 10).

305 Trace element abundances in clinopyroxenes (Table 3, Table S1 and Fig. 11) are
306 quite variable showing also in some crystals compositional intra-mineral zoning (e.g., cpx-
307 4 in the TP-TAB1 sample). Primitive mantle normalized patterns of clinopyroxenes show an
308 overall similarity with differences in the degree of enrichments of the incompatible elements
309 (Fig 11). This is clearly evidenced, for instance, by the variation in the depth of the Nb, Pb,
310 Zr and Ti negative anomalies with respect to the adjacent elements (Fig. 11). With the
311 exception of the cpx-4 rim in the TP-TAB1 sample that displays a distinctive pattern,
312 variations in incompatible element abundances of Tufo del Palatino clinopyroxenes reflect
313 those observed for major element compositions that, on the basis of diopside (Di) and
314 Tschermak (ΣTs) components, suggested the presence of three clinopyroxene populations
315 (Fig. 4). Crystals having low ΣTs (<0.20) and high Di and Mg# values (Di >0.73 and Mg#
316 >0.67) are characterized by relatively low trace element contents (e.g., Nb =0.07-0.29 ppm,
317 Zr = 100-409 ppm, La = 13-28 ppm) whereas in clinopyroxenes whose Mg# is <0.62 with
318 relatively low Di and high ΣTs (i.e., Group II and III), the concentration of Nb, Zr and La
319 are significant higher (Nb = 0.38-8.37 ppm; Zr=317-939 ppm; La=23-68 ppm). In particular,
320 in Group III clinopyroxene have the highest Nb, Zr and La contents (Fig. 11, Table 3, Table
321 S1). As mentioned above, the incompatible element composition of cpx-4 rim in the TP-
322 TAB1 sample differs from the others because it is characterized by lower contents in Y,
323 LREE/MREE (La_N/Sm_N >3 compared to La_N/Sm_N <2) and LREE/HREE and (La_N/Yb_N =
324 51-65 compared to La_N/Yb_N = 11-36) possibly as a result of the crystallization in equilibrium

with HREE-rich phase. Actually, the distinctive pattern of cpx-4 rim is similar to that of clinopyroxenes crystallized in equilibrium with garnet in the leucite -bearing, granular rocks of Colli Albani (i.e., italites and/or fergusites, Freda et al., 1997; Fabbrizio et al., 2018; Dallai et al., 2004; Shaw, 2018).

5. Discussion

5.1. K-foiditic parental magma

Effusive eruptions in the Colli Albani were fed by phonotephritic to K-foiditic magmas (e.g., Gozzi et al., 2014) while the large explosive eruptions almost exclusively by K-foiditic magmas (e.g., Gaeta, 1998; Palladino et al., 2001; Marra et al., 2009; Freda et al., 2011; Biagio et al., 2013; Leicher et al., 2016). Nevertheless, evidences of the parental phonotephritic magma are common in the products of the large explosive eruptions. A large-scale example is the phonotephritic Vallerano lava flow that predates, without temporal gap, the K-foiditic Pozzolane Rosse eruption (Freda et al., 2011). At smaller scale, clinopyroxene antecrysts in equilibrium with primitive melts are relatively common in the Colli Albani pyroclastites (e.g., Dallai et al., 2004).

The Di-rich population of clinopyroxenes (Group I, Fig. 4) indicates that the Tufo del Palatino scoria clasts are no exception to the rule because these clinopyroxenes are in equilibrium with the Mg#>0.6 typical of the Coli Albani primitive magmas (Table 2). Actually, on the basis of the Fe-Mg distribution coefficient between clinopyroxene and melt ($K_D(\text{Fe-Mg})^{Cpx\text{-}melt} = Fe_{Cpx} \times Mg_{melt}/Mg_{Cpx} \times Fe_{melt}$, calculated assuming all Fe as Fe^{2+} in both phases) the Group I clinopyroxenes (Fig. 4) are not in equilibrium with the K-foiditic melts, but in equilibrium with the phonotephritic compositions of the primitive Colli Albani lava flows (Table 1).

The latter, as well as the primitive magmas of the Roman Province show peculiar, if not unique, geochemical features (e.g., $K_2O/Na_2O \geq 2$; high LILE/HREE ratio; $^{87}Sr/^{86}Sr \geq 0.709$) and this singularity is due to the composition of the metasomatizing agents that modified the pristine peridotite mantle (e.g., Ammannati et al., 2016; Avanzinelli et al., 2018). Moreover, to better constrain the composition of possible parental magma Tufo del Palatino products, it should be noted that the temporal geochemical variations observed in the Colli Albani magmas indicate that the ultrapotassic magmas originated from a metasomatized mantle source in which phlogopite is the potassium-bearing phase. This is consistent with the $^{87}Sr/^{86}Sr$ and the incompatible trace element decrease of primitive magmas during the eruptive history of the volcanic district (e.g., Gaeta et al., 2006; Boari et al., 2009; Gaeta et al., 2016). Indeed, primitive mantle normalized patterns of the younger primitive compositions (40-308 ka; MgO >5 wt %) of Colli Albani show trace element abundances that are similar or lower than in the oldest AH38f lava flow (474 ka; Fig. 10). Noteworthy, the decrease of incompatible trace element abundances by means of a fractional crystallization process is unrealistic because the younger primitive compositions have lower content of MgO respect to AH38f lava flow (i.e., 4.14-6.43 wt% and 7.07 wt % respectively). Moreover, the younger primitive compositions have lower $^{87}Sr/^{86}Sr$ ratio respect those measured in the Tufo del Palatino clinopyroxene (Table 3) which, instead, is similar those of the AH38f lava flow.

5.2. T, P, volatiles concentration in the pre-eruptive magmatic system

In addition to the clinopyroxene antecrysts (Group I, Fig. 4) in equilibrium with the phonotephritic melt other two group of clinopyroxenes occurs in the scoria clasts of the Tufo del Palatino (Table 1). The largest population (Group II , Fig. 3) has the $K_D(Fe\text{-}Mg)^{Cpx\text{-}melt}$ = 0.20-0.35 that indicate equilibrium conditions ($K_D(Fe\text{-}Mg)^{Cpx\text{-}melt} = 0.28 \pm 0.08$ according to

374 Putirka, 2008)) with the K-foiditic composition of the Tufo del Palatino glasses (Table 2).
375 The third population formed by few crystals (Group III), according to the $K_D(Fe\text{-}Mg)^{Cpx\text{-}glass}$,
376 appear in equilibrium with the K- foiditic compositions characterized by low MgO contents
377 (i.e., <2 wt%, similar to Lionato glasses, Table S1). The equation 33 of the thermometer of
378 Putirka (2008), with a standard error of 87 °C) indicates that clinopyroxene antecrysts and
379 AH38f phonotephrite equilibrate in the range of 1083-1144 °C and the Group II
380 clinopyroxenes and the K-foiditic melt (i.e., Tufo del Palatino glass) between 1048-1098 °C
381 (Table 1 and S1). Lower temperatures in the Palatino pre-eruptive system are suggested by
382 MgO-poor, Group III clinopyroxene, as well as, by the amphibole occurrence that in the
383 alkaline magmas is stable at T<1050°C (e.g., Charles, 1977; Singh et al., 2000; Bonechi et
384 al., 2017, 2020b). The HREE depletion measured in the rims of Group III clinopyroxenes
385 (Fig. 11) suggests local conditions (e.g., the peripheral portion of the magma chamber;
386 Masotta et al., 2010) of even lower temperature compatible with the garnet crystallization
387 (830-920 °C; Scaillet et al., 2008). Anyway, the garnet occurrence, as well as that of
388 amphibole, indicates relatively high pressure condition for the Tufo del Palatino pre-eruptive
389 magmatic system. Pressures of 0.32-0.36 GPa estimated from the Group I clinopyroxene
390 compositions (Table 1 and S1) using the Palk algorithm (Masotta et al., 2013; with a standard
391 error of estimate of 0.12 GPa) are similar to those obtained from the volatile contents in the
392 melt inclusions of Colli Albani mafic cumulate (Gaeta et al., 2009). Using the $H_2O + CO_2$
393 saturation values measured in the K-melts of Colli Albani at 0.20-0.50 GPa (Behrens et al.,
394 2009), the volatile content in the melt inclusion of the TP-Fall sample (Fig. 9) indicates a
395 pressure of about 0.2 GPa that is in agreement with the barometric estimation obtained from
396 the Group II clinopyroxene compositions (Table 1 and S1). The latter, as well as the
397 amphibole, show high Fe^{3+}/Fe^{2+} ratio due to redox conditions characterized by high values
398 of f_{O2} (i.e., from QFM +1 to QFM +4; Gaeta et al., 2000) but at a_{H2O} <1 as suggested by the

F, SO_3, Cl abundances in the K-foiditic glasses (Table 2). The Tufo del Palatino pre-eruptive magmatic system is definitely characterized by the a_{H2O} <1 and high CO_2 activity in the melt, as testified by the early crystallization of CO_3-bearing apatite (Fig. 6), and by the high CO_2 activity in the volatile phase which led to the calcium carbonate crystallization in the vesicles of the scoria clasts (Fig. 3d, Table S1). Noteworthy, the volatile contents in the Tufo del Palatino glasses (Table 2 and Table S1) are lower respect those estimate for the pre-eruptive system because the syn-eruptive, glass transition of the Tufo del Palatino magma occurred at low pressure (<0.1 GPa) in agreement with the hydromagmatic style of the eruption.

5.3. Phase relationships in the K-foiditic melts

Phase relationships of peculiar silicate melts like the K-foidites still remain enigmatic in spite of the availability of powerful thermodynamic software (e.g., MELTS; Ghiorso and Sack, 1995) and experimental studies of crystallization at controlled conditions (e.g., Gupta, 1972; Yoder, 1986; Melzer and Foley, 2000). Actually, in the pseudo-ternary forsterite-leucite-diopside (hereafter Ol-Cpx-Lc) system at atmospheric pressure (Gupta, 1972), the compositions of central Italy leucitites (e.g., Lustrino et al., 2019), as well as the Colli Albani K-foiditic glasses, fall around the olivine-leucite cotectic (Fig. 12), despite the petrographic characteristics of these rocks does not show evidence of olivine+leucite equilibrium in the absence of clinopyroxene. Tufo del Palatino scoria clasts show Group II clinopyroxenes in equilibrium with the K-foiditic melt but also Group I clinopyroxene, crystallized early (i.e., antecrysts), in a more primitive magma (e.g., AH38f) in equilibrium with the olivine. Moreover, in the groundmass of the K-foiditic lava flows of the Colli Albani the association clinopyroxene+leucite+olivine is also present (Gozzi et al., 2014). The petrographic features of the leucite-bearing rocks of the Colli Albani indicate that the Ol-Cpx-Lc diagram is suitable for representing the crystallization of these rocks but with a different topology from

424 that at atmospheric pressure. On the one hand, the presence of H_2O in the K-foiditic glasses
425 (Table 2 and Fig. 9) and the clinopyroxene-based barometric estimations indicate
426 crystallization conditions at P >1 atm of the phonotephritic parental magmas. On the other
427 hand, the P_{H2O}>1-2 kbar or the high F activity in the system allow the early
428 clinopyroxene+phlogopite crystallization in the phonotephritic magmas. The early
429 crystallization of phlogopite, in turn, causes the departure from the Ol-Cpx-Lc compositional
430 plane with the formation of melts characterized by high silica contents and in equilibrium
431 with K-feldspar ± leucite. Actually, the experiments on F- and H_2O-bearing Cpx-Ks-Ol-Qz
432 system indicate that crystallization, at pressure up to 1.8 GPa, in which phlogopite is present
433 on the liquidus, leads to the formation of phonolites and trachytes but not to K-foidites
434 (Melzer and Foley, 2000). Silica undersaturated melts in equilibrium with phlogopite and
435 leucite ± kalsilite are probably restricted to extremely Ca-poor magmatic system and are not
436 comparable to the composition of the K-foiditic melts of Colli Albani. The crystallization of
437 primitive K-melts at P >1 atm in dry conditions (and/or that does not allow the phlogopite
438 crystallization) it is also unlikely because it occurs at very high temperatures (>1350°C)
439 above that of geothermometric estimation obtained from Group I clinopyroxene (Table 1
440 and S1). Noteworthy, the clustering of the Colli Albani K-foidites in a relatively narrow zone
441 of the Ol-Cpx-Lc diagram suggest the occurrence of a thermal minimum towards which final
442 products of a fractional crystallization converge (Fig. 13). This zone could be represented
443 by melt compositions in equilibrium with Cpx + Lc ± Ol + vapor obtained at 0.2 GPa and
444 a_{H2O} <1 (Fig. 13), starting from a potassic phonotephrite doped with carbonate (Iacono-
445 Marziano et al., 2007; Freda et al., 2008). In particular, the Ol-Cpx-Lc multiple saturation,
446 the abruptly decreases of residual melt (i.e., 57 wt % of crystallization) and the low amount
447 of normative larnite (i.e., 3 wt %) indicate that the composition of the experimental glass
448 obtained by Iacono-Marziano et al., (2007) at 1100 °C and 0.2 GPa is almost representative

449 of a thermal minimum in the Ol-Cpx-Lc system. As the experimental clinopyroxenes are
450 solid solutions with large chemical variations it is not an invariant point. The Ol-Cpx-
451 Lc+melt+vapor equilibrium replaces at 1 atm <P <0.5 GPa (i.e. the experimental condition
452 of Freda et al., 2008) the reaction point Ol + Cpx + Melt = Cpx + Phl + Melt in the system
453 Cpx-Ks-Ol-Qz. Noteworthy, from the point of phlogopite crystallization starts the
454 univariant boundary line Cpx + Phl + Melt that is a piercing point in the Ol-Cpx-Lc plan
455 leading to differentiated compositions of the system Cpx-Ks-Ol-Qz. These compositions are
456 impoverished in magnesium and calcium, and they are in equilibrium with K-
457 feldspar±leucite (i.e., phonolitic compositions; Melzer and Foley, 2000). Otherwise, in
458 absence of phlogopite crystallization, the plane Ol-Cpx-Lc it is considered a thermal barrier
459 in the system Cpx-Ks-Ol-Qz (Yoder, 1986) that divided the crystallization paths toward K-
460 foidites (i.e., in the Ol-Cpx-Lc-Ks volume) from those towards silica oversaturated melts
461 (i.e., in the Ol-Cpx-Lc-Qz volume). It is worth stressing that in the system Cpx-Ks-Ol-Qz at
462 P >1 atm the change from reaction point involving the phlogopite to a point in which Ol +
463 Cpx-Lc + melt is in equilibrium seems to be obtainable only through the addition of calcite
464 or dolomite that through the release of CO_2 brings the system at the volatiles saturation
465 conditions but with a_{H2O} <1 (Freda et al., 2008). These peculiar conditions allow the
466 expansion of the leucite and clinopyroxene stability field at the expense of phlogopite (i.e.,
467 the a_{H2O} <1 effect) and olivine (i.e., the P >1 atm effect) and the appearance of the Ol-Cpx-
468 Lc-melt equilibrium at temperatures compatible with those here obtained from the
469 geothermometers (Table 1 and S1). The phase relationships reported in Figure 12 are valid
470 for potassic melts with a normative larnite content <10 wt %. In the Ol-Cpx-Lc-Mel
471 (melilite) volume, at 0.2 GPa and a_{H2O} <1, the equilibrium Ol-Cpx-Lc-melt disappears at Fo
472 <10 wt % and T <1100 °C and below this temperature the melt composition is in equilibrium
473 with clinopyroxene and leucite. The disappearance of olivine is due to the increase of

474 calcium activity that drives the reaction $Mg_2SiO_4 + 2CaO + 3SiO_2^{melt} = 2CaMgSi_2O_6$ to the
475 right and, in turn, changes the Ol-Cpx-Lc-melt piercing point into a reaction point. In the Ol-
476 Cpx-Lc-Mel system from the reaction point starts a divergent surface containing the Cpx-
477 Lc-melt phases. This divariant surface converges toward the thermal minimum of the Ol-
478 Cpx-Lc-Mel system where Cpx + Lc + Mel + melt coexist. The K-foiditic melts of Colli
479 Albani are contained on this surface and plot close to the Cpx + Lc cotectic line when the
480 glass composition is projected from the melilite corner on the Ol-Cpx-Lc system at $P \geq 0.2$
481 GPa and $a_{H2O} < 1$ (Fig. 12).
482
483 **5.4. Role of the carbonate assimilation**
484 The thermal barrier represented by the Ol-Cpx-Lc surface in the Cpx-Ks-Ol-Qz system does
485 not act in the first steps of the primitive potassic magmas differentiation. Actually, in the
486 Cpx-Ks-Ol-Qz system, the crystallization path starts within the olivine + melt phase volume
487 and/or on the Ol + Cpx + melt surface where the degrees of freedom of are high. In this step
488 of the magmatic differentiation, unless the magmas were not already strongly undersaturated
489 in silica, it is relatively easy that changes in pressure, volatile activities and oxygen fugacity
490 bring the primitive potassic melts towards phonolitic and/or silica oversaturated
491 compositions. The key effect of early phlogopite crystallization on the differentiation of
492 primitive potassic magmas (Melzer and Foley, 2000) has been previously discussed. The
493 lower values and narrow range of Mg# of the Tufo del Palatino phlogopite with respect to
494 Volsci Volcanic Field (VVF; Marra et al. 2021) consistently indicates a narrow phlogopite
495 stability field in the Colli Albani magmas (Fig 5). The VVF Lct-bearing scoria clasts are
496 characterized by the association of Phl with Ol in the phenocryst assemblage, which instead
497 is lacking in the Colli Albani scoria clasts (e.g., Freda et al., 1997, 2006, 2011; Palladino et
498 al., 2001; Marra et al., 2009; Gozzi et al., 2014; Gaeta et al., 2016). Other important effects

499 that increase the silica activity in the melt, during the differentiation of primitive potassic
500 magmas, are: 1) increase of the olivine stability field, caused by low oxygen fugacity and/or
501 low pressure conditions (e.g., Conte et al., 2009); 2) early crystallization of clinopyroxene
502 at high oxygen fugacity that shows a relatively low silica content due to increase of the
503 $CaFeSiAlO_6$ component in solid solution (e.g., Dolfi, 1996), and obviously 3) fractional
504 crystallization coupled with the assimilation of sialic crustal rocks (e.g., Sabatini Volcanic
505 District; Sottili et al., 2019). The assimilation of carbonate by magmas is an important open-
506 system process preventing primitive melts move away from the plane Ol-Cpx-Lc towards
507 phonolitic and/or silica oversaturated compositions. This process has been extensively
508 documented at the Colli Albani (e.g., Freda et al., 1997, 2008, 2011; Dallai et al., 2004;
509 Gaeta et al., 2006, 2009; Iacono Marziano et al., 2007; Mollo et al., 2010; Di Rocco et al.,
510 2012; Gozzi et al., 2014) and it is no coincidence that most of the known K-foidites come
511 from this district. The pristine composition of the Tufo del Palatino glasses allows to obtain
512 further information on the mass of carbonate involved in the assimilation process at the
513 origin of the K-foiditic melts. Major element mass balance calculations indicate that it is
514 possible to obtain the K-foiditic compositions of the Tufo del Palatino glasses starting from
515 the parental magma (i.e., the phonotephrite AH38f, Table 2) by subtracting a solid
516 assemblage made of Cpx (37.0 wt %) + Lc (24.9 wt %) + Mgt (3.8 wt %) + Ap (1.6 wt %;
517 mineral composition are indicated in Table S1). In order to obtain low square residuals (i.e.,
518 $\Sigma r^2 = 0.4$) in the mass balance calculations, we must also consider the assimilation of ~4 wt
519 % of calcite corresponding to a low (<0.1) M^o_a/M^o_m ratio, where M^o_m is the mass of pristine
520 melt to which assimilant mass M^o_a is added. Results of mass balance calculations are in
521 agreement with the mineralogical composition and the texture (e.g., Ti-mgt and apatite
522 inclusions in clinopyroxenes; Fig. 2a) observed in the Tufo del Palatino scoria clasts and
523 with the phase relationships observed in the assimilation experiments (Iacono Marziano et

524 al., 2007; Freda et al., 2008). Trace elements are much more sensible tracers, being able to
525 distinguish between closed-system (i.e., fractional crystallization) and open-system (i.e.,
526 magma mixing and assimilation fractional crystallization) processes, since their low
527 concentrations in crystals and melts vary significantly. Starting from the trace element
528 abundances in the AH38f phonotephrite (i.e., the parental magma) the FC model reproduces
529 well the leucite compatible elements (i.e., Rb, Cs) but increases the incompatible trace
530 elements with respect to what measured in the Tufo del Palatino glasses (Fig. 13a). A similar
531 result is obtained in the fractional crystallization of the AH38f phonotephritic magma open
532 to carbonate assimilation using the AFC algorithm proposed by DePaolo (1981). Otherwise,
533 the trace abundance in the Tufo del Palatino glasses is well reproduced (Fig. 13b) with a
534 calcite-assimilation fractional crystallization model using the FCA algorithm (Cribb and
535 Barton, 1996). The FCA model more faithfully reproduces the nature of the carbonate
536 assimilation process because implicitly considers CO_2 degassing that makes the mass
537 assimilated and the mass crystallized independent. Interesting, the FCA model based on the
538 trace elements (Fig. 13b) indicates a large amount of carbonate (~12.4 wt %) involved in the
539 assimilation process. The ability of magmatic systems to the continuous CO_2-degassing is a
540 limiting factor for the assimilation of so large amount of carbonate at low pressure (<300
541 MPa). Moreover, in case of high ratio M^o_a/M^o_m, the assimilation of cold (~350 °C) wall rock
542 induces considerable cooling of the magma. Nevertheless, magma cooling is compensated
543 by the latent heat of crystallization that, in turn, is function of two parameters: the
544 temperature interval of crystallization and the viscosity of the melt. These two parameters
545 are not independent each other. On one hand, the enlargement of the temperature interval of
546 crystallization depends by the decrease of the glass transition and solidus temperatures. On
547 the other hand, the glass transition temperature is related to the melt viscosity that controls
548 also the crystal growth rate. Actually, In isothermal conditions, the crystal growth rate is

549 function of the melt polymerization that enhancing the melt viscosity lowers the diffusivity
550 of elements in the melt (Bonechi et al. 2020a). The peculiar phase relations and the melt
551 rheology of the K-foiditic magmas, largely different from those occurring in other
552 differentiated potassic magmas (i.e., phonolite or trachyte), lead to unique distribution of the
553 latent heat across the crystallization interval of the K-foidites (e.g., Lange et al., 1994). The
554 experiments on the potassic phonotephrite doped with carbonate (Freda et al., 2008) indicate
555 that the crystallization of clinopyroxene and leucite in equilibrium with a K-foiditic melt
556 proceed over a relatively large (>200 °C) temperature interval (Fig. 14a). In the Colli Albani
557 rocks, this large temperature interval is confirmed by the occurrence of garnet in the scoria
558 clasts (Freda et al., 1997; this work), as well as by magmatic calcite ($T_{dissociation}$<900°C) in
559 the groundmass of the lava flows (Gozzi et al., 2014). Moreover, K-foiditic melts are
560 significantly less viscous than the phonolitic and trachytic melts (Fig. 14b), allowing a rapid
561 nucleation and growth of leucite and clinopyroxene (e.g., Bonechi et al., 2020a). The syn-
562 eruptive, high growth rate of leucite is clearly indicated by the star-like habit (Fig. 3b), while
563 the apatite inclusions (Fig. 2a) sustain the high growth rate of clinopyroxene during the
564 differentiation process of the phonotephritic parental magma. The phosphorus saturation in
565 the boundary layer led to apatite precipitation and its entrapment at the clinopyroxene rim.
566 As observed in many experimental studies (e.g., Bonechi et al., 2020a) high growth rates are
567 favoured by large degree of undercooling. Efficiency of the carbonate assimilation process
568 that origin K-foiditic magmas in the Colli Albani magmatic system is due to the combination
569 and/or the feedback of the low melt viscosity, the large temperature interval of crystallization
570 and the undercooling.
571
572 **6. Conclusions**

573 The K-foiditic magmas of the Colli Albani Volcanic District originate from the combination
574 of the mantle metasomatism (not discussed) and the crustal assimilation which cannot be
575 responsible for the rarity of this type of magmatism as they are active petrological processes
576 on a global scale, and they have certainly been in the past too. Nevertheless, these are open
577 system processes with high degrees of freedom that can greatly affect the final results.
578 Closed-system magmatic differentiation of the ultrapotassic primitive magmas is
579 characterized by the fractional crystallization of olivine, olivine + clinopyroxene and by the
580 early crystallization of phlogopite (i.e., together the clinopyroxene) which leads to phonolitic
581 or trachytic melts but not foiditic melts. K-foiditic magmas, similar to those that fed Tufo
582 del Palatino explosive eruption, are the result of the fractional crystallization of
583 clinopyroxene ± olivine and clinopyroxene + leucite from phonotephritic parental magmas.
584 The reduction of the olivine and phlogopite stability fields in favor of those of clinopyroxene
585 and leucite seems to occur only during the fractional crystallization in a system open to the
586 assimilation of carbonate. The efficiency of this process is due to the combination of intrinsic
587 factors of K-foiditic magmas, which can be considered of general value, such as the low
588 viscosity and the cotectic crystallization of clinopyroxene and leucite in an extended
589 temperature range and a local factor linked exclusively to the geological contest of the Colli
590 Albani Volcanic district: the thickness and the depth of the carbonate substrate.
591
592 **Acknowledgment**
593 We are very grateful to the Editor Michael Roden and two anonymous reviewers for their
594 helpful and constructive comments. We thank to C. Romano (Roma Tre University) for the
595 access to the RAMAN facility and M. Serracino (CNR-IGAG) for assistance during EPMA
596 analytical sessions.
597

598 **Funding**

599 This research has been conducted with the financial support of the HP-HT Laboratory at the
600 Department of Earth Sciences of Sapienza - University of Rome

601

602 **References**

603 Ammannati, E., Jacob, D., Avanzinelli, R., Foley, S.F., 2016. Low Ni olivine in silica-
604 undersaturated ultrapotassic igneous rocks as evidence for carbonate metasomatism in the
605 mantle. Earth Planet. Sci. Lett. 444, 64–74.

606 Avanzinelli, R., Casalini, M., Elliott, T., Conticelli, S., 2018. Carbon fluxes from subducted
607 carbonates revealed by uranium excess at Mount Vesuvius, Italy. Geology 46, 259–262.
608 https://doi.org/10.1130/G39766.1

609 Awonusi, A., Morris, M.D., Tecklenburg, M.M.J., 2007. Carbonate assignment and
610 calibration in the Raman spectrum of apatite. Calcif. Tissue Int. 81, 46–52.
611 https://doi.org/10.1007/s00223-007-9034-0

612 Bianchi, I., Piana Agostinetti, N., De Gori, P., Chiarabba, C., 2008. Deep structure of the
613 Colli Albani volcanic district (central Italy) from receiver functions analysis. J Geophys Res
614 113:B09313. https://doi:10.1029/2007JB005548

615 Behrens, H., Misiti, V., Freda, C., Vetere, F., Botcharnikov, R.E., Scarlato, P., 2009.
616 Solubility of H_2O and CO_2 in ultrapotassic melts at 1200 and 1250 °C and pressure from 50
617 to 500 MPa. Am. Mineral. 94, 105–120. https://doi.org/10.2138/am.2009.2796

618 Boari, E., Avanzinelli, R., Melluso, L., Giordano, G., Mattei, M., De Benedetti, A.A., Morra,
619 V., Conticelli, S., 2009. Isotope geochemistry (Sr-Nd-Pb) and petrogenesis of leucite-
620 bearing volcanic rocks from “Colli Albani” volcano, roman magmatic province, central
621 Italy: Inferences on volcano evolution and magma genesis. Bull. Volcanol. 71, 977–1005.
622 https://doi.org/10.1007/s00445-009-0278-6

623 Bonechi, B., Perinelli, C., Gaeta, M., 2020a. Clinopyroxene growth rates at high pressure:
624 constraints on magma recharge of the deep reservoir of the Campi Flegrei Volcanic District
625 (south Italy). Bull. Volcanol. 82, 5. https://doi.org/10.1007/s00445-019-1342-5
626 Bonechi, B., Perinelli, C., Gaeta, M., Tecchiato, V., Fabbrizio, A., 2020b. Amphibole growth
627 from a primitive alkaline basalt at 0.8 GPa: time-dependent compositional evolution, growth
628 rate and competition with clinopyroxene. Lithos 354–355, 105272.
629 Bonechi, B., Perinelli, C., Gaeta, M., Tecchiato, V., Granati, S.F., 2017. Experimental
630 constraints on amphibole stability in primitive alkaline and calc-alkaline magmas. Period.
631 Mineral. 86, 231–245. https://doi.org/10.2451/2017PM735
632 Bonechi, B., Perinelli, C., Gaeta, M., Fabbrizio, A., Petrelli, M. & Strnad L. Trace element
633 partitioning between clinopyroxene and alkali basaltic melts: investigation at high pressure
634 on a primitive composition from the Campi Flegrei Volcanic district (Italy). Geochimica et
635 Cosmochimica Acta, https://doi.org/10.1016/j.gca.2021.04.023.
636 Brocato, P., Diffendale, D.P., Giuliomaria, D.D., Gaeta, M., Marra, F., Terrenato, N., 2019.
637 A previously unidentified tuff in the archaic temple podium at sant'omobono, rome and its
638 broader implications. Journal of Mediterranean Archaeology. 32, 114–136.
639 Charles, R.W., 1977. The phase equilibria of intermediate compositions on the pseudo-
640 binary $Na_2CaMg_5Si_8O_{22}(OH)_2$, $Na_2Ca\ Fe_5Si_8O_{22}(OH)_2$. Am. J. Sci. 277, 594–625.
641 https://doi.org/10.2475/ajs.277.5.594
642 Conte, A.M., Dolfi, D., Gaeta, M., Misiti, V., Mollo, S., Perinelli, C., 2009. Experimental
643 constraints on evolution of leucite-basanite magma at 1 and 10^{-4} GPa : implications for
644 parental compositions of Roman high-potassium magmas. Eur. J. Mineral. 21, 763–782.
645 https://doi.org/10.1127/0935-1221/2009/0021-1934
646 Cribb, J., Barton, M., 1996. Geochemical effects of decoupled fractional crystallization and
647 crustal assimilation. Lithos 37, 293–307.

Dallai, L., Freda, C., Gaeta, M., 2004. Oxygen isotope geochemistry of pyroclastic clinopyroxene monitors carbonate contributions to Roman-type ultrapotassic magmas. Contrib. Mineral. Petrol. 148, 247–263. https://doi.org/10.1007/s00410-004-0602-2

De Hoog, J.C.M., Mason, P.R.D., Van Bergen, M.J., 2001. Sulfur and chalcophile elements in subduction zones: Constraints from a laser ablation ICP-MS study of melt inclusions from Galunggung volcano, Indonesia. Geochim. Cosmochim. Acta 65, 3147–3164. https://doi.org/10.1016/S0016-7037(01)00634-2

Devine, J.D., Gardner, J.E., Brack, H.P., Layne, G.D., Rutherford, M.J., 1995. Comparison of microanalytical methods for estimating H_2O contents of silicic volcanic glasses. Am. Mineral. 80, 319–328. https://doi.org/10.2138/am-1995-3-413

Di Battistini, G., Montanini, A., Vernia, L., Bargossi, G.M., Castorina, F., 1998. Petrology and geochemistry of ultrapotassic rocks from the Montefiascone Volcanic Complex (Central Italy): magmatic evolution and petrogenesis. Lithos 43, 169–195.

Di Genova, D., Sicola, S., Romano, C., Vona, A., Fanara, S., Spina, L., 2017. Effect of iron and nanolites on Raman spectra of volcanic glasses: A reassessment of existing strategies to estimate the water content. Chem. Geol. 475, 76–86. https://doi.org/10.1016/j.chemgeo.2017.10.035

Di Rocco, T., Freda, C., Gaeta, M., Mollo, S., Dallai, L., 2012. Magma chambers emplaced in carbonate substrate: Petrogenesis of skarn and cumulate rocks and implications for CO_2 degassing in volcanic areas. J. Petrol. 53, 2307–2332. https://doi.org/10.1093/petrology/egs051

Diffendale, D.P., Marra, F., Gaeta, M., Terrenato, N., 2019. Combining geochemistry and petrography to provenance Lionato and Lapis Albanus tuffs used in Roman temples at Sant'Omobono, Rome, Italy. Geoarchaeology 34, 187–199. https://doi.org/10.1002/gea.21702

673 Dolfi, D., 1996. Preliminary results on the effect of oxygen fugacity on magmatic
674 clinopyroxene and coexisting liquid compositions. Period. Mineral. 65, 5–14.
675 Ersoy, Y., Helvaci, C., 2010. FC-AFC-FCA and mixing modeler: A Microsoft® Excel©
676 spreadsheet program for modeling geochemical differentiation of magma by crystal
677 fractionation, crustal assimilation and mixing. Comput. Geosci. 36, 383–390.
678 https://doi.org/10.1016/j.cageo.2009.06.007
679 Fabbrizio, A., Gaeta, M., Carroll, M.R., Petrelli, M., 2018. Crystallization induced Sulfur
680 and REE zoning in apatite: The example of the Colli Albani's magmatic system. Eur. J.
681 Mineral. 125–133.
682 Fabbrizio, A., Schmidt, M. W., Günther, D., Eikenberg, J., 2008. Experimental
683 determination of radium partitioning between leucite and phonolite melt and ^{226}Ra-
684 disequilibrium crystallization ages of leucite. Chemical Geology. 255, 377–387.
685 Foley, S.F., Jenner, G.A., 2004. Trace element partitioning in lamproitic magmas-the
686 Gaussberg olivine leucitite. Lithos 75, 19–38. https://doi.org/10.1016/j.lithos.2003.12.020
687 Freda, C., Gaeta, M., Giaccio, B., Marra, F., Palladino, D.M., Scarlato, P., Sottili, G., 2011.
688 CO_2-driven large mafic explosive eruptions: The Pozzolane Rosse case study from the Colli
689 Albani Volcanic District (Italy). Bull. Volcanol. 73, 241–256.
690 https://doi.org/10.1007/s00445-010-0406-3
691 Freda, C., Gaeta, M., Karner, D.B., Marra, F., Renne, P.R., Taddeucci, J., Scarlato, P.,
692 Christensen, J.N., Dallai, L., 2006. Eruptive history and petrologic evolution of the Albano
693 multiple maar (Alban Hills, Central Italy). Bull. Volcanol. 68, 567–591.
694 https://doi.org/10.1007/s00445-005-0033-6
695 Freda, C., Gaeta, M., Misiti, V., Mollo, S., Dolfi, D., Scarlato, P., 2008. Magma-carbonate
696 interaction: An experimental study on ultrapotassic rocks from Alban Hills (Central Italy).
697 Lithos 101, 397–415. https://doi.org/10.6133/apjcn.092017.05

698 Freda, C., Gaeta, M., Palladino, D.M., Trigila, R., 1997. The Villa Senni Eruption (Alban
699 Hills, central Italy): The role of H_2O and CO_2 on the magma chamber evolution and on the
700 eruptive scenario. J. Volcanol. Geotherm. Res. 78, 103–120. https://doi.org/10.1016/S0377-
701 0273(97)00007-3
702 Gaeta, M., 1998. Petrogenetic implications of Ba-sanidine in the Lionato Tuff (Colli Albani
703 Volcanic District, Central Italy). Mineral. Mag. 62, 697–701.
704 https://doi.org/10.1180/002646198547927
705 Gaeta, M., Di Rocco, T., Freda, C., 2009. Carbonate assimilation in open magmatic systems:
706 The role of melt-bearing skarns and cumulate-forming processes. J. Petrol. 50, 361–385.
707 https://doi.org/10.1093/petrology/egp002
708 Gaeta, M., Fabrizio, G., Cavarretta, G., 2000. F-phlogopites in the Alban Hills Volcanic
709 District (Central Italy): Indications regarding the role of volatiles in magmatic
710 crystallisation. J. Volcanol. Geotherm. Res. 99, 179–193. https://doi.org/10.1016/S0377-
711 0273(00)00172-4
712 Gaeta, M., Freda, C., 2001. Strontian fluoro-magnesiohastingsite in Alban Hills lavas
713 (Central Italy): constraints on crystallization conditions. Mineral. Mag. 65, 787–795.
714 https://doi.org/10.1180/0026461016560009
715 Gaeta, M., Freda, C., Christensen, J.N., Dallai, L., Marra, F., Karner, D.B., Scarlato, P.,
716 2006. Time-dependent geochemistry of clinopyroxene from the Alban Hills (Central Italy):
717 Clues to the source and evolution of ultrapotassic magmas. Lithos 86, 330–346.
718 https://doi.org/10.1016/j.lithos.2005.05.010
719 Gaeta, M., Freda, C., Marra, F., Di Rocco, T., Gozzi, F., Arienzo, I., Giaccio, B., Scarlato,
720 P., 2011. Petrology of the most recent ultrapotassic magmas from the Roman Province
721 (Central Italy). Lithos 127, 298–308.

722 Gaeta, M., Freda, C., Marra, F., Arienzo, I., Gozzi, F., Jicha, B., Di Rocco, T., 2016.
723 Paleozoic metasomatism at the origin of Mediterranean ultrapotassic magmas: Constraints
724 from time-dependent geochemistry of Colli Albani volcanic products (Central Italy). Lithos
725 244, 151–164. https://doi.org/10.1016/j.lithos.2015.11.034
726 Ghiorso, M.S., Sack, R.O., 1995. Chemical mass transfer in magmatic processes IV. A
727 revised and internally consistent thermodynamic model for the interpolation and
728 extrapolation of liquid-solid equilibria in magmatic systems at elevated temperatures and
729 pressures. Contrib. Mineral. Petrol. 119, 197–212. https://doi.org/10.1007/BF00307281
730 Giaccio, B., Arienzo, I., Sottili, G., Castorina, F., Gaeta, M., Nomade, S., Galli, P., Messina,
731 P., 2013. Isotopic (Sr–Nd) and major element fingerprinting of distal tephras: an appli-
732 cation to the Middle–Late Pleistocene markers from the Colli Albani volcano, central Italy.
733 Quaternary Science Reviews 67, 190–206.
734 Giordano, G., De Benedetti, A.A., Diana, A., Diano, G., Gaudioso, F., Marasco, F., Miceli,
735 M., Mollo, S., Cas, R.A.F., Funiciello, R., 2006. The Colli Albani mafic caldera (Roma,
736 Italy): Stratigraphy, structure and petrology. J. Volcanol. Geotherm. Res. 155, 49–80.
737 https://doi.org/10.1016/j.jvolgeores.2006.02.009
738 Giordano, D., Russell, J. K. & Dingwell, D. B. (2008). Viscosity of magmatic liquids: a
739 model. Earth and Planetary Science Letters 271, 123-134.
740 Giordano, D., González-García, D., Russell, J.K., Raneri, S., Bersani, D., Fornasini, L., Di
741 Genova, D., Ferrando, S., Kaliwoda, M., Lottici, P.P., Smit, M., Dingwell, D.B., 2020. A
742 calibrated database of Raman spectra for natural silicate glasses: implications for modelling
743 melt physical properties. J. Raman Spectrosc. 51, 1822–1838.
744 https://doi.org/10.1002/jrs.5675

745 Gozzi, F., Gaeta, M., Freda, C., Mollo, S., Di Rocco, T., Marra, F., Dallai, L., Pack, A.,
746 2014. Primary magmatic calcite reveals origin from crustal carbonate. Lithos 190–191, 191–
747 203. https://doi.org/10.1016/j.lithos.2013.12.008
748 Gupta, A., 2015. Origin of potassium-rich silica-deficient igneous rocks. Springer, New
749 Delhi, India.
750 Gupta, A., 1972. The system Forsterite-Diopside-Akermanite-Leucite and its significance in
751 the origin of potassium-rich mafic and ultramafic volcanic rocks.. Am. Mineral. 57, 1242–
752 1259.
753 Hammer, J.E., 2008. Experimental studies of the kinetics and energetics of magma
754 crystallization. In: Putirka KD, Tepley III FJ (eds) Minerals, inclusions and volcanic
755 processes. Rev Mineral Geochemistry, 9–59.
756 Hawthorne, F.C., Oberti, R., Harlow, G.E., Maresch, W. V, Martin, R.F., Schumacher, J.C.,
757 Welch, M.D., 2012. Nomenclature of the amphibole supergroup. Am. Mineral. 97, 2031–
758 2048.
759 Hughes, E.C., Buse, B., Kearns, S.L., Blundy, J.D., Kilgour, G.N., Mader, H.M., 2019. Low
760 analytical totals in EPMA of hydrous silicate glass due t sub-surface charging: Obtaining
761 accurate volatiles by difference. Chem. Geol. 505, 48–56.
762 Humphreys, M.C.S., Kearns, S.L., Blundy, J.D., 2006. SIMS investigation of electron-beam
763 damage to hydrous, rhyolitic glasses: implications for melt inclusion analysis. Am. Mineral.
764 91, 667–679.
765 Iacono Marziano, G., Gaillard, F., Pichavant, M., 2007. Limestone assimilation and the
766 origin of CO_2 emissions at the Alban Hills (Central Italy): Constraints from experimental
767 petrology. J. Volcanol. Geotherm. Res. 166, 91–105.
768 https://doi.org/10.1016/j.jvolgeores.2007.07.001

769 Kimura, M., Mikouchi, T., Suzuki, A., Miyahara, M., Ohtani, E., El Goresy, A., 2009.
770 Kushiroite, $CaAlAlSiO_6$: A new mineral of the pyroxene group from the ALH 85085 CH
771 chondrite, and its genetic significance in refractory inclusions. Am. Mineral. . 94, 1479–
772 1482.
773 Lange, R.A., Cashman, K. V., Navrotsky, A., 1994. Direct measurements of latent heat
774 during crystallization and melting of a ugandite and an olivine basalt. Contrib. Mineral.
775 Petrol. 118, 169–181. https://doi.org/10.1007/BF01052867
776 Le Bas, M.J., W, L.M.R., Streckeisen, A., Zanettin, B., 1986. A chemical classification of
777 volcanic rocks based on the total alkali-silica diagram. J. Petrol.
778 https://doi.org/10.1093/petrology/27.3.745
779 Le Losq, C., Neuville, D.R., Moretti, R., Roux, J., 2012. Determination of water content in
780 silicate glasses using Raman spectrometry: Implications for the study of explosive
781 volcanism. Am. Mineral. 97, 779–790. https://doi.org/10.2138/am.2012.3831
782 Leake, B.E., Woolley, A.R., S, C.E., A, M.C.G.U.S., Canada, J.D.G., Hawthorne, F.C.,
783 Kisch, H.J., Krivovichev, V.G., Canada, J.A.M., Maresch, W. V, Schumacher, J.C., France,
784 D.C.S., Stephenson, N.C.N., Whittaker, E.J.W., 1997. Nomenclature of Amphiboles: report
785 of the subcommittee on amphiboles of the international mineralogical association,
786 commission on new minerals and mineral names. Can. Mineral. 35, 219–246.
787 Leicher, N., Zanchetta, G., Sulpizio, R., Giaccio, B., Wagner, B., Nomade, S., Francke, A.,
788 Del Carlo, P., 2016. First tephrostratigraphic results of the DEEP site record from Lake
789 Ohrid (Macedonia and Albania). Biogeosciences, 13, 2151–2178.
790 Lustrino, M., Fedele, L., Agostini, S., Prelević, D., Salari, G., 2019. Leucitites within and
791 around the Mediterranean area. Lithos 324–325, 216–233.
792 https://doi.org/10.1016/j.lithos.2018.11.007

793 Masotta, M., Gaeta, M., Gozzi, F., Marra, F., Palladino, D.M., Sottili, G., 2010. H2O- and
794 temperature-zoning in magma chambers: The example of the Tufo Giallo della Via Tiberina
795 eruptions (Sabatini Volcanic District, central Italy). Lithos, 118, 119–130.
796 Marra, F., Danti, A., Gaeta, M., 2015. The volcanic aggregate of ancient Roman mortars
797 from the Capitoline Hill: Petrographic criteria for identification of Rome's pozzolans and
798 historical implications. J. Volcanol. Geotherm. Res., 308, 113–126.
799 Marra, F., Cardello, L., Gaeta, M., Jicha, B., Montone, P., Niespolo, E., Nomade, S.,
800 Palladino, D.M., Pereira, A., De Luca, G., Florindo, F., Frepoli, A., Renne, P., Sottili, G.,
801 2021. The Volsci Volcanic Field (central Italy): an open window on continental subduction
802 processes. Int. J. Earth Sci. in press.
803 Marra, F., Karner, D.B., Freda, C., Gaeta, M., Renne, P., 2009. Large mafic eruptions at
804 Alban Hills Volcanic District (Central Italy): Chronostratigraphy, petrography and eruptive
805 behavior. J. Volcanol. Geotherm. Res. 179, 217–232.
806 https://doi.org/10.1016/j.jvolgeores.2008.11.009
807 McDonough, W.F., Sun, S. s., 1995. The composition of the Earth. Chem. Geol. 120, 223–
808 253. https://doi.org/10.1016/0009-2541(94)00140-4
809 Melzer, S., Foley, S.F., 2000. Phase relations and fractionation sequences in potassic magma
810 series modelled in the system $CaMgSi_2O_6$-$KAlSiO_4$-Mg_2SiO_4-SiO_2-F_2O_{-1} at 1 bar to 18 kbar.
811 Contrib. Mineral. Petrol. 138, 186–197. https://doi.org/10.1007/s004100050017
812 Mollo, S., Gaeta, M., Freda, C., Di Rocco, T., Misiti, V., Scarlato, P., 2010. Carbonate
813 assimilation in magmas: A reappraisal based on experimental petrology. Lithos 114, 503–
814 514. https://doi.org/10.1016/j.lithos.2009.10.013
815 Morimoto, N., 1988. Nomenclature of Pyroxenes. Mineral. Petrol. 39, 55–76.
816 https://doi.org/10.1007/BF01226262

817 Palladino, D.M., Gaeta, M., Marra, F., 2001. A large K-foiditic hydromagmatic eruption
818 from the early activity of the Alban Hills Volcanic District, Italy. Bull. Volcanol. 63, 345–
819 359. https://doi.org/10.1007/s004450100150
820 Pearce, N.J.G., Perkins, W.T., Westgate, J.A., Gorton, M.P., Jackson, S.E., Neal, C.R.,
821 Chenery, S.P., 1997. A compilation of new and published major and trace element data for
822 NIST SRM 610 and NIST SRM 612 glass reference materials. Geostand. Newsl. 21, 115–
823 144. https://doi.org/10.1111/j.1751-908X.1997.tb00538.x
824 Putirka, K.D., 2008. Thermometers and Barometers for Volcanic Systems, in: Putirka, K.D.,
825 Tepley III, F.J. (Eds.), Minerals, Inclusions And Volcanic Processes. Reviews in Mineralogy
826 and Geochemistry, pp. 61–120. https://doi.org/10.2138/rmg.2008.69.3
827 Rolandi, G., Munno, R. & Postiglione, I. (2004). The A.D. 472 eruption of the Somma
828 volcano. Journal of Volcanology and Geothermal Research 129, 291–319.
829 Scaillet, B., Pichavant, M., Cioni, R., 2008. Upward migration of Vesuvius magma chamber
830 over the past 20,000 years. Nature 455, 216–219. https://doi.org/10.1038/nature07232
831 Singh, P., Arima, M., Gupta, A., 2000. Phase equilibrium constraints on the petrogenesis of
832 nephelinites with reference to the system diopside nepheline under variable P T conditions
833 in the presence or absence of water. J. Mineral. Petrol. Sci. 95, 113–124.
834 Shaw, C.S.J., 2018. Evidence for the presence of carbonate melt during the formation of
835 cumulates in the Colli Albani Volcanic District, Italy. Lithos. 310–311, 105–119.
836 Skála, R., Strnad, L., McCammon, C., Čada, M., 2009. Moldavites from the Cheb Basin,
837 Czech Republic. Geochim. Cosmochim. Acta 73, 1145–1179.
838 https://doi.org/10.1016/j.gca.2008.11.003
839 Sottili, G., Arienzo, I., Castorina, F., Gaeta, M., Giaccio, B., Marra, F., Palladino, D.M.,
840 2019. Time-dependent Sr and Nd isotope variations during the evolution of the ultrapotassic

841 Sabatini Volcanic District (Roman province, Central Italy). Bull. Volcanol. 81.
842 https://doi.org/10.1007/s00445-019-1324-7
843 Strnad, L., Mihaljevic, M., Sebek, O., 2005. Laser Ablation and Solution ICP-MS
844 Determination of Rare Earth Elements in USGS BIR-1G, BHVO-2G and BCR-2G Glass
845 Reference Materials. Geostand. Geoanalytical Res. 29, 303–314.
846 https://doi.org/10.1111/j.1751-908x.2005.tb00902.x
847 Thompson, R. (1977). Primary basalts and magma genesis. III. Alban Hills, Roman
848 Comagmatic Province, Central Italy. Contributions to Mineralogy and Petrology 60, 91–
849 108.
850 Wallace, P.J., 2005. Volatiles in subduction zone magmas: Concentrations and fluxes based
851 on melt inclusion and volcanic gas data. J. Volcanol. Geotherm. Res. 140, 217–240.
852 https://doi.org/10.1016/j.jvolgeores.2004.07.023
853 Washington, H., 1906. The Roman comagmatic region. Carnegie Inst. Washingt. 56, 206–
854 214.
855 Yoder, H.S., 1986. Potassium-rich Rocks: Phase Analysis and Heteromorphic Relations. J.
856 Petrol. 27, 1215–1228. https://doi.org/10.1093/petrology/27.5.1215
857

858 **Figure captions**

859 **Figure 1 -** Stratigraphic successions and chronological constraints available for Colli Albani
860 Volcanic District (a). Simplified geologic map of the Colli Albani Volcanic District with the
861 same colours used in the stratigraphic successions (b). Satellite image showing the outcrop
862 area of the pyroclastic-flow deposits of Tufo del Palatino and the sites (geographic
863 coordinates in Table S1) where the analyzed samples were collected: 1) TP-Fall; 2) TP-ST;
864 3) TP-SO1; 4) TP-CH, 5) TP-RT; 6) TP-TAB; 7) TP-VM; 8) TP-VP; 9) TP-VG; 10) TP-
865 EU; 11) TP-PVF (c).

Figure 2 - Photomicrographs of the Tufo del Palatino scoria clasts in plane-polarized light. Group II, pale green, euhedral clinopyroxene with Ti-magnetite, apatite and melt inclusions (a). Group III, deep green clinopyroxene in equilibrium with MgO-poor melt and garnet (b). Microphenocryst of phlogopite in a cryptocrystalline scoria clast with star-like leucites and calcite-bearing vesicles (c). Subhedral, brown garnet (d). Cpx: clinopyroxene; Ti-Mgt: Ti-magnetite; Amph: amphibole; Cc: calcite.

Figure 3 - Photomicrographs of the Tufo del Palatino scoria clasts in plane-polarized light (a, b, c) and crossed polars (d). Aphyric, glassy scoria clast with scarce vesiculation (a). Glassy scoria clast showing scarce leucite microcrysts characterized by star-like habit and calcite-bearing vesicles (b). Glassy scoria clast showing leucite microcrysts ranging from euhedral to star-like (c). Detail of a large vesicle showing the zeolite rim and the calcite core (d). Cpx: clinopyroxene; Ti-Mgt: Ti-magnetite; Amph: amphibole; Cc: calcite.

Figure 4 - Binary covariation plot of diopside (Di) vs Tschermak (Ts) components expressed as the sum of kushiroite ($CaAl_2SiO_6$), essenite ($CaFeSiAlO_6$), CaTi-Tschermak (CaTiTs, $CaTiAl_2O_6$) and CaCr-Tschermak (CaCrTs, $CaCrAlSiO_6$) for clinopyroxenes in the Tufo del Palatino scoria clasts.

Figure 5 - Phlogopite chemical compositions from Tufo del Palatino (this work), Colli Albani (data from Gaeta et al., 2000) and Volsci Volcanic Field (yellow field, data from Marra et al., 2021) scoria clasts, reported in the Ti-Mg/(Mg + Fe^{2+}) (upper) and F-Mg/(Mg + Fe^{2+}) (lower) diagrams.

Figure 6 - Raman spectra of Tufo del Palatino apatite. Insets are Raman spectra portions (Awonusi et al., 2007) of CO_3-bearing apatite from 0.03 wt % in a-spectra to 7.9 wt % in f-spectra. Raman spectra were processed (baseline correction and smoothing) using the Spectragryph© software (F. Menges, "Spectragryph - optical spectroscopy software", Version 1.2.14, 2016-2020, http://www.effemm2.de/spectragryph/) (a). Plots illustrating a

linear relationship between: (100-$EMPA_{tot}$) + SO_3 vs $2P_2O_5$ wt % (b) and (100-$EMPA_{tot}$) + SO_3 vs $2P_2O_5$ wt % (c) in the apatite crystals of the Tufo del Palatino scoria clasts. The (100-$EMPA_{tot}$) wt % content is representative of the CO_3 content in the apatite.

Figure 7 - Total alkali versus silica classification diagram (Le Bas et al., 1986) of the Tufo del Palatino glasses and the parental magma (AH38f).

Figure 8 - Major oxide vs MgO (a,b and c) and S vs F (d) co-variations for the Tufo del Palatino glasses and the parental magma (AH38f). Symbols are as in Fig. 7.

Figure 9 – Raman spectra for the melt inclusion (TP-Fall) and glasses (TP-SO1 and TP-VM). The melt inclusion shows higher H_2O respect to the glasses and the presence of CO_3. Green field indicates the silicates region (200-1400 cm^{-1}) while the light blue field indicates the water region (2700-4000 cm^{-1}). H_2O^{Raman} is the water content estimated following the methods of Di Genova et al. (2017) (see §Analytical Methods for detail). Details of the Raman processing as in Fig. 7.

Figure 10 - Primitive Mantle normalized (McDonough and Sun, 1995) trace element abundances for Tufo del Palatino glasses and primitive lava flows from Colli Albani volcanic district. MdT, AH32, AH7a and AH38f have MgO content (wt %) of 5.15, 4.54, 6.43 and 7.07, respectively.

Figure 11 - Primitive Mantle normalized (McDonough and Sun, 1995) trace element abundances for Tufo del Palatino clinopyroxenes. Clinopyroxenes were arranged in Cpx groupI, Cpx group II and Cpx group III as function of their content in diopside (Di) and Tshermak (STs) components (see the text).

Figure 12 - Olivine (Ol), clinopyroxene (Cpx), leucite (Lc) compositional (wt%) plane showing the phase relations at 0.2 GPa and a_{H2O} <1 and at 0.001 GPa. The Ol, Cpx and Lc normative compositions reported in the diagram are calculated assuming $An_{Normative}$ = $CaAl_2Si_2O_8$ = $CaAl_2SiO_6$ + SiO_2, Cpx = $Di_{Normative}$ + $CaAl_2SiO_6$ and Lc = $Lc_{Normative}$ +

$Ne_{Normative} + SiO_2$, Ol = $Ol_{Normative}$. K-foiditic glasses of Colli Albani after Gaeta (1998) and Marra et al. (2009). Experimental data after Gupta (1972), Iacono Marziano et a*l*. (2007) and Freda et al. (2008).

Figure 13 - Primitive Mantle normalized (McDonough and Sun, 1995) trace elements patterns for phonotephrite (AH38f, Table 3 and S1), the average of the Tufo del Palatino glass compositions, and the predicted composition of differentiated melts obtained after fractional crystallization (FC in a), combined (AFC in b) and decoupled (FCA in c) fractional crystallization and assimilation from the AH38f phonotephrite assumed as primitive parental magma. In the three models the amount of residual melt is 37 wt % and removed solid is formed by clinopyroxene (38.9 wt %), leucite (19.3 wt %), Ti-magnetite (3.6 wt %) and apatite (1.2 wt %). The relative ratio of assimilated material to crystallized material (r) in the AFC and FCA models is r = 0.2 with the assimilated calcite composition after Gozzi *et al*. (2014). The modelled compositions were calculated by using the Excel© spreadsheet program of Ersoy and Helvaci (2010) implemented with the $K_{Dleucite/melt}$ (Foley and Jenner, 2004) and $K_{Dclinopyroxene/melt}$ (Bonechi *et al*., 2021).

Figure 14 - Phase relationships for the hydrous-carbonated parental phonotephritic composition reported in the pressure vs temperature space (modified from Freda et al., 2011). The diagram illustrates the large temperature range of clinopyroxene and leucite crystallization in equilibrium with K-foiditic melt (a). The diagram shows the variation of the viscosity with the SiO_2 content for K-foiditic glass (in blue; this study) and phonolitic and trachytic glasses (in green; database of Giordano et al., 2019). Viscosity data were calculated using the Excel© spreadsheet of Giordano et al. (2008) at atmospheric pressure and T = 1000°C (b).

Figure 1

Click here to access/download;Figure;Fig 1 revised Gaeta et al.pdf

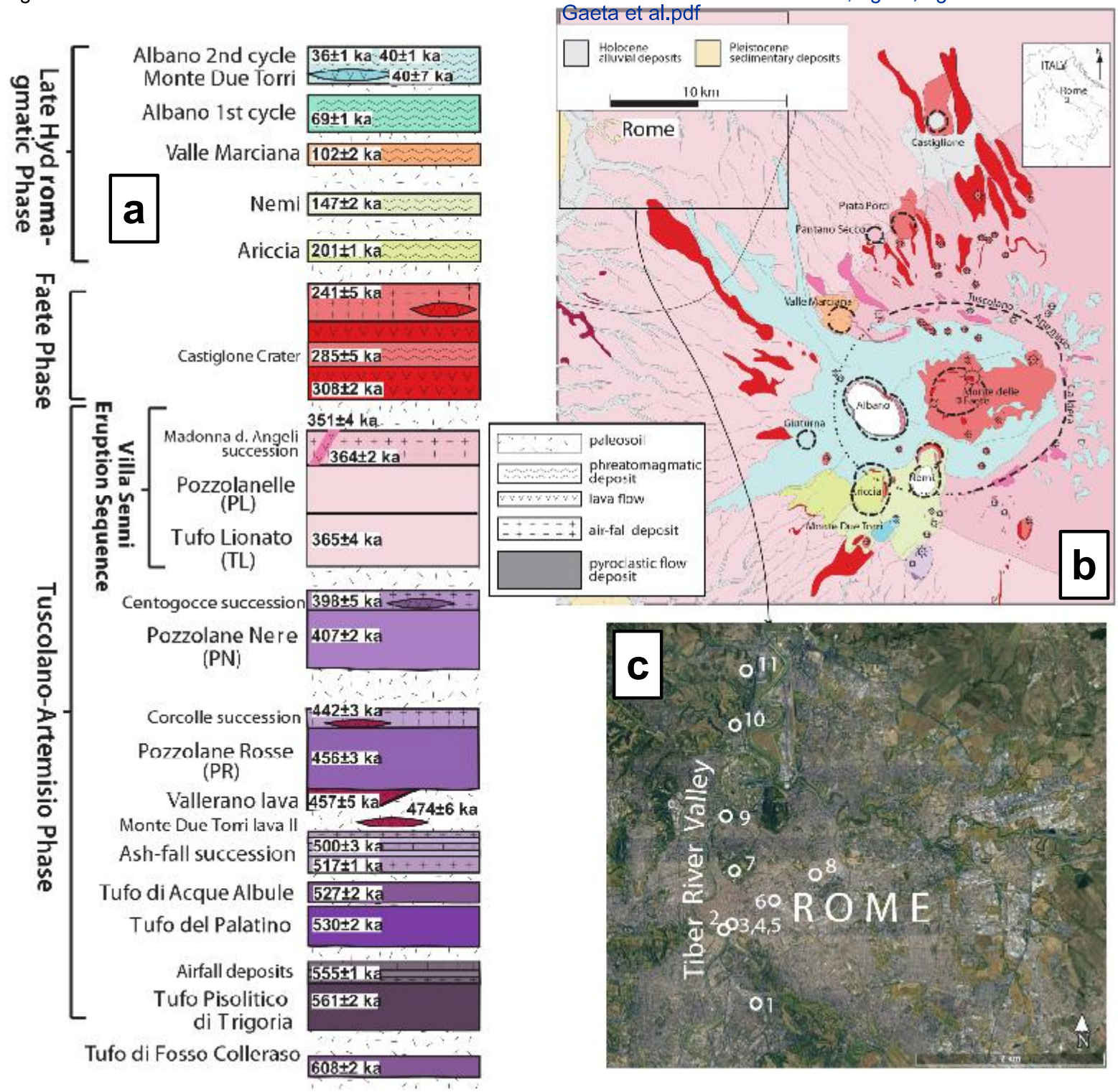

Fig. 1

Figure 2

Click here to access/download;Figure;Fig 2 revised Gaeta et al.pdf

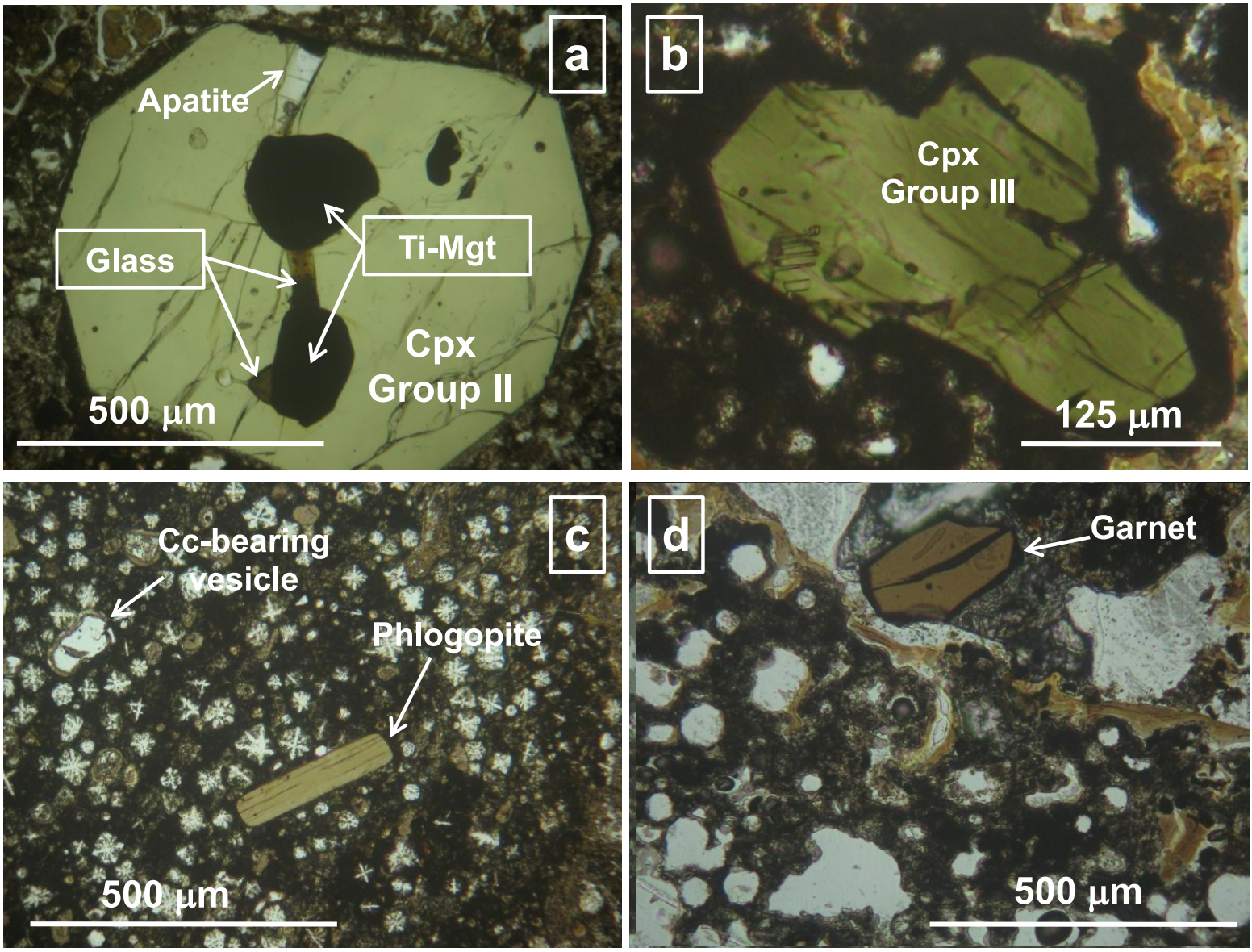

Figure 3

Click here to access/download;Figure;Fig 3 revised Gaeta et al.pdf

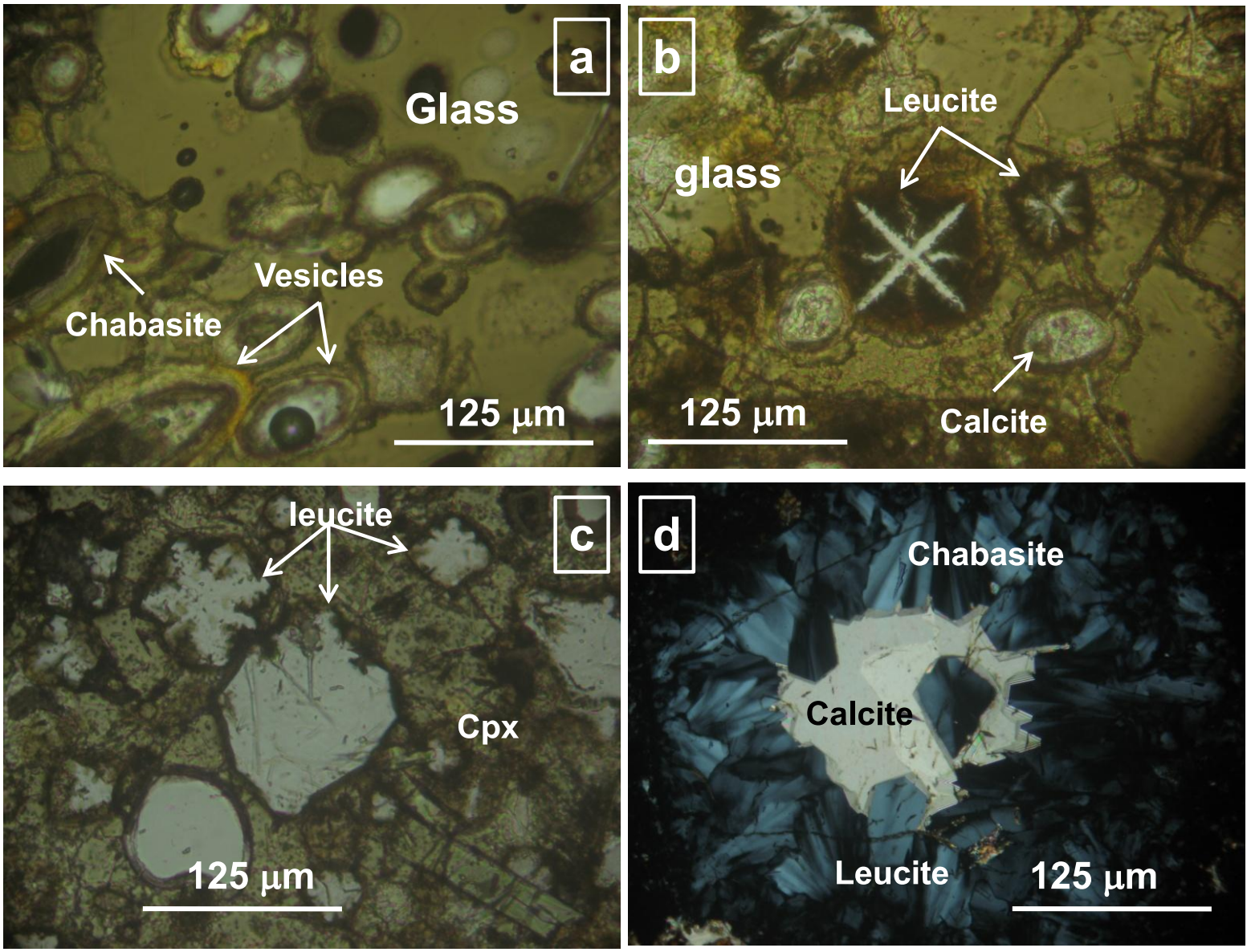

Figure 4

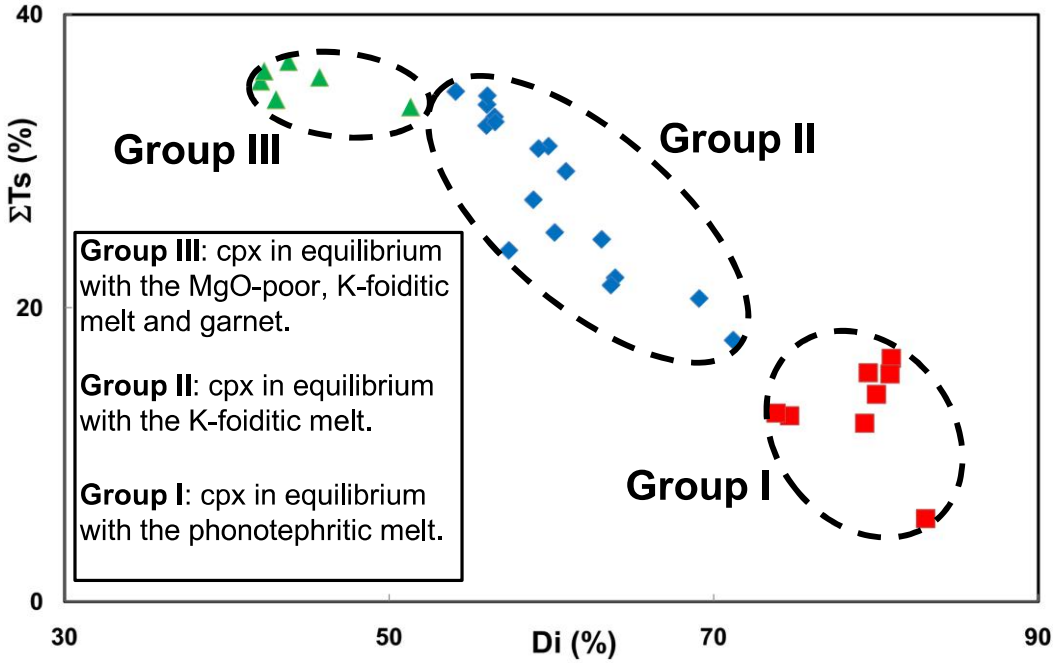

Fig.4

Figure 5

Click here to access/download;Figure;Fig 5 revised Gaeta et al.pdf

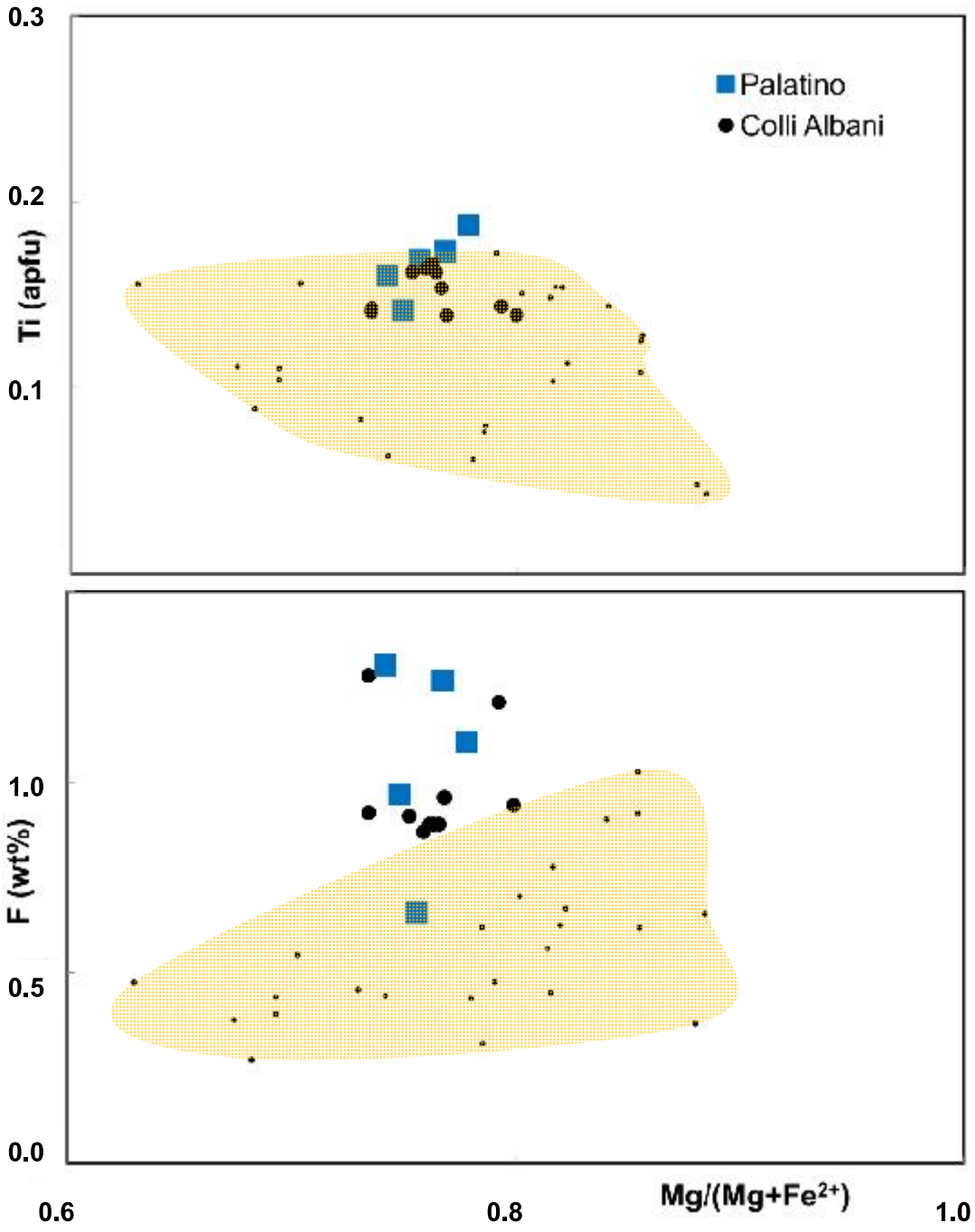

Fig. 5

Figure 6

Click here to access/download;Figure;Fig 6 revised Gaeta et al.pdf

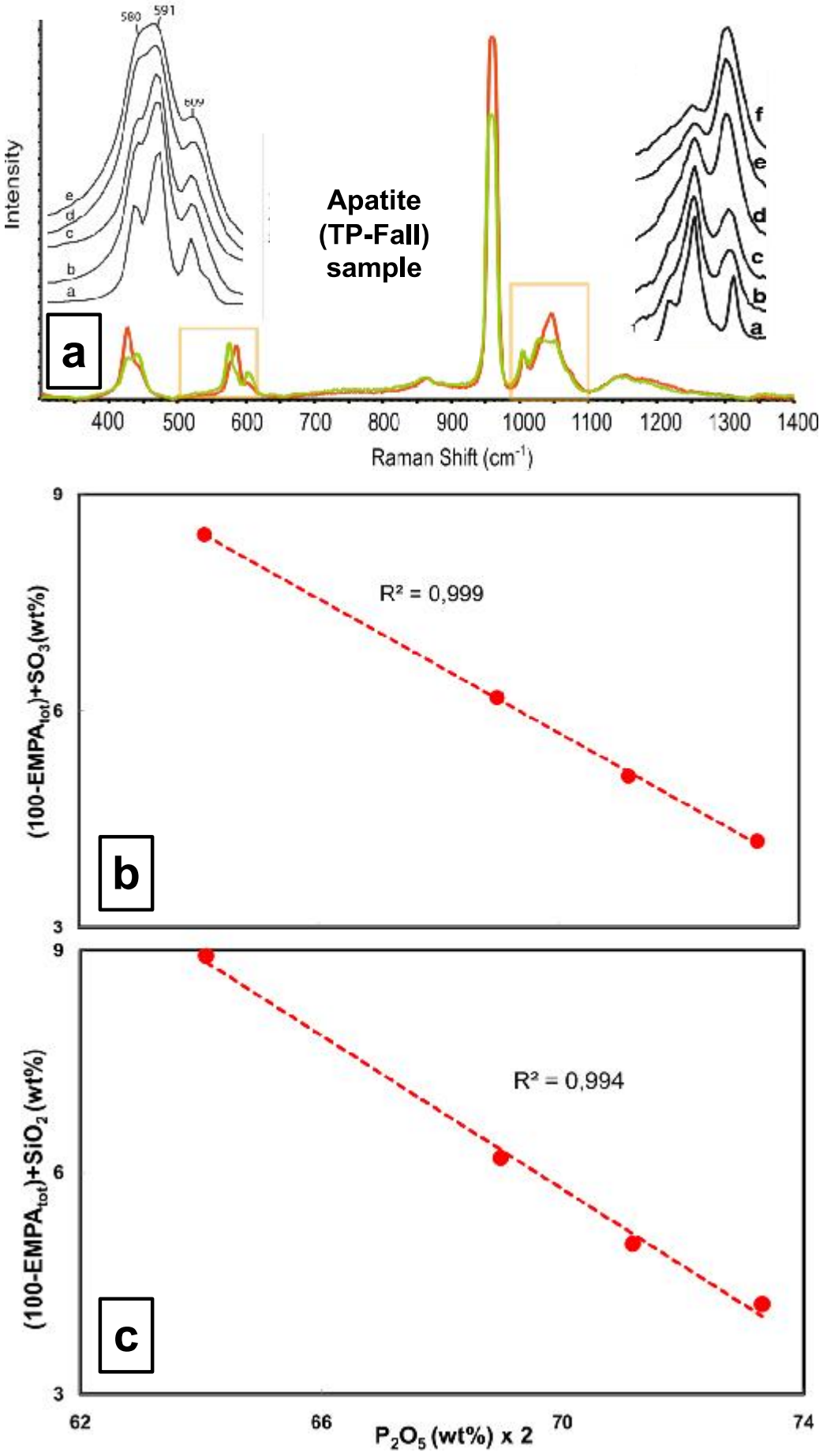

Fig. 6

Figure 7

Click here to access/download;Figure;Fig 7 revised Gaeta et al.pdf

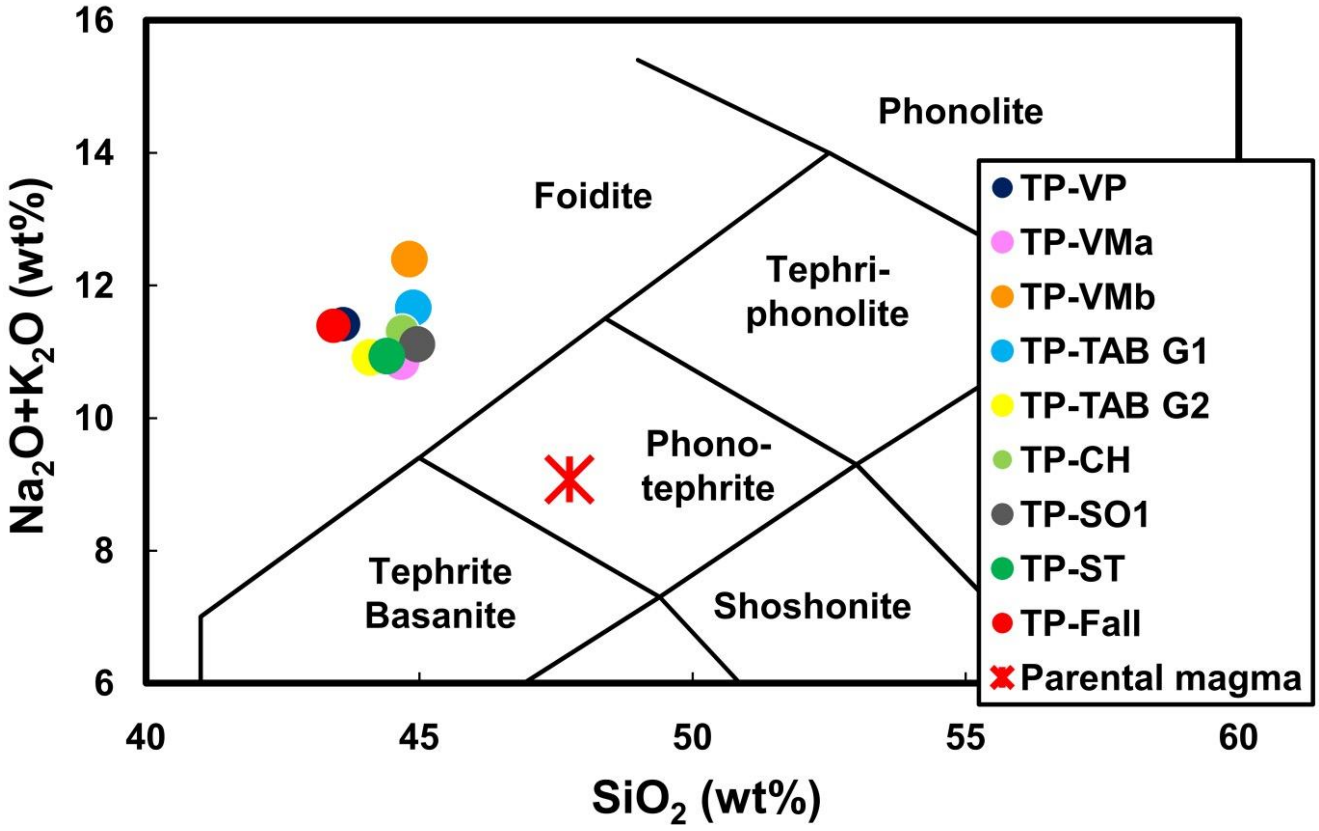

Fig. 7

Figure 8

Click here to access/download;Figure;Fig 8 revised Gaeta et al.pdf

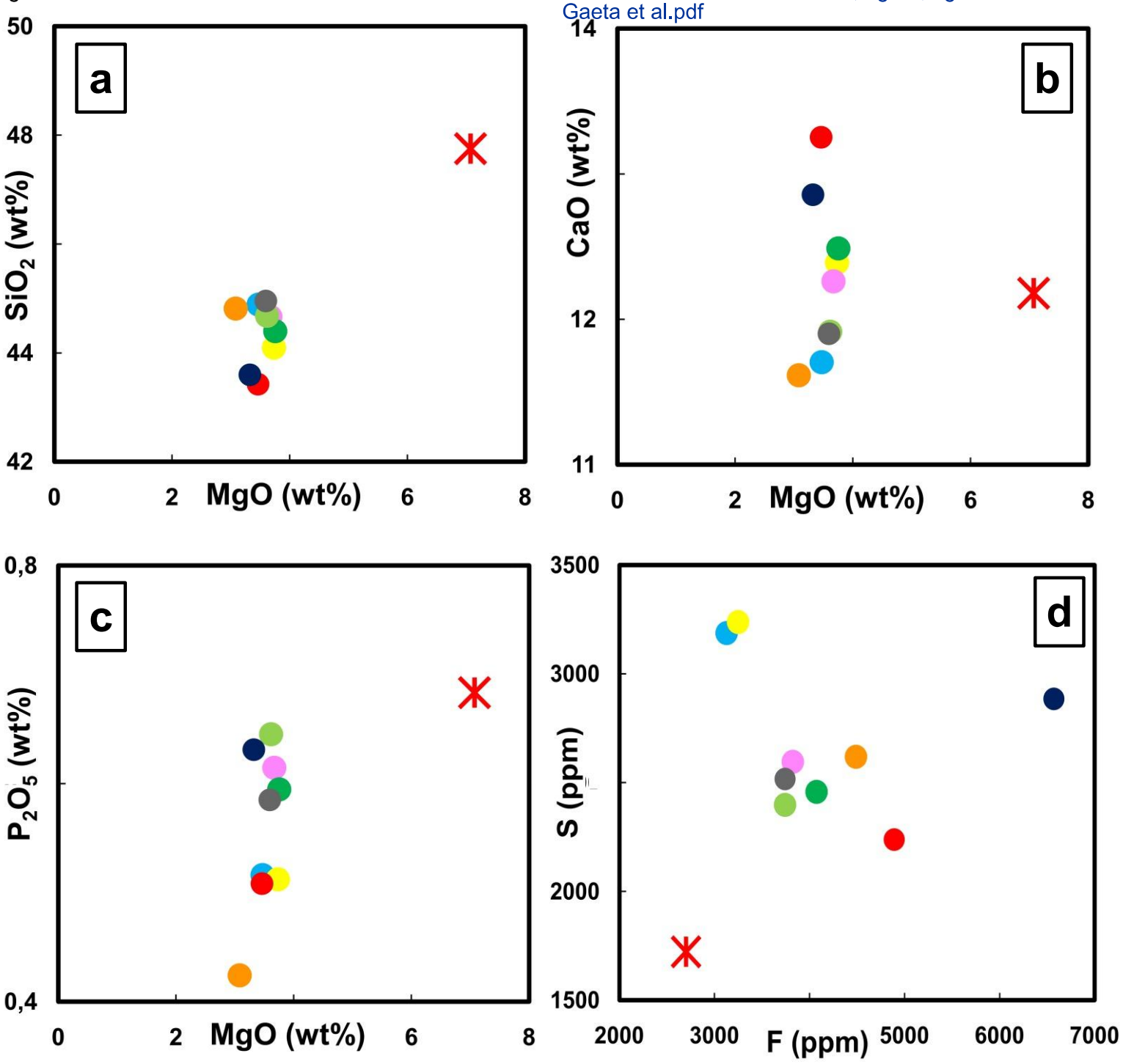

Fig. 8

Figure 9

Click here to access/download;Figure;Fig 9 revised Gaeta et al.pdf

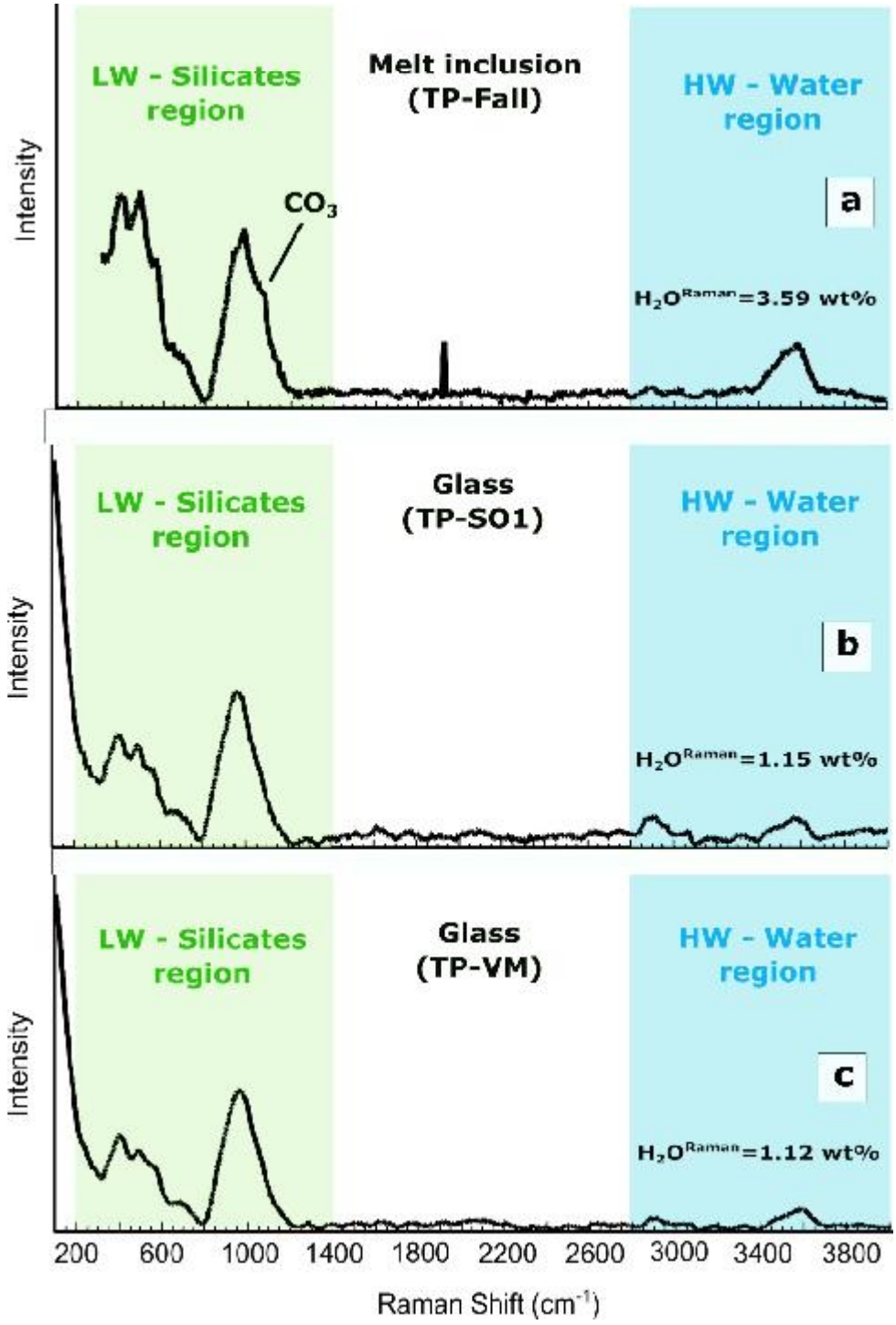

Fig. 9

Figure 10

Click here to access/download;Figure;Fig 10 revised Gaeta et al.pdf

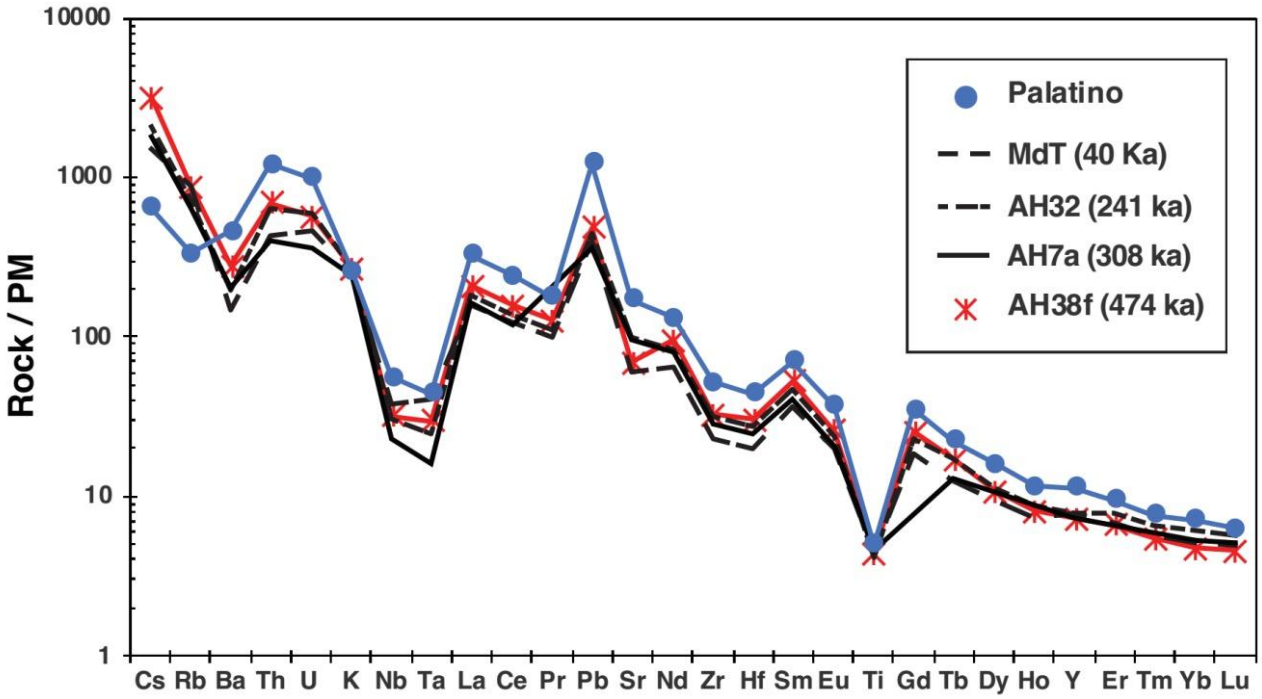

Fig. 10

Figure 11

Click here to access/download;Figure;Fig 11 revised Gaeta et al.pdf

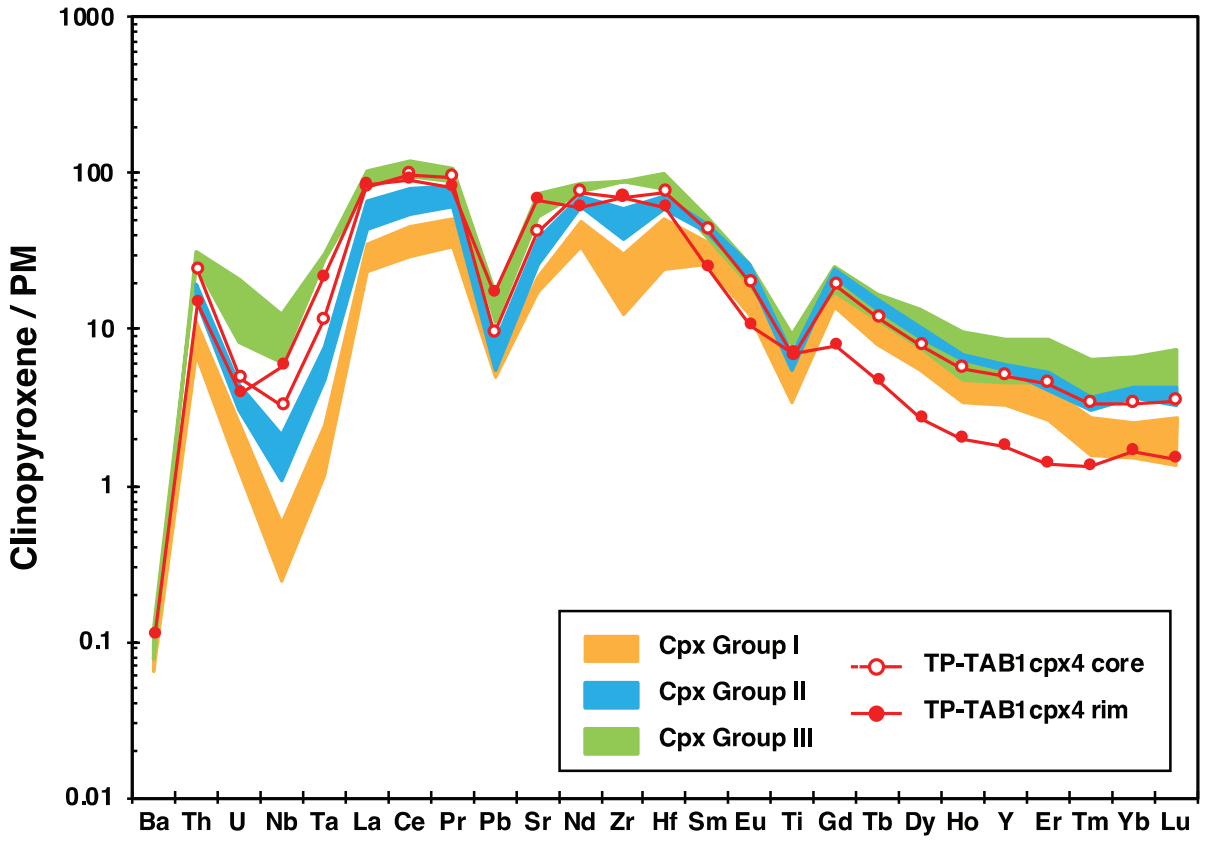

Fig. 11

Figure 12

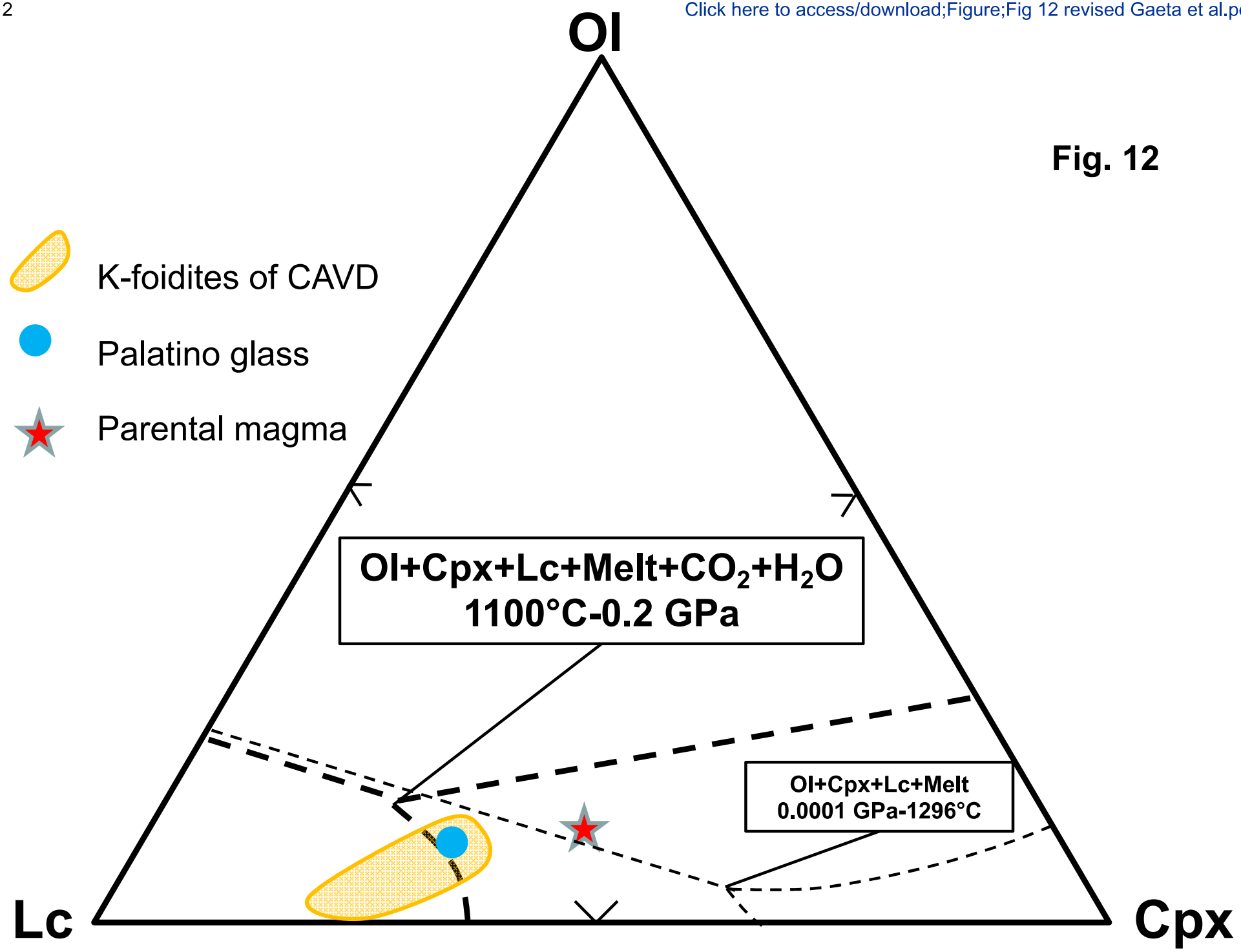

Figure 13

Click here to access/download;Figure;Fig 13 revised Gaeta et al.pdf

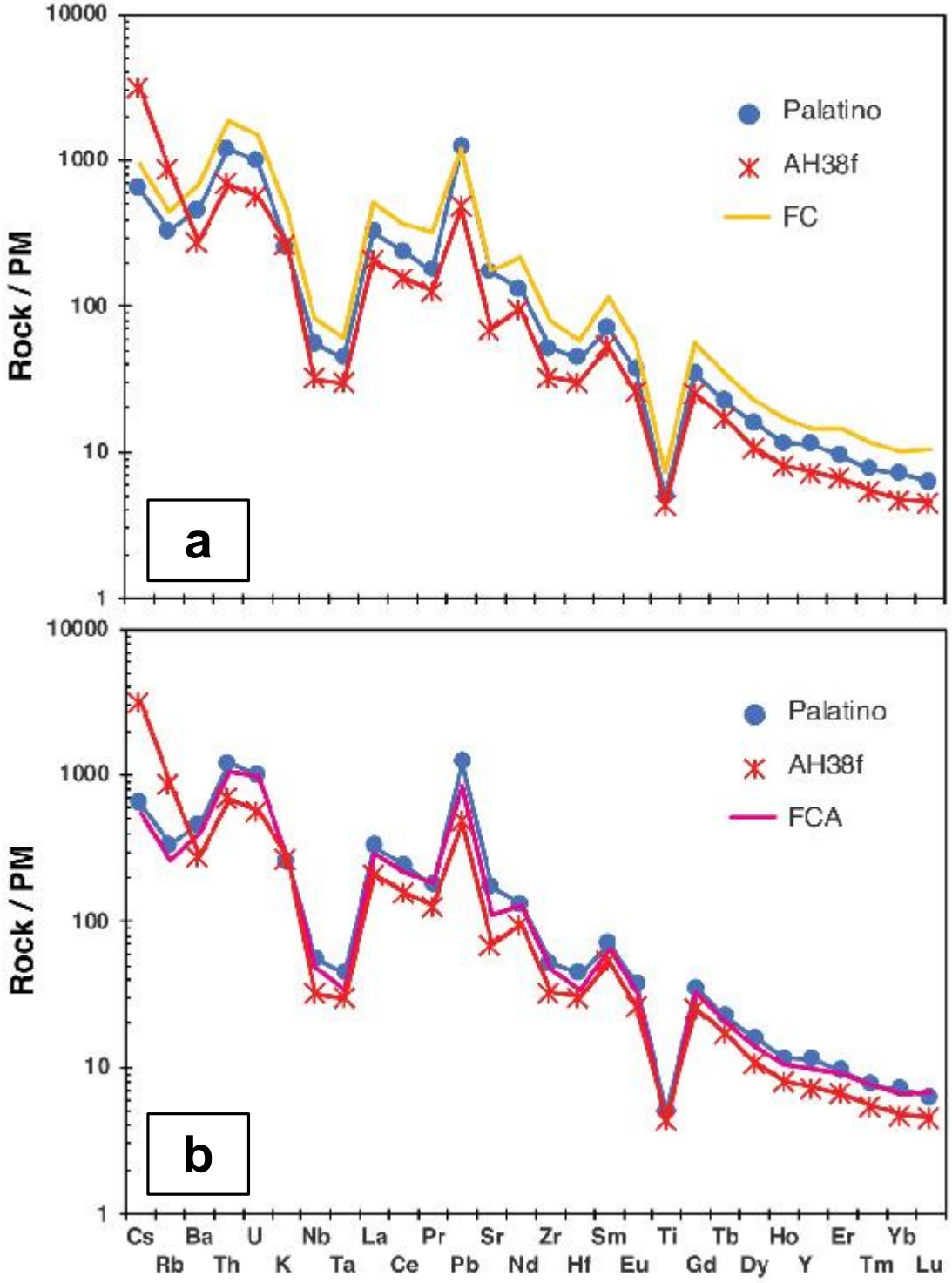

Fig. 13

Figure 14

Click here to access/download;Figure;Fig 14 revised Gaeta et al.pdf

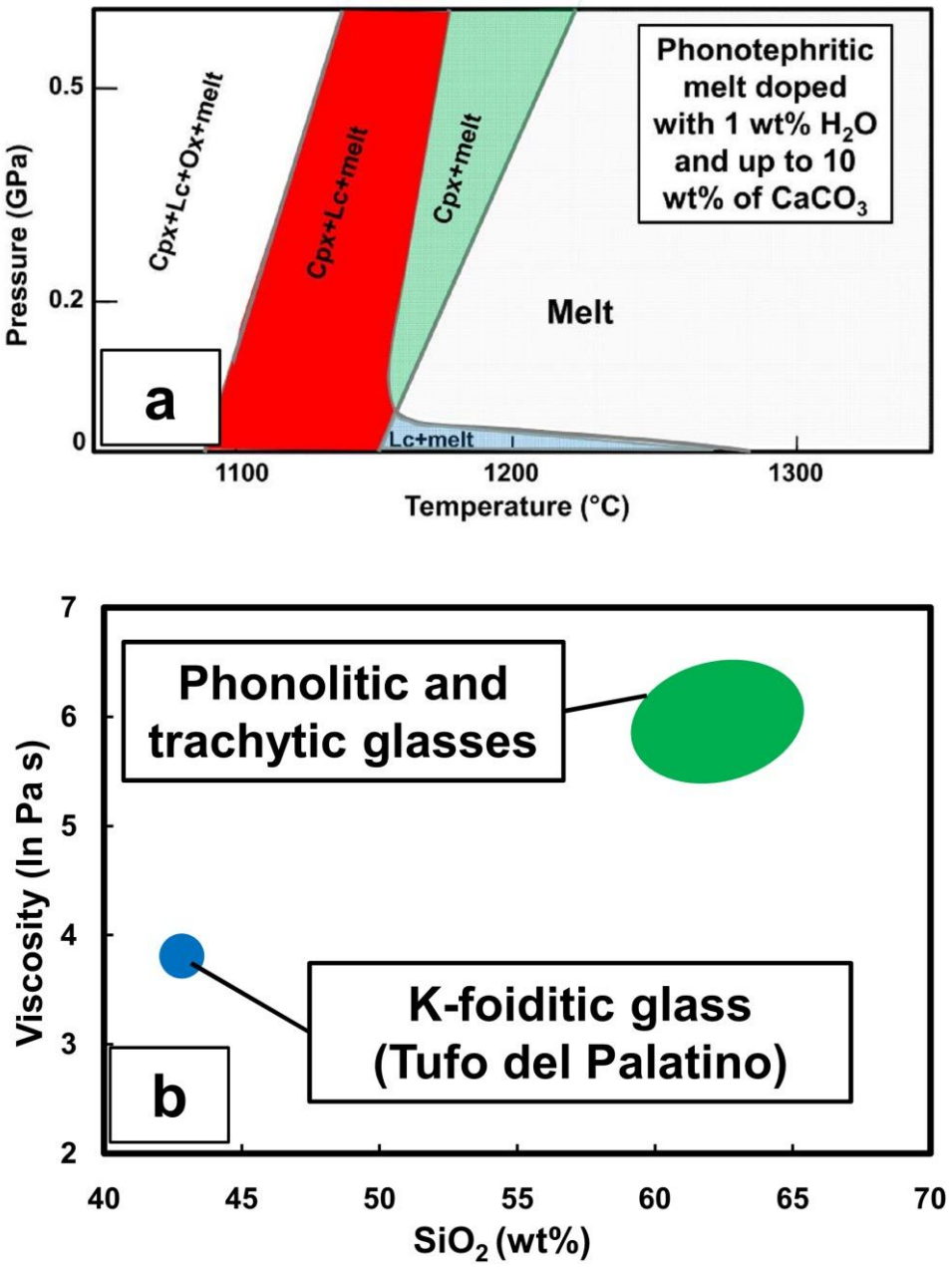

Fig. 14

Table 1. Chemical composition of clinopyroxenes in the Tufo del Palatino scoria clasts.

Sample	Group I TP-Fall		Group II TP-Fall		Group II TP-VG		Group III TP-Fall	
	Core	Rim	Rim	Core	Rim	Core	Rim	Core
SiO_2	52.07	50.67	45.72	43.94	46.27	46.17	40.97	40.97
TiO_2	0.45	0.82	1.48	2.11	1.34	1.22	1.99	2.17
Al_2O_3	2.51	4.09	7.41	8.30	6.65	6.58	10.17	10.08
FeO	4.50	5.27	9.11	9.75	9.00	8.84	14.16	14.55
MnO	0.15	0.09	0.11	0.12	0.17	0.19	0.27	0.30
MgO	14.89	14.33	10.91	10.07	11.13	10.93	6.81	6.87
CaO	24.23	24.72	24.86	24.61	24.49	24.55	23.83	23.77
Na_2O	0.18	0.19	0.31	0.27	0.24	0.27	0.42	0.49
K_2O	0.00	0.04	0.00	0.00	0.00	0.00	0.00	0.01
Cr_2O_3	0.00	0.04	0.03	0.03	0.03	0.00	0.02	0.00
Total	98.96	100.26	99.92	99.19	99.32	98.75	98.65	99.21
Cations on the basis of 6 oxygen								
Si	1.933	1.861	1.712	1.666	1.744	1.750	1.590	1.582
Ti	0.013	0.023	0.042	0.060	0.038	0.035	0.058	0.063
Al^{IV}	0.067	0.139	0.288	0.334	0.256	0.250	0.410	0.418
Al^{VI}	0.043	0.038	0.039	0.037	0.040	0.044	0.056	0.041
Fe^{3+}	0.012	0.070	0.187	0.196	0.158	0.156	0.269	0.288
Fe^{2+}	0.127	0.092	0.098	0.113	0.126	0.124	0.191	0.182
Mn	0.005	0.003	0.003	0.004	0.006	0.006	0.009	0.010
Mg	0.824	0.785	0.609	0.569	0.625	0.618	0.394	0.396
Ca	0.964	0.973	0.998	1.000	0.989	0.997	0.991	0.983
Na	0.013	0.014	0.023	0.020	0.018	0.020	0.032	0.037
K	0.000	0.002	0.000	0.000	0.000	0.000	0.000	0.000
Cr	0.000	0.001	0.001	0.001	0.001	0.000	0.000	0.000
En	<1	<1						
Di	83	79	61	57	63	62	40	40
Hd	13	9	10	11	13	12	19	18
ΣTs	6	12	25	27	22	22	35	36
Jd+Acm	1	1	2	2	2	2	3	4
Kd[a]	0.24	0.29	0.27	0.31	0.26	0.26	0.47	0.47
T(°C)[b]	1112	1121	1069	1069	1068	1056		
P(GPa)[c]	0.32	0.33	0.21	0.22	0.21	0.21		

a:clinopyroxene-melt exchange coefficients Kd is calculated using as equilibrium melt the compositions of AH38f (Group I), Tufo del Palatino (Group II) and Lionato (Group III) glasses (chemical compositions of AH38f and glasses in Table 2 and Table S1); b: calculated using the Eq.33 algorithm of Putirka (2008); c: calculated using the algorithm Palk2012 of Masotta et al. (2013); En: enstatite; Di: diopside; Hd: hedembergite; ΣTs: Tschermak-molecules; Jd: jadeite; Acm: acmite.

Table 2. Chemical composition of glasses in the Tufo del Palatino scoria clasts and AH38f lava flow assumed as parental magma.

Sample	TP-Fall	TP-ST	TP-SO1	TP -CH	TP-TAB1	TP-TAB1	TP-VM	TP-VM	TP-VP	AH38f
RT	G	G	G	G	G1	G 2	G1	G 2	G	LF
NA	5[a]	3	9	4	3	3	8	4	2	
SiO_2	41.33	42.37	43.08	42.92	43.51	42.39	42.81	43.22	41.37	47.52
TiO_2	1.11	1.09	1.08	1.02	1.03	1.11	1.07	1,02	1.11	0.88
Al_2O_3	14.97	14.74	15.23	15.30	15.68	15.11	15.08	16.13	15.56	13.25
FeO	10.29	10.54	10.20	10.22	9.97	10.78	10.42	9.30	10.05	7.25
MnO	0.24	0.18	0.18	0.18	0.22	0.25	0.20	0.23	0.33	0.14
MgO	3.29	3.58	3.44	3.47	3.36	3.59	3.52	2.97	3.17	7.04
CaO	12.61	11.92	11.40	11.44	11.35	11.91	11.75	11.20	12.26	12.12
Na_2O	4.76	3.15	2.95	2.86	2.99	3.10	3.13	4.51	4.61	1.30
K_2O	6.08	7.29	7.71	8.00	8.31	7.40	7.27	7.45	6.27	7.73
P_2O_5	0.48	0.57	0.56	0.62	0.50	0.49	0.59	0.41	0.60	0.68
SO_3	0.56	0.61	0.63	0.60	0.80	0.81	0.65	0.65	0.72	[b]0.43
F	0.49	0.41	0.37	0.37	0.31	0.32	0.38	0.45	0.66	[b]0.27
Cl	0.18	0.11	0.11	0.11	0.10	0.10	0.11	0.16	0.16	
Total	96.39	96.56	96.94	97.14	98.13	97.37	96.99	97.71	96.86	98.61
H_2O[c]			1.15					1.12		[d]0.60
Mg#[e]	0.36	0.38	0.38	0.38	0.38	0.37	0.38	0.36	0.36	0.63
Fe_2O_3[f]	4.49	4.39	4.22	4.24	4.17	4.46	4.31	4.04	4.33	
FeO	6.25	6.59	6.41	6.41	6.22	6.77	6.54	5.67	6.15	

RT: rock type; G: glass; LF: lava flow; NA: number of EMP analyses; a: standard deviations in S1 Table; b: values of primitive glasses (Gaeta et al., 2009); c: obtained from Raman spectra; d: LOI value; e: Mg# = MgO/(MgO+FeO) calculated on the molar basis considering all the iron as FeO; f: iron partition calculated at the oxygen fugacity of QFM+2 buffering conditions.

Table 3. Trace element abundances and $^{87}Sr/^{86}Sr$ ratio.

	Glass		LF	Clinopyroxene				
Sample	TP-TAB1	TP-VM	AH38f	TP-TAB1/TP-VM				
NA	16	10		10	11	16		
				Group I	Group II	Group III	Cpx4[a] Core	Cpx4[a] Rim
Li	nd	nd	nd	2.89	3.03	4.86	2.77	9.15
Cs	14	14	66	bld	bld	bld	bld	bld
Rb	199	203	528	bld	bld	bld	bld	bld
Ba	3080	2988	1822	0.54	0.73	0.80	bld	1.00
Sr	3414	3382	1363	404	554	1015	825	1321
Pb	184	183	73	0.90	1.05	1.69	1.43	2.68
Th	96	95	55	0.62	1.27	2.03	1.89	1.23
U	20	20	11.5	0.04	0.07	0.15	0.10	0.13
Zr	544	536	341	202	449	792	746	699
Hf	13	12	8.6	9.3	18.0	23.1	21.2	16.0
Ta	1.65	1.64	1.10	0.07	0.16	0.62	0.42	0.60
Y	50	48	31	17	24	24	21	8
Nb	37	36	21	0.25	0.73	2.93	2.13	3.10
Sc	11	11	31	86	64	32	38	9
Cr	4	4	170	71	28	45	51	3
Ni	15	14	80	91	49	39	20	1
Co	35	34	35	39	41	57	33	23
V	343	340	243	150	215	333	278	386
La	214	212	136	18	32	55	53	53
Ce	411	403	261	61	104	168	162	153
Pr	46	45	32	10	17	24	24	21
Nd	165	162	119	50	76	98	96	71
Sm	28.3	28.8	21.5	11.8	17.0	17.7	17.3	9.2
Eu	5.76	5.45	3.98	2.4	3.4	3.4	3.1	1.6
Gd	19.0	19.2	13.9	8.8	12.0	11.5	10.6	4.7
Tb	2.25	2.20	1.70	1.0	1.3	1.3	1.2	0.6
Dy	10.9	10.7	7.3	4.4	6.1	6.2	5.4	1.9
Ho	1.74	1.68	1.20	0.63	0.93	0.92	0,84	0.31
Er	4.14	4.25	2.90	1.35	2.02	2.16	2.00	0.74
Tm	0.52	0.51	0.37	0.15	0.23	0.27	0.23	0.12
Yb	3.19	3.07	2.10	0.97	1.49	1.81	1.45	0.56
Lu	0.43	0.42	0.31	0.14	0.22	0.30	0.23	0.14
$^{87}Sr/^{86}Sr$			0.710831[b]	0.710893[c]				

a: in equilibrium with garnet; b: after Gaeta et al. (2016); c: after Gaeta et al. (2006); NA: number of ICP-MS point analyses; nd: not determinated; bdl: below detection limit.